SEARCH FOR EXOTIC DOUBLE TRACKS

with the IceCube Neutrino Telescope

SANDRO KOPPER

Dissertation

zur Erlangung des Doktorgrades der Naturwissenschaften
(Dr. rer. nat.)

BERGISCHE
UNIVERSITÄT
WUPPERTAL

Fachbereich C - Mathematik und Naturwissenschaften
(Astroteilchenphysik)
Bergische Universität Wuppertal

April 2017

Die Dissertation kann wie folgt zitiert werden:

urn:nbn:de:hbz:468-20170511-093419-2
[http://nbn-resolving.de/urn/resolver.pl?urn=urn%3Anbn%3Ade3Ahbz3A468-20170511-093419-2]

Sandro Kopper: *Search for Exotic Double Tracks* with the IceCube Neutrino Telescope, April 2017 (first version February 2016)

GUTACHTER:
Prof. Dr. Klaus Helbing
Prof. Dr. Lutz Köpke

– Dedicated to my parents, my brother and my friends.

ABSTRACT

Physics theories beyond the Standard Model, like supersymmetry and models with extra dimensions, often invoke $\mathbb{Z}_2$-symmetries in order to avoid new couplings that lead to unobserved new physics, like unnaturally fast proton decay. This gives rise to the possibility of heavy new particles being produced in pairs with the lightest of them being (meta-)stable. Thus, under favorable conditions, neutrinos in the PeV range can produce pairs of exotic, charged particles that can be seen in a km^3-sized detector as two parallel, muon-like tracks with a track separation of a few hundred meters.

This thesis discusses methods for simulating and reconstructing these exotic double tracks for the case of the IceCube neutrino observatory located at the geographic South Pole. It deals with techniques to separate them from other air shower or neutrino-induced muon events in a model independent way.

The search for such events with data taken by the IceCube detector in its 79-string configuration between May 2010 and May 2011 resulted in no candidate events. This result can be used to derive limits that can be applied to explicit exotic models.

As this is the first analysis of its kind, the prospects and requirements of future double track searches are also addressed.

I love deadlines.
I love the whooshing noise they make as they go by.

— Douglas Adams, *The Salmon of Doubt*

ACKNOWLEDGEMENTS

Many thanks to everybody whose assistance and support made this work possible and helped me to finish it. For this I would like to acknowledge everyone in the astroparticle physics group in Wuppertal but also the members of the IceCube collaboration worldwide.

First and foremost, I want to thank my supervisor Professor Klaus Helbing for giving me the chance to work within the IceCube collaboration and pursue this interesting field of study. Here I also want to thank our secretary Ms. Schaarwächter who always helped with any organizational issues that might come up in a fast and friendly way.

I want to thank everyone in Wuppertal I shared the workplace with, both those still present and those who already moved on. They always made the time I spent at the office enjoyable. This goes for the whole astroparticle group at large, all of whom I can not name here in person, but especially those within the IceCube group with whom I had many lively discussions. I especially want to mention those I shared an office with: Benjamin Semburg, Jonas Posselt, Dennis Soldin and Anna Pollmann. Dennis not only was always open for conversations about all kinds of scientific questions but also helped me with input about this thesis and its contents in particular. In this regard I also want to mention Stephanie Hickford who helped me proof-read the text you currently hold.

Finally I want to thank my family, my parents Gabriele and Wilfred Kopper and my brother Claudio, as well as my friends who supported me throughout these years and everyone I forgot to mention to whom I also want to apologize hereby.

CONTENTS

ADD	Arkani-Hamed, Dimopoulos, Dvali
AGASA	Akeno Giant Air Shower Array
AGN	Active Galactic Nucleus
AHA	Additionally Heterogeneous Absorption
AMANDA	Antarctic Muon And Neutrino Detector Array
AMSB	Anomaly Mediated Supersymmetry Breaking
ANTARES	Astronomy with a Neutrino Telescope and Abyss environmental RESearch
ATLAS	(originally) A Toroidal LHC ApparatuS
ATWD	Analog-to-digital Transient Waveform Digitizer
AUGER	Pierre Auger Observatory
BATSE	Burst And Transient Source Experiment
BCS	Bardeen-Cooper-Schrieffer
BDT	Boosted Decision Tree
CC	Charged-Current
CHAMP	CHArged Massive Particle
CMB	Cosmic Microwave Background
CMS	Compact-Muon-Solenoid experiment
cMSSM	constrained MSSM
CoG	Center of Gravity
CORSIKA	COsmic Ray SImulations for KAscade
CR	Cosmic Ray
CTEQ	Coordinated Theoretical-Experimental project on QCD
DAQ	Data AcQuisition
d.o.f.	degree of freedom
DOM	Digital Optical Module

DOR DOM Readout

DUMAND Deep Underwater Muon And Neutrino Detector Project

fADC fast (flash) Analog-to-Digital Converter

FCNC Flavor Changing Neutral Current

FERMI Fermi Gamma-ray Space Telescope

FPGA Field Programmable Gate Array

GEANT GEometry ANd Tracking

GMSB Gauge Mediated Supersymmetry Breaking

GPS Global Positioning System

GRB Gamma Ray Burst

GUT Grand Unified Theory

GZK Greisen-Zatsepin-Kuzmin

HiRes High Resolution Fly's Eye Cosmic Ray Detector

HLC Hard Local Coincidence

IC22 22-string IceCube detector

IC40 40-string IceCube detector

IC79 79-string IceCube detector

IC86 (complete) 86-string IceCube detector

ICT Imaging Cherenkov Telescope

KASCADE KArlsruhe Shower Core and Array DEtector

KK Kaluza-Klein

LAT Large Area Telescope

LED Large Extra Dimensions *or* Light-Emitting Diode

LHC Large Hadron Collider

LKP Lightest Kaluza-Klein Particle

LHEF Les Houches Event Files

LSP Lightest Supersymmetric Particle

LPM Landau-Pomeranchuk-Midgal

M.C. Monte Carlo

MChits Monte Carlo hits

MIP Minimum Ionizing Particle

MMC Muon Monte Carlo

MPE Multi Photo-Electron

MSSM Minimal Supersymmetric Standard Model

mSUGRA minimal SUperGRAvity

mUED minimal Universal Extra Dimensions

NC Neutral-Current

NCh Number of Channels (i.e. signal DOMs)

NEMO NEutrino Mediterranean Observatory

NESTOR Neutrino Extended Submarine Telescope with Oceanographic Research

NLKP Next-to-Lightest Kaluza-Klein Particle

NLSP Next-to-Lightest Supersymmetric Particle

NPE Number of Photo-Electrons

NUHM Non Universal Higgs Mass

RAPcal Reciprocal Active Pulsing calibration

PDF Probability Density Function *or* Patron Distribution Function

PE Photo-Electron

pMSSM phenomenological MSSM

PREM Preliminary Earth Reference Model

RGE Renormalization Group Equation

RS Randall-Sundrum

SLC Soft Local Coincidence

SLHA SUSY Les Houches Accord

SM Standard Model

SMT Simple Majority (Multiplicity) Trigger

SNR SuperNova Remnant

SPICE South Pole ICE

SPE Single Photon-Electron

SPS Snowmass Points and Slopes

SUSY SUperSYmmetry

TMVA Toolkit for MultiVariate data Analysis

ToE Theory of Everything

ToI Tensor of Inertia

UED Universal Extra Dimensions

UHE Ultra High Energy

UTC Coordinated Universal Time

WIMP Weakly Interacting Massive Particle

WMAP Wilkinson Microwave Anisotropy Probe

To summarize the summary of the summary:
people are a problem.

— Douglas Adams, *The Restaurant at the End of the Universe*

INTRODUCTION AND SUMMARY

This work is about charged particles that have an origin in exotic physics of cosmic ray interactions and the prospect of their detection in a modern neutrino telescope as parallel tracks.

Chapter 1 is a recapitulation of the phenomenon of so called *cosmic rays*. Due to the high energy some cosmic ray particles have, they can cause particle interaction cascades in the atmosphere known as *air showers* which are discussed in Chapter 2. Understanding the behavior of charged particles in bulk matter like the atmosphere or the Earth itself are thus vital in order to conduct cosmic ray observations (Chapter 3). However, not all cosmic ray particles are charged. Neutrinos, some of which can have very high energies, are being produced in both air showers and the sources of cosmic rays and can help to answer questions about the origins of the latter. They are of interest for astroparticle physics and are being observed in experiments known as neutrino telescopes. Their history and detection principles are discussed in Chapter 4 and Chapter 5 then goes into more detail for one specific such experiment with the name IceCube that forms the basis of this work.

Physics beyond the current *Standard Model* is needed in order to explain a number of facts in current particle physics. This is examined in Chapter 6. It goes into detail on two of the most popular such frameworks - supersymmetry and models with extra dimensions. Both share several aspects and a common prediction by both of them is new, yet unobserved particles with rest masses in the TeV range.

The speed of light $c = 1$ is a common convention in particle physics.

Taking all these aspects together cosmic ray and especially neutrino interactions can, under favorable conditions, lead to parallel tracks of said particles in neutrino telescopes as a unique event signature. This, along with the simulation of both the exotic tracks and possible standard model backgrounds, is the topic of Chapter 7. The contents of Chapter 8 then show a way to reconstruct the properties of such events and how to use their topology to distinguish them from other events in a km^3-neutrino telescope. The cut parameters for the special case of IceCube in its 79-string configuration and their chosen values is topic of Chapter 9. A discussion of the difficulties of finding a rare signal with the low amount of background simulation in a *blind* analysis and the influence on the final cut parameters can also be found here. In Chapter 10 and Chapter 11 the results of *unblinding* the data and the limits set on exotic double tracks together with how systematic uncertainties of the IceCube detector modify them are shown.

Finally a discussion of the analysis and the prospect of extending it to more recent and future years of IceCube data taking, especially requirements of background simulation and improvements in filtering, is done in Chapter 12. Possibly needed improvements when it comes to reconstruction are also considered here.

Part I

THEORY AND EXPERIMENT

In the beginning the Universe was created.
This had made many people very angry and has been widely regarded as a bad move.

— Douglas Adams, *The Hitchhiker's Guide to the Galaxy*

1 COSMIC RAYS

It has been more than a century since the discovery of *cosmic rays* and their function as ionizing particles high in the atmosphere by Victor Hess which made him the co-recipient of the Nobel Price in 1936 [1]. Yet, we still do not know their exact origins to date. The spectrum of the particles comprising the cosmic radiation follow roughly a power law $dN/dE = E^{-\gamma}$ over many orders of magnitude and shows very little structure (compare Figure 1). The main exceptions to this are the so called *knee*, corresponding to a softening of the spectrum where the spectral index changes γ from ≈ 2.7 to ≈ 3.1 at around 10^{15} eV, and the *ankle* at $\approx 5 \cdot 10^{18}$ eV where the index goes back to $\gamma \approx 2.7$ [2] (compare Figure 2). At lower energies at least, cosmic rays are mainly made up by protons [3]. At higher energies, especially between the knee and the ankle, the elemental composition and its change with energy becomes important when trying to distinguish between different origins of the spectral structure. It also, however, becomes harder to measure directly and so data and interpretations give a conflicting picture [4, 5, 6].

1.1 SOURCES OF COSMIC RAYS

The onset of the knee structure is usually interpreted as the energy range where high energy particles can no longer be contained within the galaxy and its associated magnetic fields. For particles with lower energy it is known that the cosmic rays must have been contained within the galaxy for a long time before reaching the Earth due to a very high abundance in spallation products within the cosmic ray nuclides [2]. If this view is correct, and since the galactic magnetic field strength is a fixed, albeit unknown, variable, the energy *cut-off* should be directly linked to the rigidity

$$R = \frac{p}{q} = r \cdot B$$

where r is the gyroradius in the magnetic field B, p is the momentum and q the charge of the particle. Higher charge generally means higher mass of chemical elements. Thus, the cut-off is indirectly also linked to the mass of the cosmic rays. While there have been supporting observations of a change in cosmic ray composition to heavier and heavier constituents to support this idea, there are still ongoing analyses in this energy range to prove the relation beyond a reasonable doubt [9].

Sometimes a faint feature at $E \approx 0.4 - 0.7 EeV$ is instead interpreted as the point of transition from galactic to extragalactic cosmic rays [10, 11, 12].

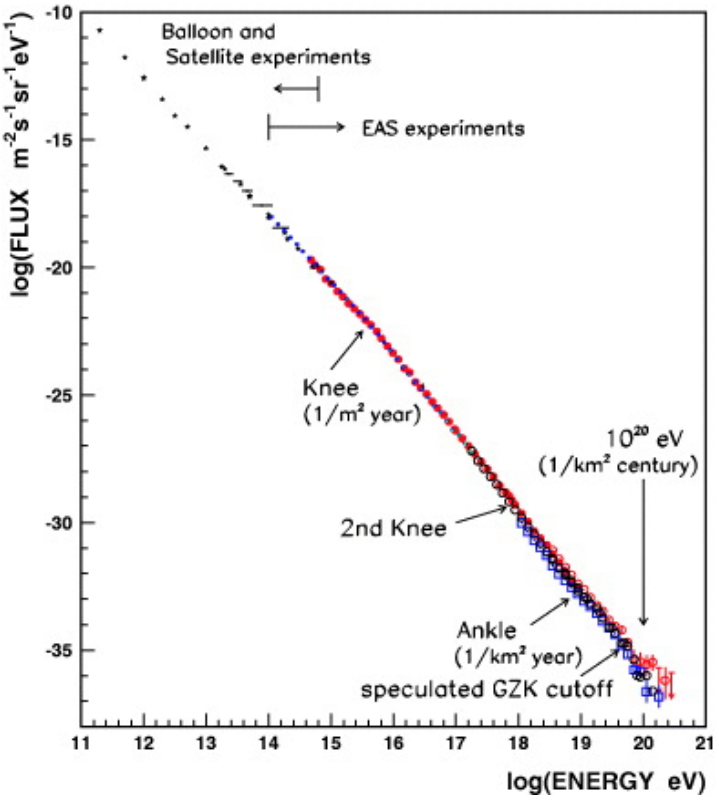

Figure 1: The cosmic ray spectrum shows very little structure over many orders of magnitude. Taken from [7].

Energies above the ankle are usually interpreted as at least mostly extragalactic in origin. If this is the case the spectrum has to steepen again at some point since the particle energy is eventually high enough to interact with the cosmic microwave background over the distance to our galaxy. This phenomenon has been predicted by Greisen, Kuzmin, and Zatsepin at particle energies of around $5 \cdot 10^{19}$eV [13, 14] and is often refered to as the *GZK-effect*. Results of the Pierre-Auger-Observatory (and earlier results of the HiRes collaboration) point in this direction [4, 6], even though there is tension with the results of the AGASA collaboration that observed conflicting behavior of the particles at highest measured energies [5].

The AGASA events exceeding the theoretical GZK cutoff could possibly be interpreted a sign of a nearby source.

If the GZK-effect really is the main feature that limits the energy of cosmic rays - instead of it being the lack of sources for such high energy particles - the drop off in the spectrum should be associated with very high energetic neutrinos produced by the decay of charged pions.

$$\gamma + p \to \Delta^+ \to p + \pi^0$$

$$\gamma + p \to \Delta^+ \to n + \pi^+$$

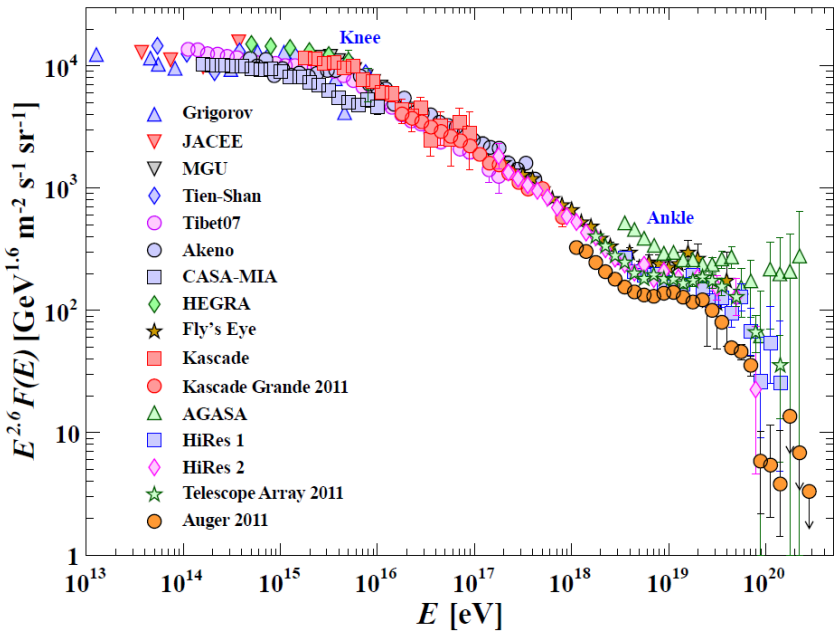

Figure 2: The structure of all-particle cosmic ray spectrum. Taken from [8].

Yet another explanation for the decrease in extragalactic cosmic rays is photo-disintegration due to the CMB or extragalactic background light. This is conceptually very close to the GZK-effect - its name is usually only used for pion production - but both models have dependent cut-off shapes, especially for different nucleons [15, 16, 17, 18, 19].

For not too high energies the source of the hadronic part of the cosmic ray spectrum can be - in principle - found by looking for gamma ray emission with imaging Cherenkov telescopes (ITCs) [20] or satellite experiments like FERMI [21]. Hadronic sources will lack the associated synchrotron emission that links a source to electron acceleration. Though in practice this observation of a source in multiple, often quite different, wavelengths can be hard to accomplish.

H.E.S.S., MAGIC, CTA, etc.

Good source candidates for galactic cosmic rays are objects with the energetic properties to accelerate particles to the required energies that are already showing gamma ray emission. An example are supernova remnants [22]. The supernova itself is also a prime source candidate for cosmic rays in our galaxy. The rate of supernova explosions in a galaxy like ours is only $\mathcal{O}(1/\text{century})$, but even this might be sufficient to produce the diffuse content of cosmic rays originating in our galaxy if even only a small part of the star's mass is converted to energy and used in the acceleration of particles [23].

When looking for source candidates outside the Milky Way there is a special class of objects showing high rates of gamma-ray emission, the so called *gamma-ray-bursts* (GRB). These events are usually interpreted as supernova or supernova-like explosions and seem to

Short GRBs *generally have a duration of less than 2 seconds.*

fall into roughly two distinct classes (see Figure 3). The *short GRBs* are, like the name implies, shorter in duration and can be found outside regions of heavy star formation [24]. Together this hints at an origin associated with the merger of compact objects like black holes or neutron stars.

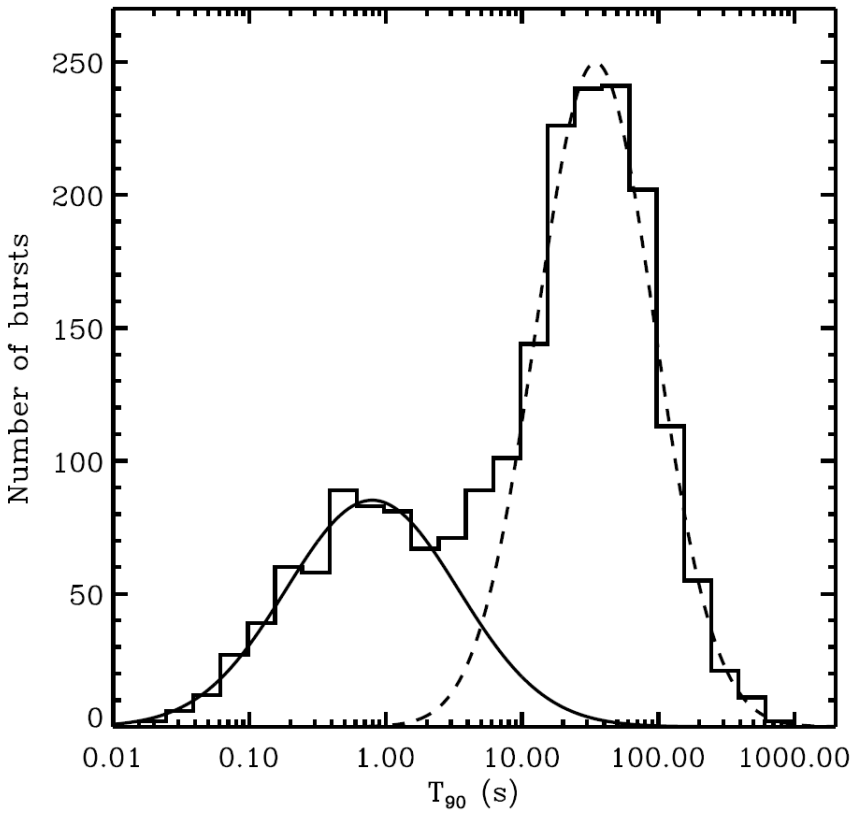

Figure 3: Duration of gamma ray bursts in the BATSE catalogue [25]. One can see two populations that can be roughly divided in two main contributions. Taken from [24].

Long GRBs *generally have a duration of* more *than 2 seconds.*

The long duration GRB population on the other hand is found (almost) exclusively in regions of heavy star formation [26]. Older stars and objects eventually leave the region of space where they have been formed, while young stars - and very massive stars are always young - are in the vicinity of their origin. While this does not completely rule out the scenario of a merger origin if it happens within a short time frame after formation, long GRBs have been regularly followed by supernova detections and thus make it likely that they are a special case of core collapse supernova of massive stars [28].

A good example is the 2006aj type Ic supernova [27].

The so called collapsar model is a popular view that makes the additional assumption of a fast rotating star that can thus form a rotating *Kerr black hole* in its core as well as an accretion disk around it [29]. At the poles of the star jets can form and then escape if the star has shed its hydrogen hull during its lifetime.

The jets can be viewed as relativistic fireballs to explain the spectral features of the GRBs. Highly variable, non-thermal, multi-peak structure is explained by the formation of shocks. Whether as internal shocks that can potentially collide with one another or as external shocks that collide with the medium outside the star, both can cause the acceleration of electrons to a power law spectrum. These emit photons via synchrotron radiation which also explains the typical GRB *afterglow* feature that has been observed. The leading shock wave during this process becomes highly relativistic due to the decreasing density as it travels towards the surface of the star. When it is reaching this point a large part of the energy gets released in the form of gamma rays.

There are also other sources for cosmic rays that can possibly accelerate particles to the required energies. These include neutron stars with unusually strong magnetic fields (*Magnetars*) and active galactic nuclei (AGN) [30, 31]. The latter again has a (this time super-massive) black hole at its center that is *fed* by an accretion disk generating large scale jets at its poles.

The conflicting views on possible cosmic ray particles beyond the GZK-cutoff energy also have lead to speculations about scenarios for cosmic rays at the highest energies that do not depend on particle acceleration. Instead, super heavy, meta-stable particles could have been produced as relics during the Big Bang or produced when topological defects tied to GUT (*Grand Unified Theory*) physics collapse or annihilate. The highest energies for cosmic rays could thus be directly tied to a scale in fundamental physics [32].

1.2 ACCELERATION MECHANISMS

Since magnetic fields can not accelerate charged particles in a way that changes their energy, the mechanism has to be directly tied to electric fields $\mathbf{E}$. Most astrophysical conditions are plasmas and thus excellent conductors. In these situations it is very hard to produce large scale electrical currents in the whole plasma volume. The current is confined to surfaces that divide different magnetic domains [33]. Here the condition

$$\langle \mathbf{E} \rangle \neq 0$$

can be fulfilled on large scales. In the field line picture these are regions where magnetic field lines reconnect. They allow for efficient particle acceleration with rotating neutron stars and black holes can be thought of as unipolar inductors that have these additional environmental characteristics where acceleration can occur [34].

The other option for particle acceleration is that there are no large scale electrical currents but there are electrical (and thus magnetic) irregularities [35]:

$$\langle \mathbf{E} \rangle = 0 \text{ and } \langle \mathbf{E}^2 \rangle \neq 0 \,.$$

One can no longer accelerate a particle in a direct fashion in such an environment but there is a way to do it in a stochastic sense with repeated collisions. Enrico Fermi first imagined the (here: large scale) irregularities as magnetic clouds that act similiar to a *magnetic mirror* [36]. In one dimension one can easily see that a particle hitting a mirror will gain energy if the mirror is moving towards the particle. It will lose energy if the mirror is moving away. Since there will be more collisions of the first type in a random environment there is a net gain in energy for the particle. In practice there will generally not be a total reflection due to magnetic fields but rather an isotropization of direction of the particle momentum. The effect of scattering is the same, if slightly smaller. Since a process like this has energy gains ϵ that are proportional to the square of the speed of the clouds v_c

$$\frac{\Delta\epsilon}{\epsilon} \propto v_c^2$$

it is known as *second order Fermi acceleration*. The relative energy gain per time

$$\alpha = \frac{1}{E}\frac{dE}{dt}$$

only depends on this energy gain and inversely on the mean free path L between the clouds:

$$\alpha \propto \frac{v_c^2}{L} .$$

Assuming an escape time scale τ for the particle one ultimately gains a power law for the particle spectrum

$$N(\epsilon)dE \propto \epsilon^{1+1/(\alpha\tau)}dE$$

that is not very universal since the combination of parameters τ, L, and v_c are not really fixed in a general situation [37].

One can also see that it would be more efficient to find process that has always direct gain in energy for each collision (and thus be first order in energy gain) instead of just having an average energy gain (and thus being second order like discussed above). This is actually realized in the case of shock waves that have said magnetic inhomogeneities on both sides. Here a particle crossing the shock front in either direction effectively experiences a head-on collision. The situation also naturally leads to a rather universal power law dependence because the escape probability of a particle is only linked to the dynamics near the shock. So one gets for the number of particles $N(\epsilon)$:

This mechanism is known as first order Fermi acceleration *or* diffusive shock acceleration.

$$\frac{dN}{d\epsilon} \propto \epsilon^{-\lambda}$$

with the spectral index $\lambda \gtrsim 2$ [38].

λ only depends on the compression ratio of the shock.

So instead of the observed $\lambda \approx 2.7$ of cosmic rays *at the Earth* one gets a harder spectrum *at the source of acceleration*. If one assumes that

the change in spectral shape has its origin in energy losses of the cosmic ray particles later on, one can assume that these losses will probably be absent for neutral particles such as neutrinos. A natural assumption for the spectral shape of neutrinos produced by interactions of the charged cosmic rays nearby a source still is a power law with $\lambda \approx 2$.

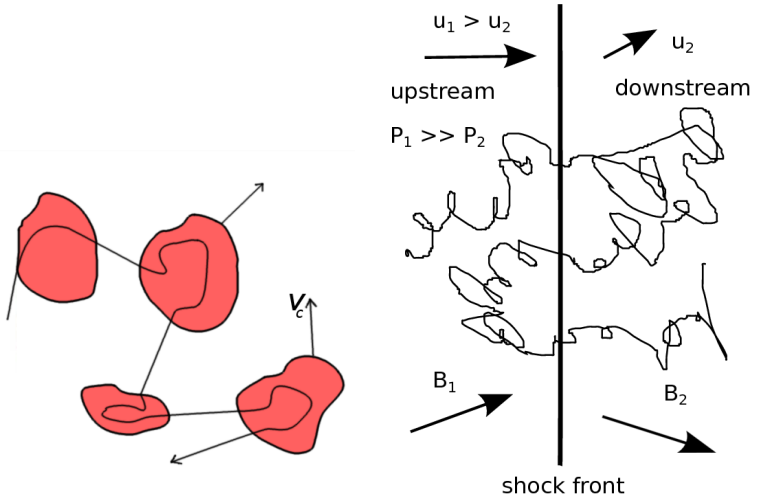

(a) Second order acceleration due to magnetized clouds

(b) First order (diffusive shock) acceleration. Taken from [38].

Figure 4: Scheme of Fermi acceleration mechanisms

1.3 NEUTRINO PRODUCTION IN GAMMA RAY BURSTS

Being tied to cosmic rays production, neutrinos at the highest energies have been linked to most scenarios for cosmic ray acceleration [39, 40, 41] and especially GRBs [42]. Neutrinos are neutral particles and so can not be accelerated in the stated ways. High energy neutrinos are instead mostly linked to the decay of charged high energy pions.

$$\pi^+ \to \mu^+ + \nu_\mu \to e^+ + \nu_e + \bar{\nu}_\mu + \nu_\mu$$
$$\pi^- \to \mu^- + \bar{\nu}_\mu \to e^- + \bar{\nu}_e + \nu_\mu + \bar{\nu}_\mu \,.$$

Pions are produced naturally in inelastic collisions of the nucleons ($p-p$ or $p-n$) of the accelerated charged nuclei. If protons are accelerated to high energies they can also react with photons already present in the ambient medium or parts of the synchrotron radiation and produce pions. The most important of these so-called *photo-meson* production processes go via the production of a Δ-resonance:

$$\gamma + p \to \Delta^+ \to p + \pi^0$$
$$\gamma + p \to \Delta^+ \to n + \pi^+$$

Apart from the origin of the photons this is a similar situation as the one described earlier for the GZK-cutoff effect [43]. Neutrinos are ultimately tied closely to charged cosmic rays and their sources, so much so that Eli Waxman and John Bachall could set a rather model independent limit on the neutrino flux from cosmic ray observations

$$E_\nu^2 \Phi_\nu < 2 \cdot 10^{-8} \mathrm{GeV/cm^2 s\ sr}$$

which has long been used as a general benchmark point for observations and a lower prediction for GRBs in particular

$$E^2 dN/dE \approx 0.3 \cdot 10^{-8} \mathrm{GeV/cm^2 s\ sr}$$

in the range $10^{14}\mathrm{eV} < E < 10^{16}\mathrm{eV}$ [44].

In 2012 GRB models got strongly constrained by the results of the IceCube experiment as main source of cosmic rays [45], though the implications can be weakened depending on model assumptions [46]. Still, recent results with neutrinos in the PeV range show promise as a start of the exploration of the neutrino sky [47].

All you really need to know for the moment is that the universe is a lot more complicated than you might think, even if you start from a position of thinking it's pretty damn complicated in the first place.

— Douglas Adams, *The Hitchhiker's Guide to the Galaxy*

2

AIR SHOWERS

Primary high energy cosmic ray particles entering the atmosphere will interact with molecules in the air and produce a number of secondary particles. Due to their high energy these secondary particles have also a high chance to interact with the air themselves. This process, if it is repeated several times, results in a cascade of interactions. With each step the energies of the initial primary particle gets shared, at best, between more and more particles that get produced in each interaction with an air molecule or when an unstable particle decays. This process can result in particles on the ground that can be many kilometers apart and thus the whole phenomenon is known as extensive air shower (EAS) [48]. The exact properties involved and the particles produced depend on both the energy and type of primary particle causing the shower.

Electromagnetic Cascades

Pure electromagnetic cascades are caused by gamma radiation, electrons and possibly positrons. In contrast to hadronic interactions, the situation is comparatively simple. A high energy gamma photon will most likely produce an electron-positron pair in the vicinity of an atomic nucleus. These particles in turn can cause one or more gamma photons to be produced as bremsstrahlung when they in turn interact with a nucleus and get decelerated. The shower development stops rapidly when the average energy loss from radiative effects drops below the scale of other energy losses. The rough phenomenology of the processes can be easily understood in simplified models such as the Heitler model [49] that fixes parameters such as the interaction length and number of produced particles in each interaction (see Figure 5, left). Still, this model does not reflect all the properties accurately, such as relative photon to e+/e- particle numbers.

Hadronic Cascades

In contrast to the case of electromagnetic cascades, hadronic primary interactions produce a more varied class of air showers. An important part of hadronic cascades are mesons, especially pions, that are very commonly produced in hadronic interactions. Charged pions with very high energies commonly re-interact with matter possibly producing more pions in another step. Neutral pions can be produced in a similar number, but unlike charged ones they decay so fast that

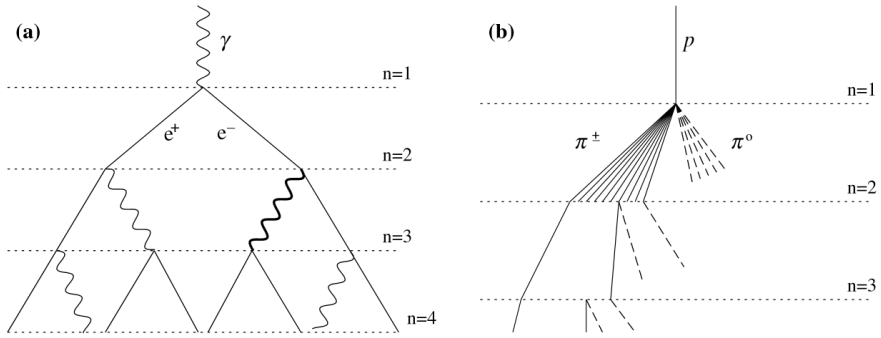

Figure 5: Left (Right): Scheme of the Heitler-(Matthews) model for electromagnetic (hadronic) air shower development. Taken from [50].

re-interaction is extremely suppressed. The dominant decay of a π^0 is into two photons (or otherwise electromagnetic) and it can cause an electromagnetic sub-shower [50]:

$$\pi^0 \to 2\gamma \ (98.823\%) \ [51]$$
$$\pi^0 \to e^+ + e^- + \gamma \ (1.174\%)$$

The probability for charged pions to decay into muons and neutrinos

$$\pi^\pm \to \mu^\pm \bar{\nu}_\mu \ (99.9877\%)$$

gets bigger compared to the probability to interact with a nucleus in the atmosphere the lower their energy E_π is. In the lower energy limit nearly all pions will decay. Since the pion and muon mass is similar the daughter muon will carry most of its primary pion energy at the point of decay [3]:

As can be seen the atmospheric muon and neutrino spectrum are closely related.

$$\langle E_\mu \rangle = 0.79 \cdot E_\pi$$
$$\langle E_\nu \rangle = 0.21 \cdot E_\pi$$

The kind of particle spectrum expected at the ground is further modified by the probability of muons to decay and their energy losses traveling through the atmosphere. This produces a low energy cut-off for muons on the ground while also producing additional neutrinos [3].

The energy loss of a muon traversing the atmosphere is typically $\mathcal{O}(2\text{GeV})$ [3].

Going higher in energy (above a few GeV) where the importance of muon decay starts to diminish fast, the muon spectrum starts to mimic the primary spectrum. This is the case until at around 100 GeV where the probability of pions to interact with air starts to become dominant (compare Figure 6). While pions that interact with the air can still produce more daughter pions that might eventually decay, these will always have much lower energy than the original pion and thus, together with the sharply falling flux of cosmic rays, have only a small contribution to the overall muon spectrum. The probability

to interact with the air rather than to decay rises with energy and thus the spectrum becomes progressively steeper. This asymptotically reaches a situation where the interaction cross section becomes independent of the energy [3]. This can be thought of as a case where the particles and nucleons can basically be viewed as *hard targets*, any time where they geometrically hit, they will also interact.

One can easily see that within a certain time frame the probability to decay decreases with $1/E$ due to time dilation but the number of possible target particles stays the same ($v_{muon} \approx c$). Thus, due to the nearly constant cross section, the probability to interact stays the same. In this limit, the situation also directly leads to an inverse scaling of the muon flux with energy. For a primary cosmic ray spectral index λ, the muon spectral index so becomes $\lambda - 1$.

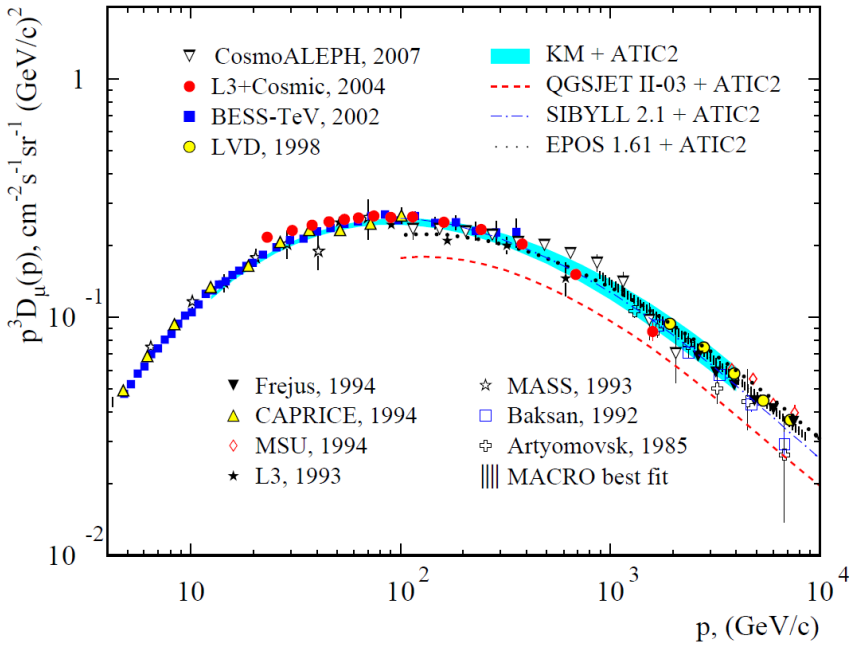

Figure 6: Spectrum of (vertical) atmospheric muons at ground level. Taken from [52].

The competition between interaction and decay leads to an additional angular dependence. For not too inclined air showers (zenith angle $\lesssim 60°$) the Earth's curvature does not yet play a role and it can be described as flat.

A useful , if not fully correct, toy model of the atmosphere's density ρ in a height h from the ground is the barometric formula

$$\rho(h) = \rho_0 \cdot \exp(-h/h_0) \; . \tag{1}$$

More realistic models of the atmosphere also have to take additional effects, such as chemical composition and heat transport, into account. In general seasonal variations in atmospheric parameters play a role that can not be neglected for air shower physics.

The probability distribution P of cosmic ray particles interacting in the atmosphere at different distances $l = h/\cos(\theta)$ from the ground and an incident zenith angle θ is governed only by its cross section with air σ and the particle column density X of air along the path to that point.

For $\theta = 0$ the parameter X is very closely related the pressure at the interaction point.

$$P \propto \exp(-X \cdot \sigma)$$

with

$$X = \int_l^\infty \rho \, dl = \int_l^\infty \rho_0 \cdot \exp(-l \cos(\theta)/h_0) \, dl$$

The cross section σ scales only slowly with energy and is mostly dependent on the mass of the primary particle. A particle with a higher number of nucleons, like iron, will have a much higher chance to interact than a proton [3].

Using Equation 1 the parameter X can be easily translated into a local density at the point of primary interaction

$$\rho = \frac{d}{dl} X = \frac{X \cos\theta}{h_0}$$

with which the probability p_{interact} of the pion to interact scales linearly. At some point in the atmosphere the pion will have to either interact or decay. The fraction of pions ϵ decaying, and thus producing observable muons, follow a probability ratio

$$\epsilon = \frac{p_{\text{decay}}}{p_{\text{interact}} + p_{\text{decay}}} \approx \frac{p_{\text{decay}}}{p_{\text{interact}}} \propto \frac{\frac{1}{E}}{\frac{X \cos(\theta)}{h_0}} = \frac{h_0}{EX \cos(\theta)} \, .$$

This discussion is not only applicable to pions but any particles produced in the air shower. The steeply falling efficiency with energy means that eventually components other than pions, such as kaons, become important for the muon flux. The individual branching ratios for muon decay and muon energy efficiency might differ. For

$$K^\pm \to \mu^\pm \nu_\mu (\bar{\nu}_\mu)$$

the branching ratio is $\sim 63.5\%$ [51]. For the so called *unflavored* component the branching ratio to muons is very low ($< 3.1 \cdot 10^{-4}$ for η particles [53]).

Still the behavior of the components all follow the same behavior from first mimicking the primary spectrum with a uniform angular distribution and then, when interaction with the air becomes slowly dominant, moving to a steeper spectrum with a spectral index roughly changed by one that shows an enhancement at higher zenith angles compared to vertical showers. At the highest energies the atmospheric muon spectrum thus is expected to again be uniform and follow the primary cosmic ray spectrum since heavy hadrons such as those with a charm component will decay almost instantly and never interact with the air. For a comparison of the critical energies ϵ when

ϵ_π	ϵ_K	ϵ_{charm}
151	850	$\sim 5 \cdot 10^7$

Table 1: Critical energies in GeV. Taken from [54].

the individual components (mostly π, K, and c) move from mostly decaying to mostly interacting see Table 1 [54].

Of course in reality each air shower does not have only a single high energy particle in it that might decay to a muon but a produces a number of suitable parent particles. This can be taken care of by either analytically solving the cascade equations governing the shower [55] or with the help of Monte Carlo methods such as utilized in computer codes for air shower simulation like CORSIKA [56].

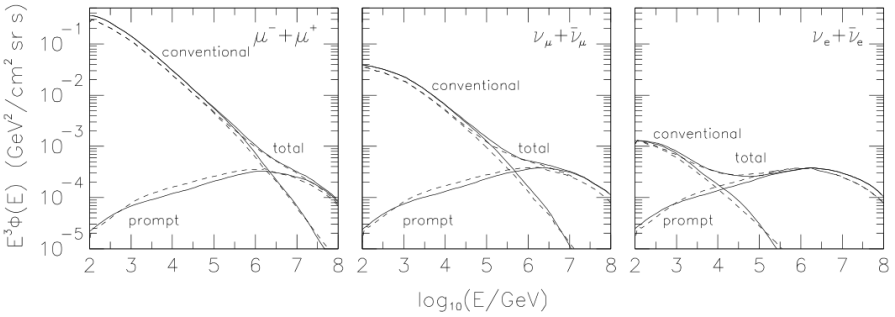

Figure 7: Contributions to the muon and neutrino flux for the main components divided in conventional (pion/kaon-like) and prompt (charm-like) flux. Taken from [55].

Atmospheric Neutrinos

Muon neutrinos are often, but not always, produced in the same air shower interactions that also produce muons and so their energy and angular dependence at the ground is very similar. Unlike muons, however, they can penetrate hundreds of kilometers of rock and more because their cross section with matter is so low. This means that they can also be produced in the atmosphere on the other side of the Earth, traverse it, and then interact near the detector to come from *below*. Oscillation effects may cause the flavour of the neutrino to be possibly not conserved after traversing the respective distance for low energy neutrinos [57]. Above 100 GeV this effect this effect starts to be extremely low for atmospheric neutrinos. For neutrinos coming from outside the solar system the path lengths are so long that one expects a 1:1:1 flavour ratio at the Earth, no matter what was initially produced at their source.

At roughly 50-100 TeV or more the neutrino cross section finally starts to get high enough for there to be significant absorption (or

scattering with significant energy loss) and the Earth starts to act as a shield even for neutrinos [58]. So in the typical energy range for a detector such as IceCube (discussed in Chapter 5) one expects the ν_μ to ν_e ratio to be comfortably above 1 for the lower energy case and then eventually reaching 1 once an astrophysical neutrino source becomes dominant at high energies. Theoretically this is also the first time ν_τ contribution plays any significant role since they are usually not produced in standard atmospheric cosmic ray interactions.

Nothing travels faster than the speed of light with the possible exception of bad news, which obeys its own special laws.

— Douglas Adams, *The Hitchhiker's Guide to the Galaxy*

3 RELATIVISTIC CHARGED PARTICLES IN MATTER

For (astro-)particle experiments the main goal of a measurement usually is both particle identification and measurement of the kinematics. Energy and direction as well as cross sections or, more directly, rates of certain particle interactions are related to the fundamental physics questions being asked. For all these specific tasks one needs to first understand the basic interactions the primary cosmic ray particles, and often their daughters and further secondary particles, will have in matter and how to exploit them for reconstruction. For a large astroparticle experiment the atmosphere and the natural medium that is instrumented is part of the detector. Particle behavior in these very media is usually tied to the prime detection principle. The *actual* detector electronics then measure the photons produced in said media. The following sections will give a brief overview of the most important particle interactions in matter and phenomena that are important for large neutrino telescopes.

For a Cherenkov telescope the medium is usually water or ice.

3.1 CHERENKOV RADIATION

A particle passing through a dielectric medium can cause coherent light emission if its velocity exceeds the phase velocity of light in the respective material [59]. In case of a charged particle it can polarize the atoms in the medium directly. The polarization and subsequent return to equilibrium results in the emission of photons. Unlike the phenomenon called scintillation (or radio-luminescence), where there is an additional step of excitation and de-excitation of an atom or molecule before the emission of a photon, this is basically instantaneous and as such coherent. This so called *Cherenkov radiation* is not directly restricted to any specific wavelength of emitted light and its intensity generally rises when going from radio to shorter wavelengths until it reaches its maximum. For water as surrounding medium this maximum is in the ultraviolet range. However when going to X-ray frequencies the refractive index of materials generally drops below one and thus Cherenkov radiation is no longer possible without violating relativity.

Note that scintillation and radio-luminescence are conceptually the same thing, even though the typical lifetime of an excited state can be quite different.

Light emission for Cherenkov radiation is non-uniform. It's properties can be visualized by simple Huygens construction of the wavefronts (see Figure 8). The direction of light emission follows a fixed angle θ that only depends on the ratio of the speed of the charged particle $v_{\text{particle}} = c\beta$ and the phase speed of light $v_{\text{phase}} = c/n$:

$$\cos\theta = \frac{v_{\text{phase}}}{v_{\text{particle}}} = \frac{1}{n\beta} .$$

Similar phenomena can also be achieved not only by the primary relativistic particle itself but by secondary charged particles it produces along its way. Any disruption of the electromagnetic field due to a non isotropic charge distribution and return to a equilibrium results in light emission.The coherency of this emission depends on the wavelength of the light. Even a non charged ultra high energy neutrino can produce coherent radiation in the microwave and radio range when passing through materials such as ice or lunar regolith [60]. This effect was postulated by Gurgen Askaryan in 1962 [61].

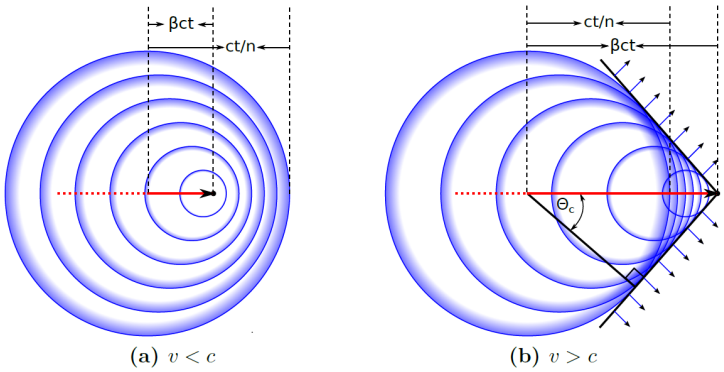

(a) $v < c$ (b) $v > c$

Figure 8: Huygens construction of a Cherenkov cone. Taken from [62].

In practice both the light yield and the characteristic arrival direction of the light can be used to detect relativistic particles.

3.2 ENERGY LOSSES IN MATTER

When fast charged particles pass through matter they mostly lose energy in single collisions that can lead to diverse effects such as ionization, atomic (or collective) excitation, or even production of new particles in very high energy collisions. While certain processes can also lead to larger variances, most energy losses are small and thus the energy loss a particle suffers along a (density weighted) distance x or *stopping power* $\langle -dE/dx \rangle$ in a medium is a very useful property.

3.2.1 *The Muon Case*

The stopping power of charged particles that are heavier than electrons (such as muons, protons, alpha particles) are usually described by the well known Bethe formula [63]. This is often done with various low and high energy corrections taking into account effects of the atomic shell structure of the material or the density dependent shielding effects of the electrical field far from the particle path at higher

energies. The stopping power can be parameterized and split into two main contributions to the energy loss. One term $a(E)$ that dominates the intermediate energy range where ionization plays the biggest role and another for the high energy part where radiative losses that all roughly scale with the energy E become important. In total one gets

$$\left\langle -\frac{dE}{dx} \right\rangle = a(E) + b(E)E$$

with the parameter b being the sum of the contributions from bremsstrahlung, direct pair production, and photonuclear interactions:

$$b = b_{brems} + b_{pair} + b_{nucl} \, .$$

The total energy dependence of the stopping power for the case of muons can be seen in Figure 9. The exact energy loss depends on the structure and mass of the particle in question. For the case of the energy losses being close to the minimum of their respective stopping function the behavior of different particles is extremely similar and particles showing such energy losses are often grouped together as minimum ionizing particles (MIPs). They are all but indistinguishable by most detectors. A useful parametrization [64] of the ionization loss is

$$a(\beta\gamma) \simeq 0.08 \frac{\text{MeV}\,\text{cm}^2}{\text{gr}} (17 + 2\ln\beta\gamma) \, .$$

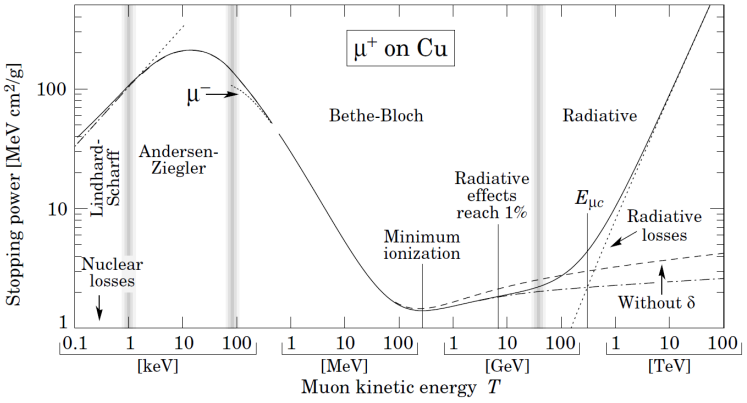

Figure 9: Energy dependent stopping power for muons. Taken from [65].

3.2.2 *Very Heavy Charged Particles*

As will be discussed in Chapter 6, new physics models often introduce heavy new particles. When it comes to direct detection, especially for charged particles, it is important to understand their energy losses in matter. This both determines typical detector responses as well as the attenuation due to energy losses these particles might

suffer as they pass through large amounts of rock or other bulk material. This is especially important to consider when studying particles reaching underground sites - such as in the case of neutrino telescopes. The particle mass itself is often the most important parameter for the magnitude of energy losses and other parameters such as spin often only play sub-dominant roles [66, 64, 67]. Only at high energies (10^8 GeV) weak interactions with matter start to contribute to the energy loss. Here the spin structure of the exotic particles and aspects like left-right hand mixing of exotic particles change the overall picture [64]. This means that many of the exotic versions of leptons introduced later on will show basically the same energy loss behavior for a wide energy range.

CHAMP is a general term used for heavy particles, but here the focus lies on lepton-like ones.

A useful approximation is thus to see a lepton-like CHAMP[1] as a *heavy muon* when doing energy loss calculations [68]. Since ionization losses are rather independent of particle mass the main changes for heavy particles come from changes to the radiative processes which all are subject to a mass suppression for any new particles in the mass range of hundreds of GeV and more. The biggest change is for bremsstrahlung processes which scale inversely with the squared mass of the CHAMPs which makes them negligible for all energy ranges. This also means that unlike for TeV muons where a catastrophic bremsstrahlung loss often can lead to highly variable event-to-event variations for initially similar particles, energy losses for heavy particles can be rather accurately treated as mostly continuous.

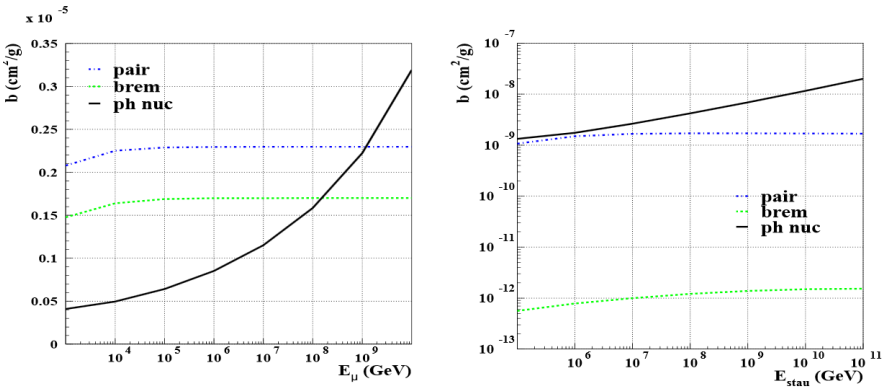

Figure 10: Energy loss contribution for a muon and a heavy, exotic particle (here: $\tilde{\tau}$, a so called *stau*). Taken from [64].

As can be seen in Figure 10, direct pair production and photonuclear losses are roughly suppressed by a factor $m_\mu/m_{\tilde{l}}$ for a particle with mass $m_{\tilde{l}}$ compared to a several orders of magnitude lighter muon with mass m_μ [68]. Taking this rough scaling into account and

1 CHArged Massive Particle

comparing the typical range of muons and particles like this in rock in a continuous approximation one gets

$$\left\langle -\frac{dE}{dx} \right\rangle \approx -\frac{dE}{dx} \approx a_\mu + \frac{m_\mu}{m_{\tilde{l}}} b_\mu E$$

and thus roughly $\mathcal{O}(1000\,\mathrm{km})$ for the range in standard rock ($\rho \approx 2.5 \mathrm{g/cm}^3$). This is in the same order of magnitude as the radius of the Earth.

For a moment, nothing happened.
Then, after a second or so, nothing continued to happen.

— Douglas Adams, *The Hitchhiker's Guide to the Galaxy*

4 NEUTRINO ASTRONOMY

As seen in the previous chapters, one of the open questions of astrophysics is the origin of cosmic rays at the highest energies. Candidates are extremely energetic cosmic environments, such as Active Galactic Nuclei, Gamma Ray Bursts, and radio lobes of FR II galaxies [69]. Tracing the sources of CRs over galactic or cosmic distances is difficult. Protons, the main component of CRs, with energies below 10^{19} eV are deflected by galactic magnetic fields and lose all directional information. At higher energies they travel in straight lines but the flux is suppressed due to interactions with photons from the cosmic microwave background (see Chapter 1). When cosmic rays are accelerated, a fraction of the particles will interact with the ambient matter present in the source. As discussed before, this astrophysical beam dump results in the production of pions, which decay into high energy photons and neutrinos.

Since both do not possess charge, they are unaffected by magnetic fields and point straight back to their source. High energy photons may, however, interact with the cosmic microwave background via pair production. Hence, the probability to observe high energy photons decreases with distance to the source. Neutrinos, on the other hand, need to have much higher energies for such interactions to matter in a significant degree and they only play a major role at the highest energies. Neutrinos are thus an ideal candidate to probe this open question.

4.1 NEUTRINO TELESCOPES

Not long after the neutrino was observed in 1956 [70] there were speculations on its role in astronomy due to its unique properties. Like a photon it has no electric charge and thus can not be deflected by magnetic fields. Unlike gamma rays, which can also be produced by cosmic ray electrons, neutrinos are an unambiguous sign of hadronic interactions in a source.

Neutrinos have an extremely small rest mass [71] and only only interact weakly with matter. As such it eventually became clear that for both the observation of neutrinos from potential cosmic ray accelerators like AGNs or GRBs [72] and the equally interesting neutrinos produced by interaction of cosmic rays at the highest energies with the microwave background radiation both would require a detector with a size in the range of a cubic kilometer [73] (compare Chapter 1).

One gets < 0.23 eV for the summed neutrino mass [71].

DUMAND[1] [74] was the first project that developed the basic design and technologies still employed by current neutrino telescopes. Water is used as a medium for a Cherenkov detector made up by photomultiplier modules that can observe the light produced by relativistic charged particles from neutrino interactions near the detector. After the cancellation of the project due to technical issues there have been multiple smaller sized efforts to build a detector. One such project was realized in lake Baikal by a collaboration of the same name (BAIKAL) [75], other projects chose the Mediterranean sea as a location. The latter is the site explored by the ANTARES[2], NESTOR,[3] and NEMO[4] collaborations [76, 77, 78].

A slightly different kind of detector that uses ice instead of liquid water as a medium is the IceCube detector and its precursor experiment AMANDA[5] at the South Pole in the Antarctica. IceCube is the first experiment to reach the previously mentioned scale of 1km^3 and already has produced promising results for cosmogenic neutrinos [47]. It is also the detector that - in its 79 string configuration - provides the data this work is based on.

The word cosmogenic *here is used only in the sense of originating outside the Earth's atmosphere.*

4.2 DETECTOR SIGNATURES OF STANDARD MODEL ν-INTERACTIONS

When neutrinos interact in a suitable medium for their secondary particles to produce Cherenkov radiation there can be several different event topologies observed in a km^3-sized underground detector. These each correlate with the initial neutrino flavor, its energy, as well as the arrival direction.

In a *neutral current* interaction (Figure 11, *top*) the neutrino transfers parts of its energy to a nuclear target which then causes a hadronic cascade. In a *charged current* interaction (Figure 11, *bottom*) the neutrino not only produces such a cascade (Figure 13a) but also a lepton that carries a large part of its initial energy.

If the lepton is an electron or tau, it - or it decay products - form another, this time electromagnetic, cascade. In practice those two kinds of particle cascades are hard, if not impossible, to distinguish and the electromagnetic cascade of an electron will overlap with the hadronic cascade of its production. But for taus at PeV energies it is possible that they travel far enough before their decay for the two cascades to be geometrically separated (Figure 13c). Since tau decay also produces a tau neutrino the situation is more complicated. A ν_τ signature in the detector is *not necessarily* the first reaction at the Earth a cosmogenic ν_τ has been part of [79]. The original ν_τ could also have

Still, there are some properties that do differ between both kinds of cascades.

This is know as a so called double bang *signature.*

1 Deep Underwater Muon And Neutrino Detector
2 Astronomy with a Neutrino Telescope and Abyss environmental RESearch
3 Neutrino Extended Submarine Telescope with Oceanographic Research Project
4 Neutrino Ettore Majorana Observatory
5 Antarctic Muon and Neutrino Detector Array

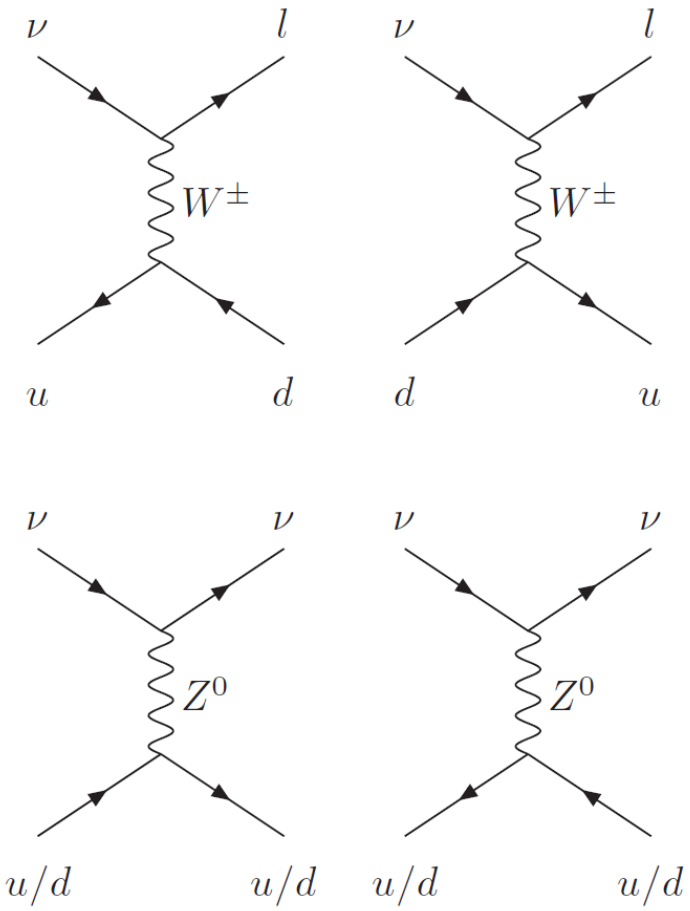

Figure 11: Feynman diagrams for neutrino-quark interactions. *Top*: charged current interactions. *Bottom*: neutral current interactions.

reacted, possibly repeatedly, on the way to the detector. Each time the tau produces another - but lower energy - ν_τ neutrino.

For an electron the light of the overlapping total cascade seen in the detector is an excellent energy estimator, since the whole neutrino energy is contained within the constituting particles. But just like for an observed tau, the energy deposited in the detector for a simple cascade event is technically only a lower limit of the primary neutrino energy. The cause could always be a neutral current reaction.

If a muon gets produced in the primary neutrino interaction the situation changes significantly from the electron case. As seen in Chapter 3 muons can have such a high range (multiple kilometers, up to tens of kilometers for extremely high energy muons [80]) that for high energy neutrinos it is likely that the initial interaction happens outside the detector volume. This means that both the energy in the hadronic cascade and the energy losses of the muon on the way to the detector can not be observed and one only sees a particle *track* inside the detector (Figure 13b). On the other hand the direction of the muon track is mostly aligned with the primary neutrino and much

The misalignment of the initial neutrino and the daughter muon sets a natural limit on the angular resolution of any neutrino telescope.

easier to reconstruct than the almost point-like cascade signatures. It should be noted that cascades still have a non isotropic light emission with a preference for the Cherenkov angle that can be used for a rough directional reconstruction [81].

Neutrinos producing long muon tracks can also be seen if their interaction vertex lies *outside* the detector. This directly leads to a much higher effective detector area - or rather volume (see Figure 12). On the other hand one has to deal with the contamination of muons produced in cosmic ray air showers. These have a much higher rate than any neutrino signal and have to be distinguished using their direction (the bulk of the Earth acts as shield for cosmic ray air showers from below) or their energy (the atmospheric muon energy spectrum is much steeper than expected for neutrinos produced outside the Earth's atmosphere). Alternatively one can only select for tracks *starting inside* the detector, but one then loses the increase in effective volume.

Using the Earth as a shield and only observing *up-going* particles eventually becomes less useful at higher energies when it becomes opaque to neutrinos (especially ν_e and ν_μ get absorbed directly). As mentioned before the situation for ν_τ is slightly different, but even here energy information gets lost on the way [82].

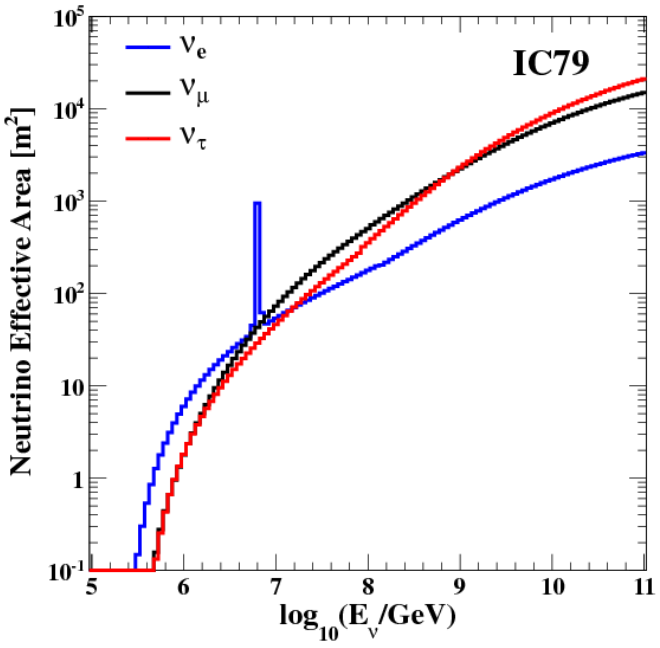

Figure 12: Increase in effective detector area for long (i.e. high energy) tracks (ν_μ,ν_τ) compared to electron neutrino cascades for the IceCube neutrino observatory. The peak in the distribution for ν_e is caused by the so called *Glashow resonance* [83]. Taken from [84].

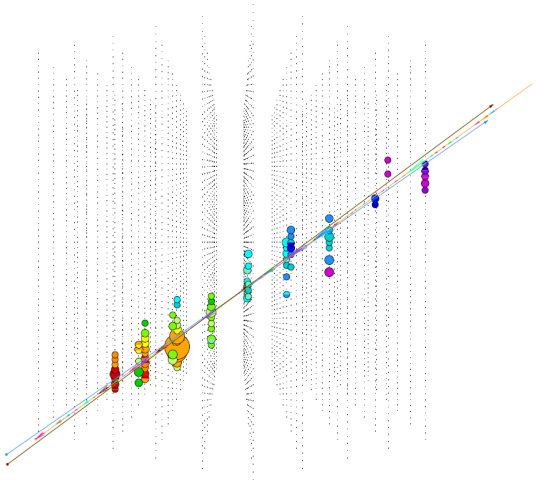

(a) Electromagnetic *cascade* produced in an ν_e interaction.

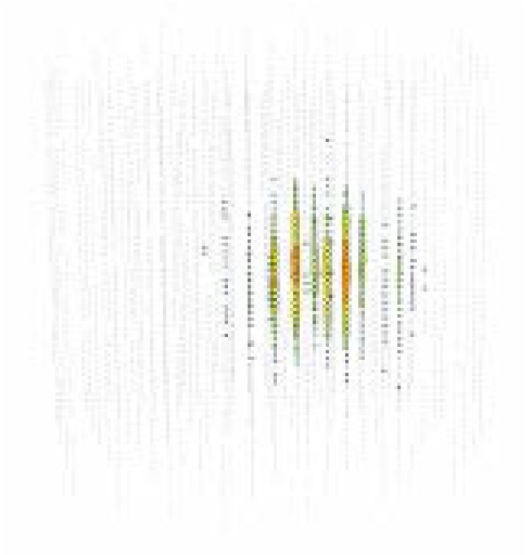

(b) Muon *track* as produced by a ν_μ interaction.

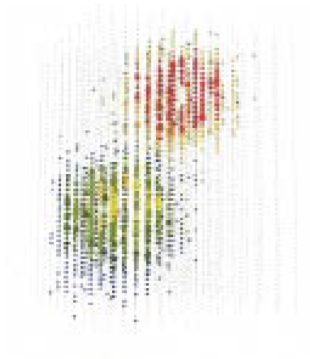

(c) Possible *double bang* signature caused by a ν_τ interaction and subsequent τ decay.

Figure 13: Neutrino event topologies in a neutrino telescope. Taken from [85].

It is a mistake to think you can solve any major problems just with potatoes.

— Douglas Adams, *Life, the Universe and Everything*

5 THE ICECUBE EXPERIMENT

IceCube is a cubic kilometer scale high-energy neutrino observatory near the Amundsen-Scott South Pole Station in Antarctica [86]. Its main goal is to map the high-energy neutrino sky, which is expected to include both a diffuse neutrino flux and point sources [87, 88]. The (initial) detector design allows observation and study of neutrinos with energies from several 100 GeV up to the EeV range.

The Amundsen-Scott station itself is located at the geographic South Pole.

The scientific motivation for such a detector and its detection principle have already been discussed in Chapter 4. This chapter deals with the structural design, data acquisition, calibration, as well as aspects of basic event selection and filtering.

5.1 THE ICECUBE DETECTOR

The detector is composed of two parts. A km^2 surface detector for general cosmic ray observations (and veto capabilities) called IceTop and the km^3 IceCube array inside the ice that is a neutrino and muon detector.

5.1.1 *The Surface Detector*

IceTop is made up by pairs of 81 polyethylene ice-filled tanks that are equipped with two digital optical modules (DOMs) each. The DOMs are run at different gains to increase the dynamic range of any signal in the tank. They are located on a roughly hexagonal grid (see Figure 14). The tank array is designed to detect air showers in the energy range around 100 TeV - 1 EeV [89].

5.1.2 *The IceCube Array*

The neutrino and muon detector array is an instrumented volume 1450-2450 m within the ice and so is also sometimes called the *InIce* array. It is made up of 86 long cables called *strings*, 78 of which house 60 optical modules for light detector. The strings were deployed using a hot-water drilling technique that created the *holes* the strings were originally deployed in. The water refreezes after deployment of such a string so recovery is impossible. The strings follow the IceTop configuration on top and they have an inter-string spacing of roughly 125 m. The optical modules are approximately 17 m apart. The other 8 strings are deployed to form a denser instrumented sub-detector called *DeepCore* [91] inside the main configuration. The optical mod-

The surrounding normal *detector strings are sometimes also counted as part of* DeepCore.

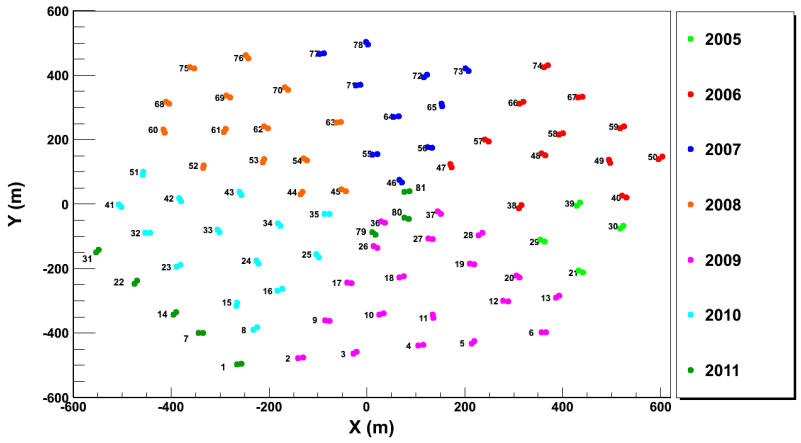

Figure 14: IceTop tanks deployed in different years of the IceCube construction. Taken from [90].

ules on these strings have a higher efficiency. Six of them are deployed with an inter-string spacing of 72 m in a regular pattern. The vertical spacing of 50 of these DOMs on each string is 7 m. Additionally 10 DOMs on each string are deployed with a spacing of 10 m each. They form a *veto layer* above the main DeepCore volume for background rejection. Additionally to this basic layout two strings that were initially planned to be on the edge of the basic hexagonal pattern of the IceCube detector have been converted to be part of the DeepCore volume and were deployed within this layout [86]. This leads to the smallest inter-string spacing within the DeepCore volume of 42 m. Overall the design has been done in order to lower the detection threshold of the IceCube detector to neutrinos with energies as low as 10 GeV. For this the main volume has been deployed in very clear ice to avoid efficiency losses from scattering and absorption. The ice properties on site will be discussed in the next section.

5.2 ICE PROPERTIES AT THE ICECUBE SITE

Years with increased volcanic activity will have higher than average amounts of dust that is introduced via the atmosphere in their respective ice layers.

The ice around IceCube formed over a time of around 100,000 years in many, mostly horizontal, layers. Each thin layer formed originally due to snowfall and their optical properties strongly depend on the impurities like dust that were introduced at the year they formed. They are thus linked strongly to the changing short and long term dust levels in the atmosphere.

These impurities strongly affect the optical properties in the ice. Ice layers with high concentrations of dust will results in lowered optical transmission coefficients due to both increased scattering and absorption [92].

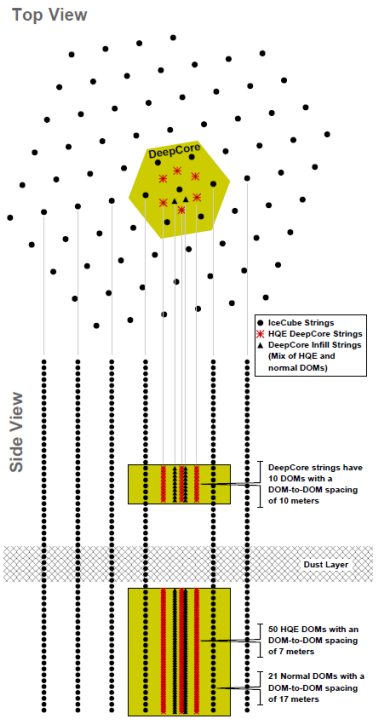

Figure 15: Schematic layout of the IceCube array and the DeepCore sub-detector. Taken from [91].

Scattering is frequency dependent and usually parameterized via an effective scattering length λ_{eff} that depends on the mean scattering angle θ per scattering event

Light scattering is in the forward region is the most important part contributing to detector effects.

$$\lambda_{\text{eff}} = \frac{\lambda_{\text{scat.}}}{1 - \langle \cos\theta \rangle}$$

The measurement of absorption and scattering is done in two ways. IceCube DOMs are fitted with *flasher* LEDs [93]. The photon arrival time distributions of data produced with this artificial signal can be used to measure both absorption and scattering length - albeit with limited resolution in depth.

The other method was done via so called *dust logger* devices deployed into the still unfrozen holes directly after the hot-water-drilling procedure [94]. This method has a much better depth resolution ($\approx$ 2 mm) and can also be used to can again access about additional information such as the tilt of individual layers. While scattering in the ice on top of the detector is dominated by air bubbles, the situation in the vicinity of the actual instrumented area of IceCube is different. All air bubbles in this depth will have been converted to air hydrates due to the high pressure. Instead, dust has the dominating effect on ice properties. Generally the ice gets clearer towards the bottom of the detector apart from a large *dust layer* structure at around 2100 m depth that shows very high absorption [95, 92].

The ice column near the DOMs that has refrozen is often called hole ice. *It shows a much higher amount of scattering ($\lambda_{scat.} \approx 50\ cm$) compared to its surroundings.*

It should also be noted that the drilling and deployment of the DOMs of course also leads to different ice properties around each string of the detector. All these factors and measurements are put into the different ice models used for IceCube simulation and reconstruction [93]. One such ice model can be seen in Figure 16.

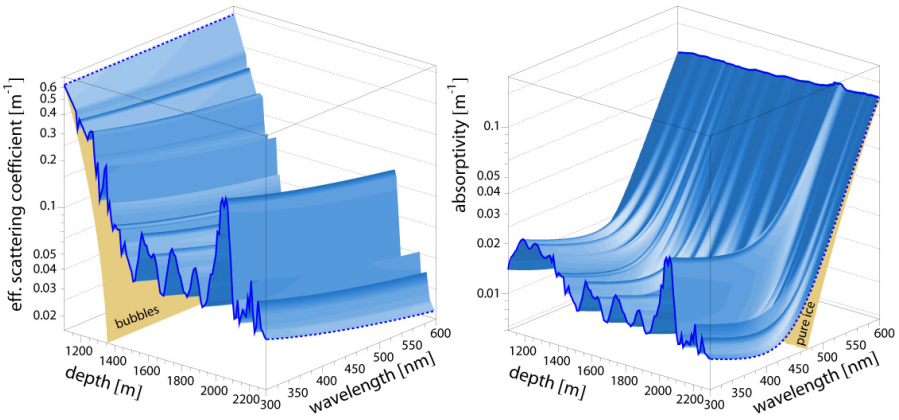

Figure 16: Scattering and absorption at the IceCube site, taken from [92]. Clearly visible are the high amount of effective scattering closer to the surface and the prominent *dust layer* structure deep within the clear ice.

5.3 ICECUBE HARDWARE AND SOFTWARE

In order to comprehend how IceCube data-taking is done one has to understand both the hardware and the software components that go into reconstructing a basic event. This includes all parts from basic layout of the optical modules up to software-filtering of events before they get sent to the north.

5.3.1 *Digital Optical Modules*

Radioactive decays in this glass sphere actually contribute significantly to the dark noise in the PMT.

The sphere-shaped pressure vessel that makes up the outer part of the IceCube DOMs are made up by 0.5 inch thick borosilicate glass spheres that transmit light with a wavelength of around 350 nm or more [96].

It is connected to a photo multiplier tube (PMT) inside using a optical coupling gel. The sphere also houses additional electronics on the DOM main board and light-emitting diodes for calibration purposes. A schematic drawing of a DOM and its components can be seen in Figure 17.

The DOMs use Hamamatsu R7081-02 PMTs and are sensitive to photons with a wavelength of 300-650 nm [98]. While these PMTs have a peak quantum efficiency at around 25%, the PMTs used in the DeepCore DOMs of the detector reach a higher efficiency of up

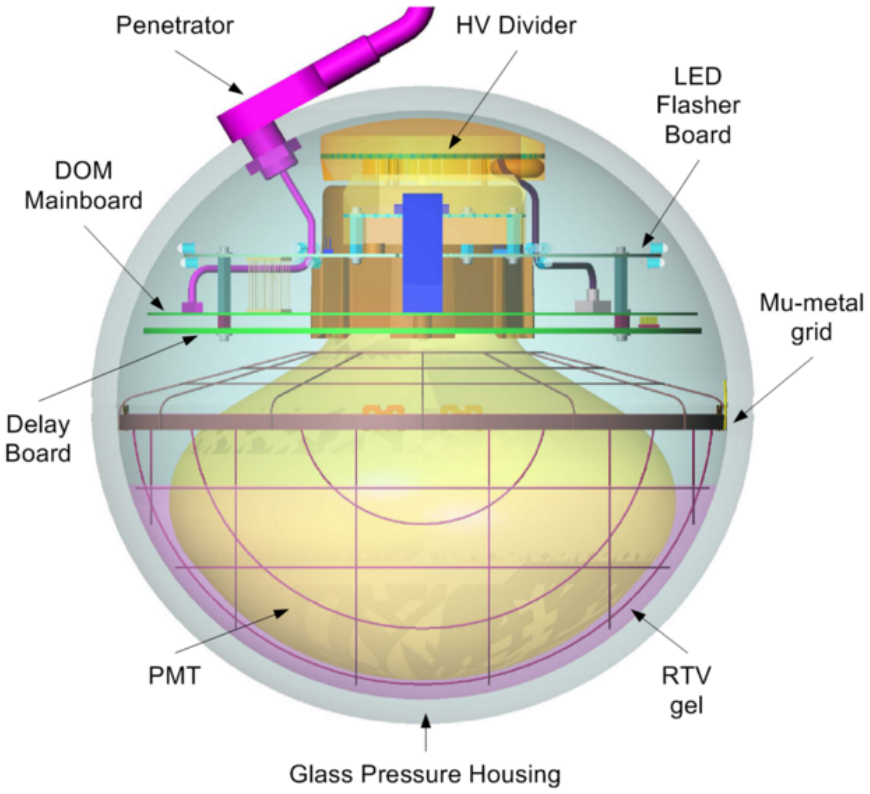

Figure 17: Schematic drawing of an IceCube digital optical module and its components. For details see [97].

to 33%. The PMTs are encased in a mu-metal shield that reduces the effect of the Earth's magnetic field. The range of the signal response in the ice is much smaller than for air showers near the surface. And so, unlike the PMTs in the IceTop detector that are operated at two different gains of 10^5 and $5 \cdot 10^6$ [89], the PMTs in the DOMs deep in the ice are operated at a single gain of 10^7.

The PMTs have their cathode on ground level and the anodes are coupled to the main board via a toroidal transformer designed for a frequency from 8 kHz up to more than 100 MHz. The decay time for a square wave signal is > 15 µs for most DOMs. Only the first 1200 DOMs built have a 1.5 µs decay time and so can show some droop. This, however, is later removed in a digital filter [96].

A muon crossing the whole *detector takes a few* µs *at best (1 km/c ≈ 3.3* µs*).*

Figure 18 shows the single photo electron response of a PMT measured via illumination by a low intensity LED. The low charge structure as well as the secondary structures for delayed hit times are thought to be caused by backscattering at the first dynode in the PMT. The main peak of the charge spectrum has a resolution of approximately 30% if described as a Gaussian. The main peak for the time structure has a resolution of 2 ns but around 4% of the hits come more than 25 ns later with some structure at a delay of up to 130 ns [98].

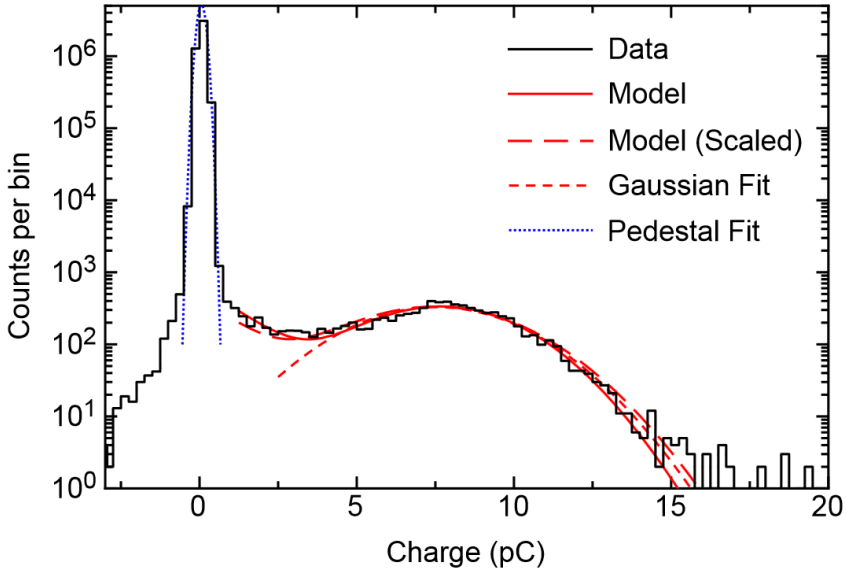

Figure 18: Single photo electron response of an IceCube PMT with a clearly visible two peak structure. Taken from [98].

5.3.2 *Data Aquisition Electronics*

The main components of the data acquisition (DAQ) system within the DOMs are responsible for the waveform digitization [97, 99]. These are the Analog Transient Waveform Digitizer (ATWD) and the *fast* analog-to-digital converter (fADC). Digitization is triggered by a voltage threshold corresponding to 1/4 photon electrons.

The 40-MHz-system clock is used to give an event a time stamp with a corresponding 25 ns resolution when the DOM has *launched*. A better time resolution can later be achieved by analyzing the whole waveform. An ATWD chip has multiple input channels connected to the PMT signal. Three of which have different gains (ration 16:2:1/4) to get an increased dynamic range. If any of the AWTD channels overflows the next lowest gain is used in digitization. Each DOM has two ATWD chips to reduce the dead-time, if one is currently digitizing the other one is *live*. Since the trigger signal formation in the FPGA[1] takes some time, the PMT signal is sent to the ATWD through a 75 ns delay line. A schematic drawing of the electronics can be seen in Figure 19.

The fADC system uses a continuously running 40 MSPS[2] digitizer chip and is preceded by a shaping amplifier (180 ns shaping time). All in all this setup covers a time window of 6.4 µs, records 256 fADC samples, and has a photon arrival time resolution of better than 5 ns. The fADC gives valuable information for late arriving photons but

1 Field Programmable Gate Array
2 Mega Samples Per Second

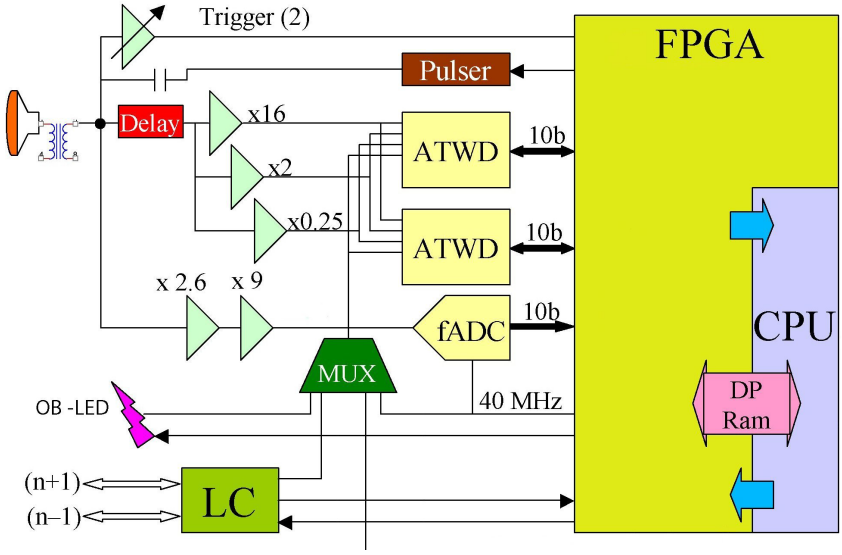

Figure 19: Scheme of the main board electronics. Taken from [97].

since it suffers from a limited dynamic range it already overflows for medium sized signals [97].

IceCube has two basic modes for sending DOM data to the surface. In *hard local coincidence* (HLC) mode the full waveforms are being transmitted if there has been any signal in one of neighboring or next-to-neighboring DOMs on the same string within a 1 µs time window, else the data is discarded. Most HLC hits are caused by muons and only very rarely by pure noise. Full *launch* waveform information is made up of all the required ATWD waveforms, the time stamp, and then additionally local coincidence signals from adjacent DOMs. The different waveform information is illustrated in Figure 20.

IceCube has run exclusively in HLC mode until early 2009.

The other mode is the so called *soft local coincidence* (SLC) mode [86]. Here no outside signal in the coincidence time window is required but instead of the whole waveform information only the three highest of the first 16 fADC samples and the timing of the highest sample is being sent to act as a coarse charge stamp. Unlike HLC data, SLC hits are clearly noise dominated and their rate is at the DOM dark rate (typically around 350 Hz). SLC hits have to be cleaned later on in software to get physics event information. Still, once an physics event has been identified, SLC hits retain additional physics information and can be used to improve reconstructions.

The name soft local coincidence is slightly misleading since there is no real coincidence requirement at all.

5.3.3 *DOM Calibrations*

There are multiple calibration techniques used in IceCube that ensure stable time and amplitude information of observed light pulses. A low intensity on-board LED is used for intensity calibration of single photo electrons. The charge distribution of these measurements is

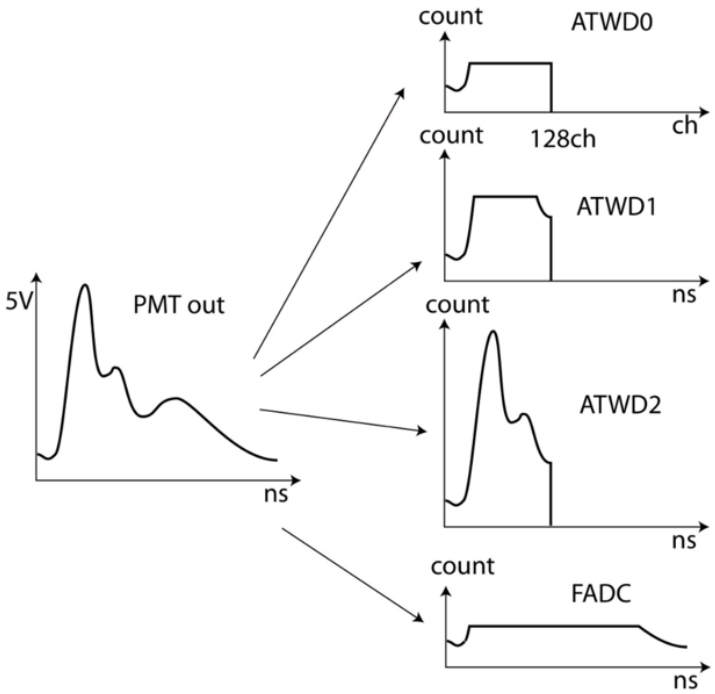

Figure 20: Sketch of the waveform information of the different channels. Once one channel with high gain saturates, lower gain channels become important in order to not lose information on the initial waveform. Taken from [100].

sent to the surface where the single photo-electron (SPE) peak is fitted. When the LED is pulsed the delay time between the pulse current and to the PMT response in the ATWD is measured to determine the total PMT transit time along with the pulse delay in the delay line. The second timing calibration is done by sending a pulse to the surface of the detector along the cable and an identical signal back. By comparing both signals the transmission time can be measured to a precision of around 3 ns [96]. The technique is called reciprocal active pulsing calibration (RAPcal).

Note that even though the RAPcal timing precision is quite good the actual pulses get widened to $\approx 1\,\mu s$ *along the* ≈ 3.5 *km of cable.*

Additional calibration can also be done with 337 nm nitrogen lasers mimicking Cherenkov light emission via a reflective cone acting as standard candles [101] or directly via cosmic ray muons. The latter are especially useful for accurately determining the horizontal positions of individual DOMs since this is hard to do with string-to-string measurements. Even though the overall wavelength of the standard candles is a bit shorter than typical Cherenkov radiation they also can be used to get a reasonable *hardware* simulation of particle cascades up to the PeV range.

The two standard candles *are deployed on string 40 (between DOM 22 and 23) and string 55 (between DOM 42 and 43).*

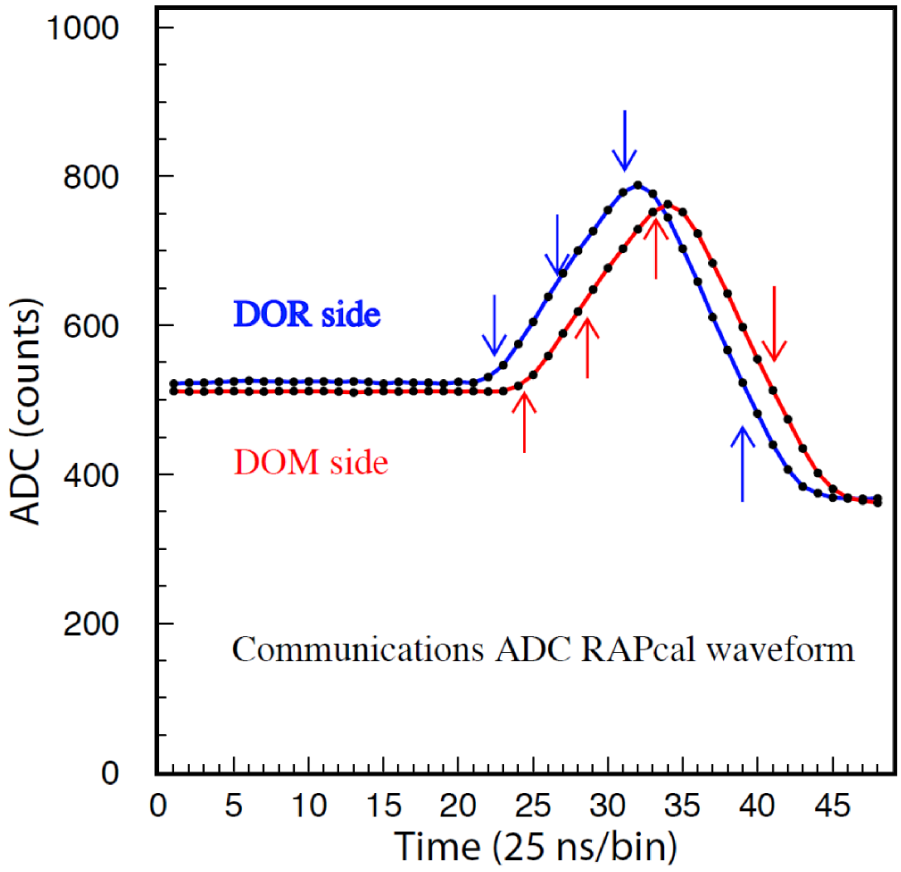

Figure 21: A RAPcal waveform including several time marks (arrows). The relative shift of the waveform is used to determine the offset between the DOM clock and the DOR master clock. Taken from [97].

5.3.4 *Surface Hardware and Software*

The IceCube Laboratory (ICL) near the center of the IceTop detector houses the surface DAQ hardware. The ICL is also the location where data is later either saved on tape or sent north via satellite after pre-processing and filtering. Each string of DOMs is connected to an industrial PC called *DOM-Hub* that receives data via multiple DOM readout (DOR) cards controlling, receiving data and powering up to 8 DOMs each. Each DOM-Hub hosts *String Hub* software components where the time calibration of the DOM time stamps is being done with the help of GPS receiver acting as *master clock*. The calibrated information is cached and partially sent to the trigger handlers that work on multi-string conditions. The full information gets read out if one of the trigger conditions is met [86].

The two main trigger conditions are 8 HLC hits firing within 5 µs or 5 ouf of 7 adjacent DOMs on a string with hits in a time window of 1.5 µs. This is known as the *simple majority* (or sometimes *simple multiplicity*) *trigger* - or simply SMT8. There exist additional triggers that

Even though there are ideas to build triggers with topological hit information on all hits to improve sensitivity on low energy horizontal events [102], the trigger building is currently being done exclusively with HLC data.

use topological information. Examples are triggers requiring multiple hits on a single string (*string/cluster-trigger* [103]) or triggers for more specialized cases. This can be triggers for very slow track-like events (for magnetic monopole searches) or triggers for the DeepCore low energy extension. When a trigger occurs all data within a ± 10 µs window is saved. If multiple windows overlap they are merged and saved in the same event (Figure 22).

The situation for IceTop is slightly different when it comes to the coincidence criterion that initiates data taking. If one tank has a signal in the high gain channel and the nearby tank has a low gain signal the pair of tanks is considered to be hit [89]. If either 3 or 8 pairs of tanks are hit the event is triggered. Only a pre-scaled subset of the 3 hit condition is used for trigger building.

The pairs of two nearby IceTop tanks are usually called stations.

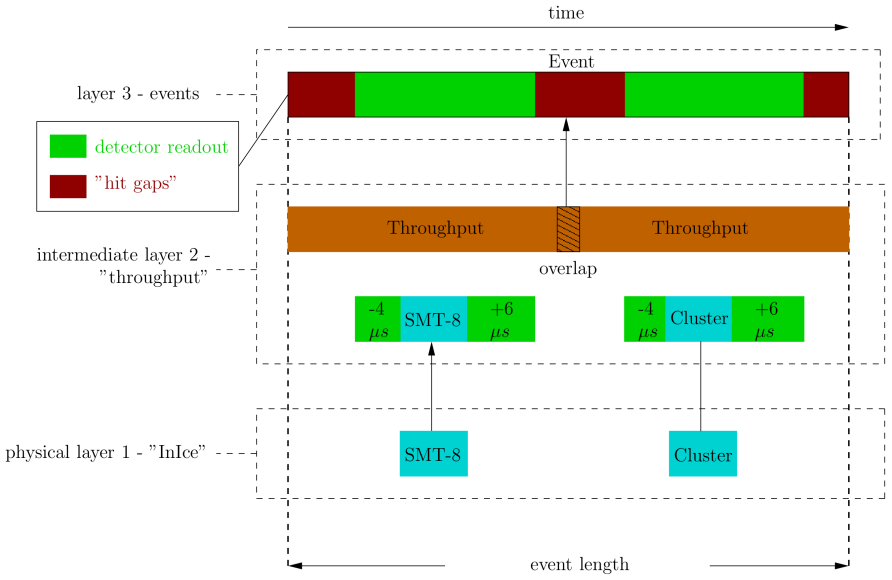

Figure 22: Individual triggers get combined into a global trigger with a shared readout. Note that the time-frame for combining triggers is longer than the individual readout windows in older detector configurations. Current detector configurations realize so called *hit-spooling* [104] and sub-threshold hits are no longer lost. Scheme taken from [105].

5.4 DATA FILTERING

While all triggered events are saved on tape there is only limited bandwidth for immediate transmission to the Northern Hemisphere via satellite. Thus a significant amount of reconstruction and on-line filtering is being done directly at site for a pre-selection of possibly interesting physics data to be sent.

The IceCube location at the South Pole is inaccessible during the austral summer. The drilling and construction thus lead to a yearly

rhythm of data-taking with varying but fixed numbers of strings for each of these *seasons*. IC79 stands for the data-taking in the season 2009-2010.

Earlier seasons had configurations with 59, 40, 22, 9, and 1 string(s).

Since 2011 and the *season* with the first full 86-string detector configuration the waveforms for some data streams are also sent in a *lossy compression* in so called *superDST* format. This allows higher data rates to be sent to the North for processing. Some notable filters are the *EHE*[3] [106] filter that selects high energy events by deposited charge in the detector, the *minimum bias* filter that selects a random and thus unbiased sample of all events at a reduced rate, the *cascade filter* [107] that is based on events with a (ν_e) cascade-like structure, filters for events coming from positions correlated with the sun, the moon, or the galactic center, and the *low up filter* [108] that selects for low energy up-going events with a veto on events that trigger the top ($\approx$ 5 DOMs layer) part of the detector. The DeepCore sub-detector also has separate, specialized filters [109].

The pre-scale *rate of the minimum bias filter in IC79 is 1:100.*

A very important filter is the *muon filter* stream. As will be discussed later on, it forms the filter stream the analysis in this work is based around. It is a filter that mainly aims to select for muons produced in muon neutrino interactions near the detector. As the filter with the highest event rate in IceCube it also serves well as an all-purpose filter for track-like events. It selects for well reconstructed track-like events with an emphasis on up-going events. Selection criteria are the deposited charge, the reconstructed zenith angle and a variable that is closely tied to the the (reduced logarithmic) likelihood of a track reconstruction (see Section 5.4.1). Details on the exact muon filter criteria can be found in [110]. It is of note that the filter explicitly selects for events with a high likelihood as single tracks using a variable that is almost identical to one selected *against* in the cut strategy employed in this work (compare Chapter 8).

5.4.1 *Basic Event Reconstructions*

The physics filters discussed before are already based on information gained by a basic event reconstruction scheme used for all events. The typical reconstruction chain is done in several steps, the first of which is to calibrate the measured PMT waveforms of individual DOMs and to extract the absolute times and voltages from the recorded ATWD and fADC information. This can then be used to determine individual photon arrival times used in event reconstruction [111, 112, 113]. A *first guess* method for the event topology in the detector is done by treating the photon arrival times as if caused by a plane wave.

This kind of simple reconstruction has the name linefit.

This already gives some idea of the basic physics properties of the event, a speed close to the speed of light speaks for a muon-track-like event and a slower reconstructed speed could be caused by a

3 Extremely High Energy

particle cascade. In a second step this is then used to *seed* a likelihood hypothesis [114]. The probability of photons radiated from a track with known properties such as position and direction are described by functions fit with the help of M.C. simulations [115].

They can then be used to perform a maximum likelihood fit to the hypothesis in question - for example an infinite muon track. This gives both an improved angular resolution and a handle to veto events with a low likelihood or non-converging fit hypotheses. For details on the maximum likelihood reconstruction and the parameters used see [114].

5.4.2 *Further Event Reconstructions*

Events at this stage of reconstructions often form the basis of individual physics analyses. Further reconstruction and filtering of events no longer follows a fixed processing and filtering chain but usually depends on the event topology of the physics signal at hand. An analysis looking for electron neutrinos for instance will usually require an especially detailed reconstruction of a single particle cascade. This cascade should be fully contained within the detector to ensure the best energy resolution and to remove the danger of a single (ν_e-like) cascade being confused with a sudden bremsstrahlung loss of a high energy muon. Physics analyses with muons on the other hand will be more focused on reconstructions that look for track-like events and might even try and remove the effects of highly variable cascades along the track when it comes to energy reconstruction [116].

There are some common reconstructions in place for particular analyses looking for similar signals (cascades, muons, low and high energy events) but many searches for exotic events - like double tracks in this work - have no common processing scheme with other analyses. The simple fit (linefit) and likelihood fits already used for the muon-filter also are an important part for further reconstruction in this work as will be discussed in more detail in Chapter 8.

There is a theory which states that if ever anyone discovers exactly what the Universe is for and why it is here, it will instantly disappear and be replaced by something even more bizarre and inexplicable. There is another theory which states that this has already happened.

— Douglas Adams, *The Restaurant at the End of the Universe*

6 PHYSICS BEYOND THE STANDARD MODELL

Now that the Higgs boson has been measured in 2012 at the CMS [117] and ATLAS [118] detectors at the LHC experiment the whole particle content of the Standard Model has been observed. Many of its properties have been measured and tested, time and again, by experimentalists since its inception - often to an astonishing degree. Yet there are some problems that lead to the conclusion that it can not be a fundamental description of nature. For once, gravity is not yet part of the model and its coupling strength is far too weak to be directly measured at colliders. It is thought that only near the Planck scale ($\approx 10^{19}$ GeV) it will become as strong as the other three forces of nature [119].

Still we have reasons to believe gravity might be mediated by a massless spin-2 boson - a graviton.

This view is guided by the idea that all forces of nature will unify at a very high energy scale, just like the unification of the electric and weak force into a single electroweak force which has been accomplished within the Standard Model. This proposition is supported by the extrapolation of the gauge couplings to higher energies. They all meet at a common point at approximately 10^{16} GeV as illustrated in Figure 23. This match is, however, not exact if one assumes that there is no new particle content between the electroweak scale ($\approx$ 100 GeV) and this point. In supersymmetric extensions to the Standard Model this match becomes much more exact, so it is commonly used within so called GUT (Grand Unified Theory) models [120, 121] that treat this unification.

Another question that remains is why the mass of the Higgs boson and the electroweak scale is so much lighter than this energy scale of unification for the other forces. It requires quantum corrections that many physicists regard as *unnatural*. This is known as the hierarchy problem [122].

Yet another challenge to the Standard Model comes from cosmology. Already in 1933 Fritz Zwicky's observation of the Coma galaxy cluster suggested that its mass was not mainly concentrated in the hot X-Ray gas but made up by a yet unknown form of matter he dubbed *dunkle Materie* - dark matter [123]. Structure formation in the universe together with constraints from the formation of early elements, the so called *Big Bang Nucleosynthesis*, suggest that this dark matter is not baryonic in nature but made up by particles that interact only gravitationally and, at most, weakly. Neutrinos are the closest match within the Standard Model but they are too light to make up a significant amount of this new form of matter. This makes them highly relativis-

Usage of the viral theorem *suggests a much different velocity dispersion of the constituting galaxies than observed in galaxy clusters if only taking into account the directly observable matter dominated by X-Ray gas.*

tic and unable to realize the structure formation of as we observe it in the universe [124].

Also, in recent years an acceleration of the expansion of the universe has been measured [125]. Before, it was thought that the speed of expansion of the universe should decrease with time. An additional energy density in the universe - in the simplest form as a parameter known as the cosmological constant - is needed to explain this behavior. This is now know as *dark energy* [126]. Even less is known about the properties and origins of dark energy than about dark matter but it is another sign that the Standard Model can not be a complete description of the physics in the universe at large.

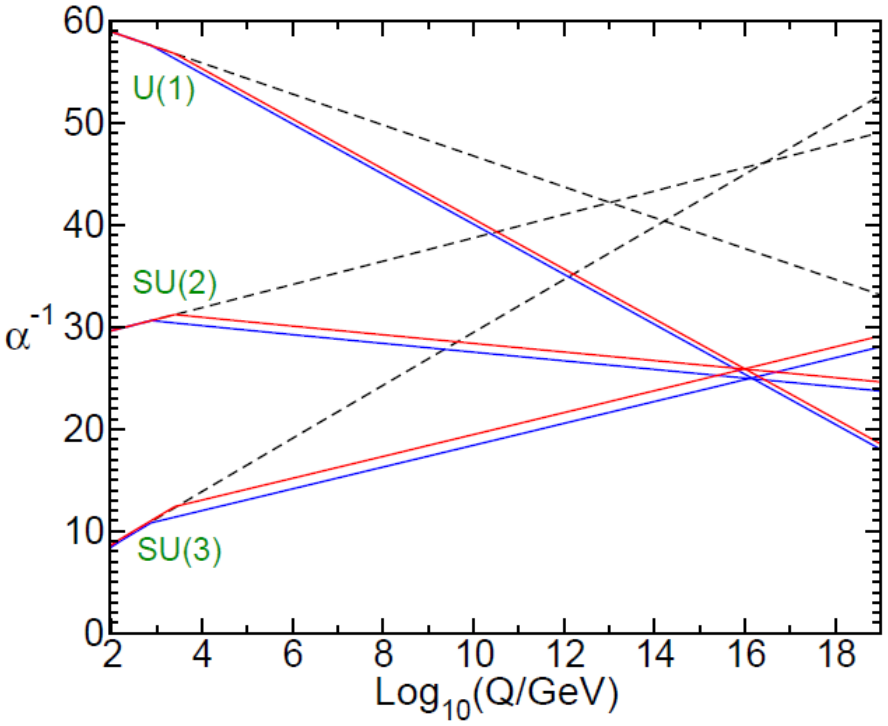

Figure 23: Two loop renormalization evolution of the inverse gauge-couplings α^{-1}. For the SM (dashed line) the couplings only meet approximately. The match is much more precise in supersymmetric models - to be exact MSSM models (solid lines). Illustration taken from [122].

6.1 SUPERSYMMETRY

Supersymmetry (SUSY) is a spacetime symmetry between bosons and fermions. It introduces (one or more) symmetry operators Q that can relate a bosonic to a fermionic state:

$$Q\,|\mathrm{boson}\rangle = |\mathrm{fermion}\rangle$$

$$Q\,|\mathrm{fermion}\rangle = |\mathrm{boson}\rangle$$

Like mentioned before, many supersymmetric models make the unification of forces easier when looking for models with a good match of the running coupling constants. This makes it likely that such a model is a better candidate for physics up to the GUT scale than the SM. This, however, was not the original motivation of supersymmetry. This motivation goes back to electro-weak symmetry breaking and the introduction of the Higgs particle.

Quantum corrections to a scalar particle

Note that the Higgs particle takes up a special place in the Standard Model since not only is it responsible to effectively give other fermions and bosons a mass term due to coupling to the Higgs field but it is also the only scalar (spin 0) particle. While all particle masses are subject to loop corrections, the loop corrections for a scalar particle are special because they do not depend on its bare mass.

Looking at the Yukawa interaction term of the Higgs H with a fermion and coupling λ_f one gets:

$$L = -\lambda_f \bar{\Psi} H \Psi$$

Given that the Higgs mechanism is used to explain masses, λ_f is proportional to the mass of the fermion in question. So for a fermion loop correction (like Figure 24) up to some cutoff scale Λ_{cutoff} for the Higgs mass-squared m_H^2 results in a term

$$\Delta m_H^2 = -\frac{|\lambda_f|^2}{8\pi^2}[\Lambda_{\text{cutoff}}^2 + ...] \tag{2}$$

that is quadratically divergent [122]. Given that λ_f never is a very large number and one wants to have a theory that works at least roughly till the coupling constants meet for *Grand Unification*, it follows that $\Lambda_{\text{cutoff}} \approx \mathcal{O}(10^{16}\ \text{GeV})$. The situation for spin-1 bosons is quite similar though corrections for a boson loop are different in sign due to their different statistics (i.e. fermionic single loop corrections are negative, bosonic positive). While the bare Higgs mass is still a free parameter, without any fine tuning one would expect to have a Higgs squared-mass that is around $(10^{16}\ \text{GeV})^2 = 10^{32}\ \text{GeV}^2$ *or higher* from the corrections alone.

The real Higgs mass on the other hand is close to the weak scale, many orders of magnitude lower in energy. This has been known by electroweak precision measurements for the Vacuum expectation value of the Higgs field

$$\langle H \rangle = (G_F\sqrt{2})^{-1/2} = 246\ \text{GeV}$$

and recently the measurements of the mass of the Higgs boson itself of ≈ 125 GeV [51, 127]. Since mass for fundamental SM particles mostly comes from coupling to the Higgs fields, the particles with the

highest mass - top quarks - will make the largest contributions, but the problem exists for the lighter SM particles as well to some degree. This whole situation is known as a *fine tuning problem* of the Standard Model.

There exist other fine tuning problem in the SM, *such as the apparent weakness of gravity (hierarchy problem) and the lack of CP violation in the strong force.*

There are two different ways to solve this problem in extensions to the Standard Model. One way is to come to the conclusion that the predicted cut-off scale Λ_{cutoff} is much lower than predicted and rather close to the TeV-scale. A way to do this will be discussed in Section 6.2. The other way is to assume an internal symmetry like SUSY that protects the quantum corrections from getting too high. Especially if one compares Equation 2 with the corrections another scalar particle $\tilde{t}$ (compare Figure 24, bottom) would give to the Higgs mass

$$\Delta m_H^2 = \frac{\lambda_s}{16\pi^2}[\Lambda_{\text{cutoff}} + ...] \,, \tag{3}$$

it is easy to notice that *two* such scalars would mostly cancel out the spin 1/2 fermion corrections under the assumption that

$$|\lambda_f| = \lambda_s] \,.$$

The situation for spin 1 vector bosons is quite similar and a spin 1/2 fermionic partner can again solve the problem [122]. In both cases the change in spin is 1/2. Both relations can be achieved by introducing supersymmetry. Note that while there are a multitude of both spin 1/2 particles and spin 1 gauge bosons in the SM, none of them seem to belong to the same group of a supersymmetry transformation. So the price to pay for SUSY is *at least* the doubling of the known particle content.

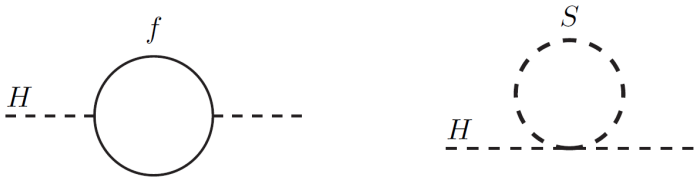

Figure 24: Feynman diagrams of a one loop Higgs-particle mass corrections for a fermion f (left) and a scalar particle S (right). Taken from [122].

6.1.1 *Broken Supersymmetry and the MSSM*

Perfect supersymmetry predicts at among other things bosonic (fermionic) states for each of the known Standard Model fermions (bosons) with the same charge structure (electric charge, weak hypercharge, etc.) - including the same mass.

When looking at how SUSY might might be realized in our world one can see quickly that it must be broken. Else it would not only

spoil the results of known particle physics experiments but also basic atomic structure as we know it. A simple reason for this is that bosons are not suffering from the Pauli exclusion principle (see Figure 25).

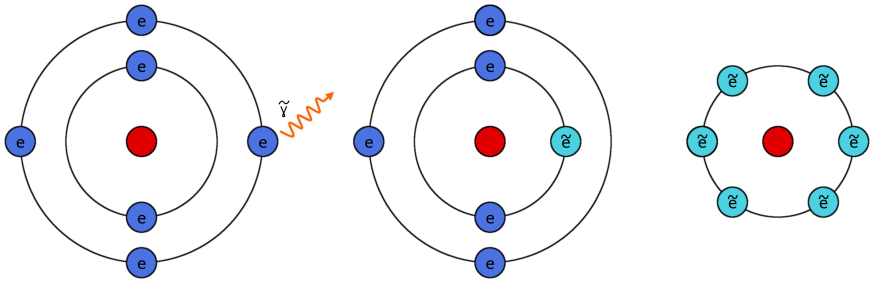

Figure 25: In perfect SUSY models an ordinary excited atom can emit a massless *photoino* $\tilde{\gamma}$ instead of a photon, turning an electron e into a selectron $\tilde{e}$. This can happen multiple times just like normal photon interactions and turn all electrons into selectrons. But the selectrons can, being bosonic, subsequently also *all* fall to the ground state. This means such an atom now has atomic interactions that are all made up by many particles in the ground state and no longer dominated by a few valence electrons, changing chemistry as we know it completely.

So it is known that supersymmetry must be broken in a way that increases the new particle masses. In particular, the mass has to be high enough to not have been observed already but at the same time can not be too high. If one wants to retain the original motivation and canceling of quantum corrections talked about earlier one can not, however, make these masses too large either. The higher the mass splitting of SM particles to SUSY partners is, the more of the original fine tuning problem will resurface. While there is no definite way to define what amount of *fine tuning* of parameters is acceptable and *natural*, it is usually thought that a mass splitting of more than $\mathcal{O}(1\text{ TeV})$ is problematic [128]. Thus supersymmetry should be in range of colliders like the LHC and cosmic ray experiments [129].

As will be seen later on, these searches can be complementary.

Even with resulting masses in the TeV range, any good SUSY model has also to (at least approximately) preserve the parameters and normal degrees of freedom of the Standard Model fields as well as all its properties (gauge invariances, etc.) while still staying supersymmetric. In practice the latter requirement is ensured when model building by promoting Standard Model fields to so called *superfields* and using the mathematical concept of (anti-commuting) *Grassmann numbers* as additional *spacial* coordinates.

Anticommuting numbers, also means eventually nilpotent. Any power series expansion will break off, in a way making such a variable seem to live in a small *extra dimension.*

Breaking supersymmetry without additional restrictions almost always leads to new effects like proton decay (as depicted in Figure 26) as well as generally high amounts of (unobserved) flavor changing neutral currents (FCNC) [130].

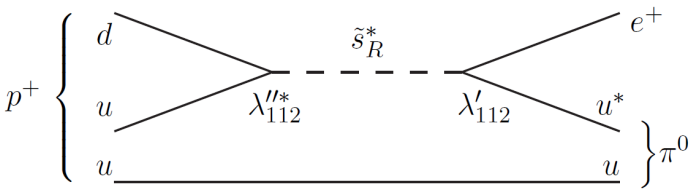

Figure 26: Randomly breaking supersymmetry without restrictions generally leads to proton decay. Depicted here is an example of a Feynman-diagram showing decay by exchange of a strange squark. Taken from [122].

Many of these requirements are difficult to realize in dynamically broken SUSY models so Howard Georgi and Savas Dimopoulos proposed what they called a *softly broken* supersymmetry [131]. The SUSY breaking terms (like gaugino and scalar field mass terms) do not spoil ultraviolet behavior but they explicitly break the supersymmetry. If one assumes that supersymmetry is a real symmetry and only spontaneously broken at some very high energy scale, a soft supersymmetry breaking Lagrangian term L_{soft} makes a SUSY theory a low energy effective theory.

MSSM

The simplest, phenomenologically viable supersymmetric extension of the Standard Model is known as the Minimal Supersymmetric Standard Model (MSSM) [132, 133]. It introduces a new particle for each of the known SM particles, referred to as *superpartner(s)* of the respective particle (see Figure 27). Per convention the superpartners $\tilde{p}$ are indicated by a $\sim$ over the respective Standard Model particle p.

Some people call all SM superpartners sparticles *even though they are not necessarily scalar.*

To be more exact, each of the two *chiral* components f of the massive SM fermions has a *scalar* superpartner $\tilde{f}$. They are called *scalar fermions* or short *sfermions*. This scheme gets repeated for individual particles, i.e. a *right-handed* tau τ_R becomes a *right-handed* stau $\tilde{\tau}_R$. Note that as scalar particles the handedness is of course not defined and only serves as a naming convention. The two states of *different handedness* have the same quantum numbers and can freely mix to form two mass eigenstates, usually named $\tilde{f}_1$ and $\tilde{f}_2$ unless they can be closely related to their apparent handedness.

For technical reasons the MSSM also introduces an additional Higgs field [135, 122]. One of the Higgs-doublets (H_u) couples to *up-type* particles and one (H_d) to down type particles and (s)leptons. This doubles the degrees of freedom in the Higgs sector while still only needing 3 degrees of freedom to give each of the spin 1 bosons (Z^0,$W^\pm$) mass. So this additional field leads to five instead of one free Higgs particles after weak symmetry breaking. The most conventional Higgs particles are the two scalars (h^0, H^0). The other ones

Field Content of the MSSM					
Super-Multiplets	Boson Fields	Fermionic Partners	SU(3)	SU(2)	U(1)
gluon/gluino	g	$\widetilde{g}$	8	1	0
gauge/	$W^{\pm}$, W^0	$\widetilde{W}^{\pm}$, $\widetilde{W}^0$	1	3	0
gaugino	B	$\widetilde{B}$	1	1	0
slepton/	$(\widetilde{\nu}, \widetilde{e^-})_L$	$(\nu, e^-)_L$	1	2	-1
lepton	$\widetilde{e}^-_R$	e^-_R	1	1	-2
squark/	$(\widetilde{u}_L, \widetilde{d}_L)$	$(u, d)_L$	3	2	1/3
quark	$\widetilde{u}_R$	u_R	3	1	4/3
	$\widetilde{d}_R$	d_R	3	1	$-2/3$
Higgs/	$(H^0_d\,,\, H^-_d)$	$(\widetilde{H}^0_d, \widetilde{H}^-_d)$	1	2	-1
higgsino	$(H^+_u\,,\, H^0_u)$	$(\widetilde{H}^+_u, \widetilde{H}^0_u)$	1	2	1

Figure 27: Scheme of the MSSM field content. Taken from [134].

are A^0, a pseudo-scalar, and the charged $H^{\pm}$. The lighter of the two scalars is named h^0 by convention and it is often very SM-Higgs-like.

The addtional Higgs particles as well as the SM vector bosons all have spin 1/2 leptonic superpartners. They are named by adding *-ino* at the end of the particle name. The *charged* Higgsinos and the gauge bosinos as well as the *neutral* Higgsinos and gauge bosinos can each mix. This leads to 2 charged and 4 neutral mass eigenstates, called *charginos* $\tilde{\chi}^{\pm}_{1,2}$ and *neutralinos* $\tilde{\chi}^0_{1,2,3,4}$ respectively. By convention the index increases with mass of the eigenstates. Note that while charginos are Dirac fermions the neutralinos are Majorana fermions and can annihilate with themselves.

Sometimes neutralinos and charginos are also written as $\tilde{N}^0_i$ and $\tilde{C}^{\pm}_i$

R-*Parity*

A prime property of the MSSM that makes sure not to spoil known precision observations is its (multiplicative) R-parity invariance. R is defined as

$$R = (-1)^{3(B-L)+2S}$$

where B, L and S are the baryon number, lepton number and spin of a particle [122]. R-parity has important phenomenological consequences. Standard Model particles always have *even* R-parity whereas their superpartners always have *odd* R-parity. So starting with any number of SM particles R-odd superpartners can only be produced in pairs. When a R-odd particle decays there will always be an odd number (and thus *at least one*) of other R-odd particles at produced. The lightest R-odd particle, called LSP (Lightest Supersymmetric Particle), takes a special place must be stable. Heavier particles like the

NLSP (Next-to-Lightest Supersymmetric Particle) can also be stable if their decay into the LSP is not kinematically allowed or meta stable if their decay is suppressed.

In the early universe such particles would have been produced in great numbers during the *Big Bang*. This means that either R-parity is not exactly conserved or the LSP is a *neutral, at best weakly interacting* particle that is hard to observe. The latter could indicate that these particles explain the *dark matter* phenomenon [136].

Extensions of the MSSM

Allowing violation of R-parity is but one of the many possible extensions of the MSSM. Almost any kind of new particles can be included as long as the general structure of the model is kept intact. Commonly explored models are the addition of fermions, like right handed (*sterile*) neutrinos ν_R and their partners $\tilde{\nu}_R$, and models that add bosons like the axion. There also exists models that include extensions in the Higgs sector like the *NMSSM* (Next-to-Minimal Supersymmetric Standard Model [137].

The most common inclusion is a particle that is expected to exist if there is a quantum theory of gravity: its hypothetical gauge boson known as the graviton (G). Theoretical considerations give it a vanishing mass, no charge and - unlike other gauge bosons - a spin of 2 [119]. The particle itself only interacts with gravitational strength and so is virtually impossible to observe but its superpartner, the spin 3/2 *gravitino* ($\tilde{G}$) might be [138].

Simplifications

It is noteworthy that the MSSM adds 105 new parameters to the Standard Model even when preserving R-parity completely [139]. But only a tiny region of the parameter space is interesting to be tested experimentally. The rest still shows meaningful FCNCs and high amounts of CP violation or they have parameters without phenomenological consequences. These considerations have lead to the *phenomenological MSSM* (pMSSM) that is only governed by 19 real parameters while staying model independent by still not considering any specific supersymmetry breaking mechanism [140, 141]. This is still a huge parameter space for SUSY searches and excluding models by sampling can possibly be prone to error. If some phenomenology only shows up because of an exact relation of multiple parameters (maybe due to the SUSY breaking mechanism) it might never show up in a (finite) random sampling of parameters. So, from both the standpoint to reduce the number of parameters further and to possibly increase the relevance of the models, efforts have been made to relate the MSSM parameters to (fewer) high energy parameters, closer to the mechanics of SUSY breaking.

The exact number is different for some other pMSSM models, but stays around 20.

Spontaneous Symmetry Breaking

Before going into details about how spontaneous SUSY breaking at high energies affects the low energy effective theory it is worthy to discuss the general effects of spontaneously breaking supersymmetry. If any continuous symmetry gets spontaneously broken it implies the existence of a *massless* particle that is tied to the generator of said symmetry. Since in most cases the symmetry has no relation to the spin of the particles, the generators of the symmetries are usually scalar particles and are called *Nambu-Goldstone bosons*. Examples where they appear is in the framework of BCS superconductivity and the theory of electroweak symmetry breaking [142, 122]. In the latter they get *eaten* by gauge-bosons as result of the Higgs-Mechanism giving the gauge-bosons an additional polarization state and thus mass. A supersymmetry generator *does* change the spin of a particle by a half-integer and so most carry a corresponding spin *charge* itself. The corresponding Goldstone particle has to be a fermion and called a *goldstino*. In the MSSM the generator(s) change the spin of the particles by $1/2$ and the goldstino is a spin $1/2$ particle with 2 spin states. Corresponding to the Higgs-mechanism this goldstino can be *eaten* by a massless spin $3/2$ fermion - the Gravitino. The gravitino so becomes a *massive* spin $3/2$ fermion with 4 spin states. Unlike the graviton it might also interact non-gravitationally since the two spin $1/2$ states relate to the goldstino modes. As a neutral particle the massive gravitino is an excellent dark matter candidate.

This mechanism is known as the Super-Higgs-mechanism.

Constrained MSSM Models

The concept of Grand Unification of the 3 Standard Model forces and maybe an eventual *Theory of Everything* (ToE) that includes gravity has driven the idea that the SUSY-breaking terms can be simplified on some high-energy scale. The scale could be the Planck scale, the GUT scale or even the scale of some *messenger* field that transmits the actual supersymmetry breaking from some *hidden sector* where it occurs.

A hidden sector consits of particles that are completely neutral with respect to the SM gauge group.

The most basic form of how to transmit SUSY-breaking to the *visible sector* is gravity. It seems to be a sound assumption that any new particles couple to it and thus it is a factor that is always present, even if it might not be the dominant one. Pure *gravity-mediated* supersymmetry breaking results in $m_{\tilde{G}}$ to be at the electroweak breaking scale. The gravitino will only interact with gravitational strength and so be impossible to produce at colliders (though it can be the LSP). A special case of gravity mediated supersymmetry breaking is *anomaly mediated* SUSY breaking where the breaking is communicated through a conformal anomaly [143].

Another possibility is *gauge-mediation* via a messenger particles that take part in gauge interactions or *direct gauge-mediation* where the par-

ticles in the SUSY-breaking sector have SM charges themselves. In these scenarios the gravitino can be in the eV to GeV mass range and will definately be the LSP. The interactions of its ± 1 helicity components will be much stronger and so it might be accessible in colliders [144, 122].

Once one has established the scale of the parameter unification and chosen the numerical value of the constrained parameter space, it is possible to compute the actual consequences for the full amount of low energy MSSM parameters via the renormalization group equations. Models built in this way are known as *constrained* MSSM. Since this renormalization group running has to be done for *each* high energy parameter combination of a model there exist computer codes that facilitate these computations. Examples of commonly used programs are SuSpect [141], SPheno [145] and SOFTSUSY [146].

mSUGRA

One of the most popular such constrained models is the mSUGRA (minimal SUperGRAvity) framework [147, 122]. It has five parameters: A unified scalar mass parameter m_0^2, a unified gaugino mass $m_{1/2}^2$, a trilinear coupling parameter A_0 as well as μ_0 and B_0, Planck scale values for the usual Higgs parameters μ and B. The last parameters $m_{3/2}$ is the gravitino mass. It is independent of all other parameters and does not influence the rest of the particle spectrum. Usually the complex A_0,B_0,μ_0 and $m_{3/2}$ are chosen to be real when model building. Sometimes the mSUGRA model with a small, commonly used parameter transformation for μ_0 and B_0 to $\operatorname{sgn}(\mu_0)$ and the weak scale parameters m_Z and $\tan\beta$ is called CMSSM.

There exist many variation of the mSUGRA model like the NUHM (non-universal Higgs mass) models that divide m_0^2 into separate parameters for the diagonal Higgs scalar squared-mass parameters and the other universal scalar mass.

GMSB

Contrary to the situation in supergravity the universality of the slepton and squark mass parameters is guaranteed in models with gauge-mediation [148, 144].

The most basic model here is called *minimal gauge mediated supersymmetry breaking* (GMSB). It's effective scale Λ is the universal mass scale for low energy phenomenology and the main parameter. The other parameters are the usual Higgs parameters μ and B already mentioned for mSUGRA. The last possible parameter is the particle content in the messenger sector.

Typical Mass Spectra

Unlike for the pMSSM where setting any a-priori probability to the combination of suitable model parameters is highly questionable, the lower amounts of parameters in the constrained models show some common properties in them that maybe can be generalized somewhat more reasonably. Generally the colored particles like gluinos ($\tilde{g}$) and squarks ($\tilde{q}$) are heavier than the ones not taking part in the strong interaction like the neutralinos or sleptons. In most mSUGRA models the lightest neutralino $\tilde{\chi}_0^0$ is the best LSP candidate. In GMSB models where the LSP is almost always the gravitino the lightest slepton, the (mostly) right handed stau $\tilde{\tau}_R$ or the $\tilde{\chi}_0^0$ can be the NLSP.

Other common models are those with stop $\tilde{t}$ LSPs due to heavy mixing in the third generation or $\tilde{\chi}_0^0/\tilde{\tau}_R$ co-NLSP scenarios. For a typical mass spectrum considered in the pre-LHC era compare Figure 28.

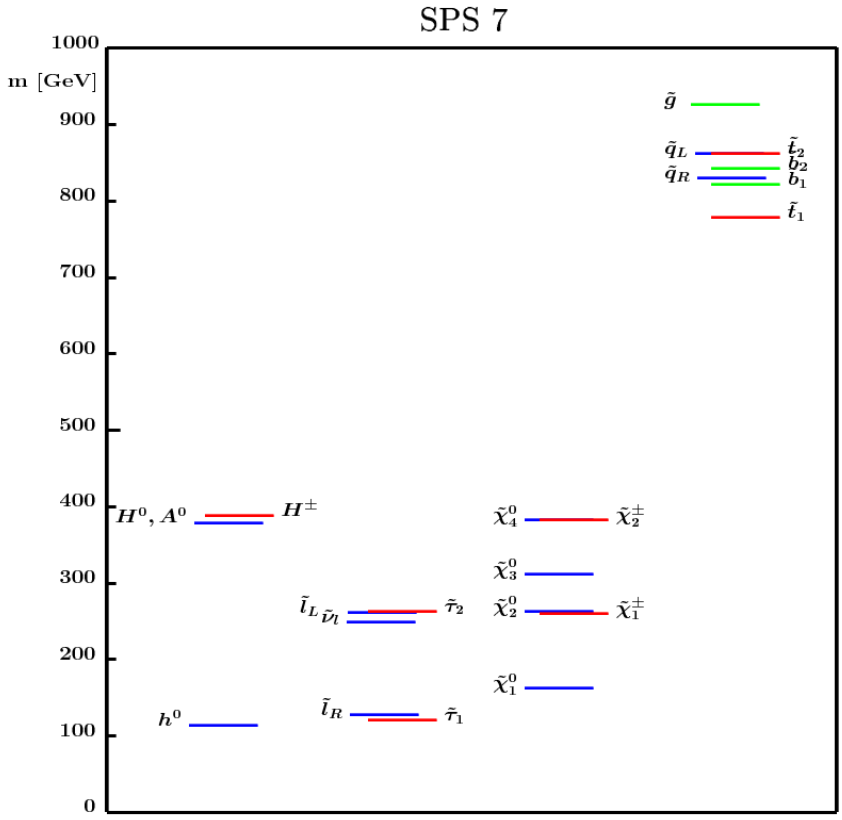

Figure 28: A constrained MSSM mass spectrum (here: GMSB with SPS7 benchmark parameters). Typical LSPs in the constrained MSSM models are gravitinos, staus and neutralinos. Taken from [149].

6.1.2 *SUSY Searches and Detector Phenomenology*

Since supersymmetry introduces such a wide range of new parameters and particles, the exact detector phenomenology is highly model dependent. The most examined collider aspect is the commonly present mass gap between the heavy squarks and gluinos and the lighter uncolored SUSY particles (compare Figure 6.1.1).

In a hadron collider like the LHC the most important SUSY production mechanism should be particles that couple to the strong force unless those are out of reach due to their high mass. From here the heavy particles produced in the primary interaction will cascade down to light and lighter SUSY particles and eventually reach the lightest supersymmetric particles (LSP) or at least the lightest SUSY particle that is detector-stable. Due to an assumed R-parity conservation there will be a SM particle produced at each step. This can lead to a high number of leptons from the multitude of slepton decays since sleptons and neutralinos are usually among the lighter SUSY particles. Also, since the lightest SUSY particle has to be neutral - and thus invisible to any tracker - another very common SUSY signal property is the *missing energy* or - in practice more often - *missing transversal momentum* in the detector (see Figure 29) [150].

This signature might be eroded if all observable SUSY particles are somewhat degenerate in mass. In this case the missing energy can only be seen in special circumstances such as the occurrence of notable initial state radiation [151].

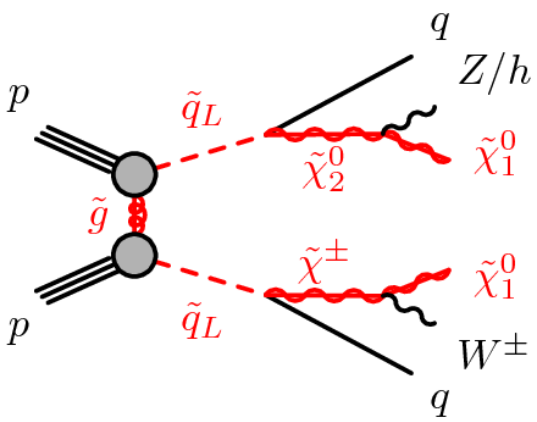

Figure 29: One of many examples for SUSY particle production and a following decay chain. Typical is the production of high energy leptons, jets and missing transversal momentum due to the escape of neutral particles. Taken from [152].

Heavy Metastable Charged Particles

If the lightest detector-stable particle is charged though and long-lived enough to only decay outside a typical detector most of the

time, the *missing energy* signature might be missing in most interactions. Such models and models with similar phenomenology are the main focus later on during this work. Here the search strategies have to use the high mass of the (meta-)stable particle and its effect on the detector. If the mass is high enough compared to its energy, its speed is noticeable slower than muon tracks in the detector which mostly have a speed $\beta \approx 1$. The speed difference to muons can either be determined directly by measuring the time of flight of the heavy particle or by observing the increased ionization energy loss such a particle will have on its way [153]. $\beta = v/c$

Cases like this are often found in GMSB frameworks but they can happen in any scenario where the NLSP is charged and the decay to the LSP is either suppressed due to kinematics or lack of interactions ($\tilde{G}$,$\tilde{\nu}_R$, etc. is LSP).

The livetime of heavy, charged particles is somewhat constrained since they can form bound systems with nuclei and catalyze the synthesis of light elements during the Big Bang nucleosynthesis [154]. Conversely, with the right livetime, they might be able to solve the primordial lithium problem [155]. Especially in bound states the decay of such a particle can cause efficient (photo-)disintegration of light nuclei.

Collider Constraints

The considerations about the Higgs mass quantum corrections at the start of this section have lead many people to believe that supersymmetry would be *just around the corner* and could possibly be observed by experiments at LHC not too long after the start of operations. These hopes were not fulfilled and the two phases the detector ran with roughly half its design center-of-mass energy (7 and 8 TeV) have so far only excluded large parts of the parameter space of constrained models [156]. Most limits on squark and gluino masses of the many diverse searches and varying model dependencies are well above 1 TeV. The Higgs mass also seems higher than can be naturally explained by most of the basic GMSB models without adjustments [157]. The masses of the other particles that do not take part in the strong interaction are less constrained than at a lepton collider probing a similar energy range. At a hadron collider they can still be created in a processes such as Drell-Yan production which have the advantage that they are quite model independent. The current limits for meta-stable charged particles (like $\tilde{\tau}_R$) produced in this way are ≈ 340 GeV [153].

While it is not impossible that the LHC will still find signs of supersymmetry with future runs, these results at least question the *naturalness* of most of the commonly used constrained SUSY models and has lead to the change to more model independent search strategies [158]. It should be noted that among all the SUSY searches at the LHC many

models with long-lived $\tilde{\tau}$ might still not be fully explored in the current searches [159].

6.2 MODELS WITH EXTRA DIMENSIONS

In 1921 Theodor Kaluza published his idea of unifying the field theories of gravitation and electromagnetism into a single one by introducing a 5th space-time dimension [160]. To simplify the equations he introduced the idea that no part of the 5-dimensional metric depends on the new 5th dimension.

The simplification that the metric is independent of the 5th dimension is known as the cylinder condition.

In the wake of the rise of quantum mechanics Oskar Klein later reinterpreted Kaluza's theory in this new setting and explained this additional condition by the assumption that the 5th dimension is small and curled up. The simplest, but still very instructive, way to view such an extra dimension is to view it as a circle of very small size. Any such compact dimension also directly leads to interesting phenomenology when viewed respective to quantization in this new dimension. Klein himself had the notion that this explained the quantization of electrical charge and calculated the size of the dimension according to this view [161].

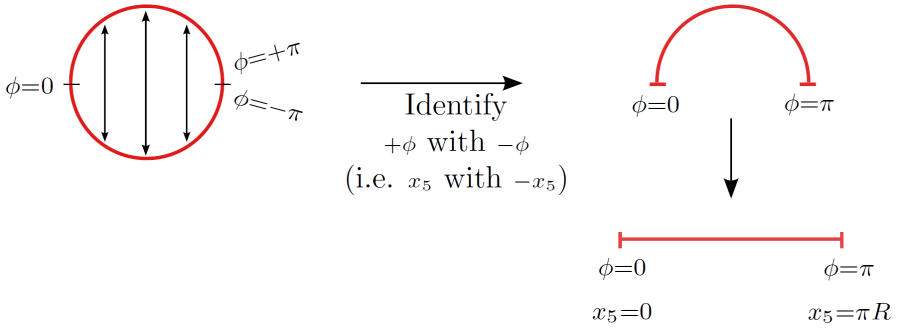

Figure 30: A circle is the simplest way for compactification of an extra dimension (called S^1 in topology). Imposing chirality defining parity breaks the translation symmetry in the 5th dimension. The extra dimension now can be topologically identified as a line. Illustration taken from [162].

It should be noted that there are multiple ways to create compact extra dimensions. For example, if the underlying theory for the field has to be invariant under parity ($\mathbb{Z}_2$) symmetry, as is commonly the case, the underlying group properties have to be taken into account during compactification. The result is that, topologically, the extra dimension is no longer a circle of radius r_c but a line of length $r_c\pi$. This is illustrated in Figure 30. This process is known as orbifold compactification [163]. The situation becomes more and more complicated as more dimensions are added.

6.2.1 *Large Extra Dimensions*

There are multiple modern particle physics models with extra dimensions that try to embed the findings of the Standard Model within them. Notable here is the model with large extra dimensions (LED) suggested by Nima Arkani-Hamed, Savas Dimopoulos, and Gia Dvali in 1998 [164, 165].

The LED model is often also refered to as ADD model after its original propoponents.

It tries to explain the weakness of gravity (as seen by $\alpha_N/\alpha_F \approx 10^{-32}$, where α_F and α_N are the typical electroweak and expected gravitational coupling constant [166]) by assuming that, unlike other fields within the Standard Model, it propagates in additional spatial dimensions. If these dimensions are large compared to the typical Planck scale there would be a much steeper power law for the law of gravity for small distances r following $\propto 1/r^{k+2}$ where k is the number of spatial dimensions above three. For larger distances that are bigger than the scale of these extra dimensions, the power law naturally changes to the well known $1/r^2$ dependency.

Thus with both physical size as well as number of these extra dimensions the actual physical Planck scale moves progressively to lower energies. It could even approach the weak scale and be in range of a collider experiments.

For a single extra dimension in this model, and for the Planck scale to be at the TeV range, the size of the extra dimension should be roughly 1mm.

6.2.2 *Warped Extra Dimensions*

Not all models try to make the size of the additional compact dimensions responsible for this behavior but instead add a warped space-time. A popular such model is the RS model of Lisa Randall and Raman Sundrum proposed in 1999 [167]. It adds a single extra dimension along which space-time is heavily warped. This can heavily influence the natural energy scale at opposing ends of this dimension. The extra dimension does no longer have to be necessarily compact (*RS1 model*) but can also be infinite (*RS2 model* [168]). The special property of the *RS* models is that the apparent weakness of gravity is now tied to the graviton being located at a different place along the extra dimension than other fields. The fundamental scale for unification of the forces can be near the TeV, but moving along the 5th dimension has strong (exponential) effects on the apparent scales of the other four dimensions - and thus the energy. This makes it look like the fundamental scale of gravity is the Planck scale and thus seemingly creating the hierarchy problem when the situation is actually only an effect of the warped space-time (see Figure 31). Since the Randall-Sundrum models no longer strongly depend on the size of the extra dimension they are viewed as more *natural* than the LED models by its proponents.

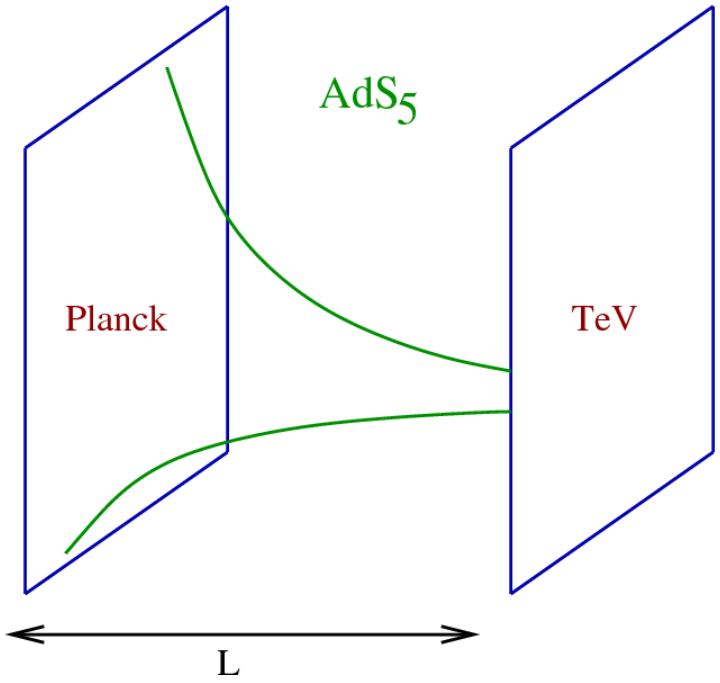

Figure 31: The situation with warped extra dimensions (here: *RS 1* model). The scale of gravity looks like it is at the Planck scale due to the heavily warped metrics in the 5th dimension that the graviton propagates into ($L = \pi r_c$). The actual fundamental scale for unification of the forces is at TeV energies - in range for collider experiments. Illustration taken from [169].

6.2.3 *Universal Extra Dimensions*

Note that all such extra dimensional models are non-renormalizable and thus should be treated as effective theories up to some cut-off scale M_s. In the simplest case a mUED model thus only two parameters: r_c and M_s.

The previous works on extra dimensions inspired theories of extra dimensions that are no longer restricted to gravity alone. For example, adding a single compact extra dimension like in the LED model, but letting *all Standard Model particles* propagate into them has some interesting phenomenological consequences. This is because a single extra dimension with some size r_c with cyclic boundary conditions leads to possible states ${m_n}^2 = n^2/r_c^2$. For Standard Model particles at tree level one thus gets $\sqrt{{m_n}^2 + {m_{SM}}^2}$ as masses for the so called *Kaluza-Klein (KK) excitations* [170]. This means that in this simple case the KK mass spectrum is nearly degenerate, though radiative corrections remove this degeneracy and can lead to a significant splitting. In any case one gets a *Kaluza-Klein tower* (Figure 32, Figure 33) of new particles above the mass spectrum of the usual Standard Model particles that in this simple model will be roughly evenly spaced in energy, the additional energy is simply the momentum in the extra dimension. Since momentum is conserved the KK-number n is also conserved. The realistic case is slightly more complex and in order to not violate SM electroweak precision measurements one has to break exact n number conservation during *compactification* but one can keep

a discrete symmetry. The implicated conserved parameter then is the so-called KK-parity $(-1)^n$. It is conserved for all interactions at all orders - unlike the KK-number n that is now only conserved at tree level [170].

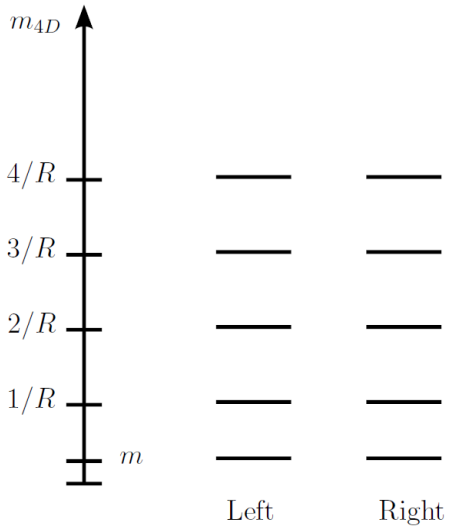

Figure 32: 4D KK-spectrum of a 5D fermion. It is sometimes known as a Kaluza-Klein tower. Taken from [162].

The collider phenomenology of these models is quite close to the one seen for supersymmetry. In this minimal model the new particles also can only be produced in pairs in SM-collisions due to KK-parity conservation that acts like the R-parity in the MSSM. The simple model discussed here is known as mUED (minimal Universal Extra Dimension). While the missing energy for interactions producing KK particles will be high, the missing transverse momentum will be low due to the quasi degeneracy. This makes the model effects more challenging to find at colliders. Just like for supersymmetry the model can be modified in many ways: KK-parity can be broken, non Standard Model particle (right handed neutrinos ν_R, gravitons G, etc.) can be introduced, more dimensions can be added or their geometry modified to get a UED version of a Randall-Sundrum model [171].

The main difference to SUSY models is that there is also an arbitrary number of additional particles due to higher order excitations at even higher masses and that the new particles keep their bosonic or fermionic nature. Like for SUSY, the lightest Kaluza-Klein particle (LKP) is very important for any observed phenomenology. If it is neutral is can also be a dark matter candidate [172, 173].

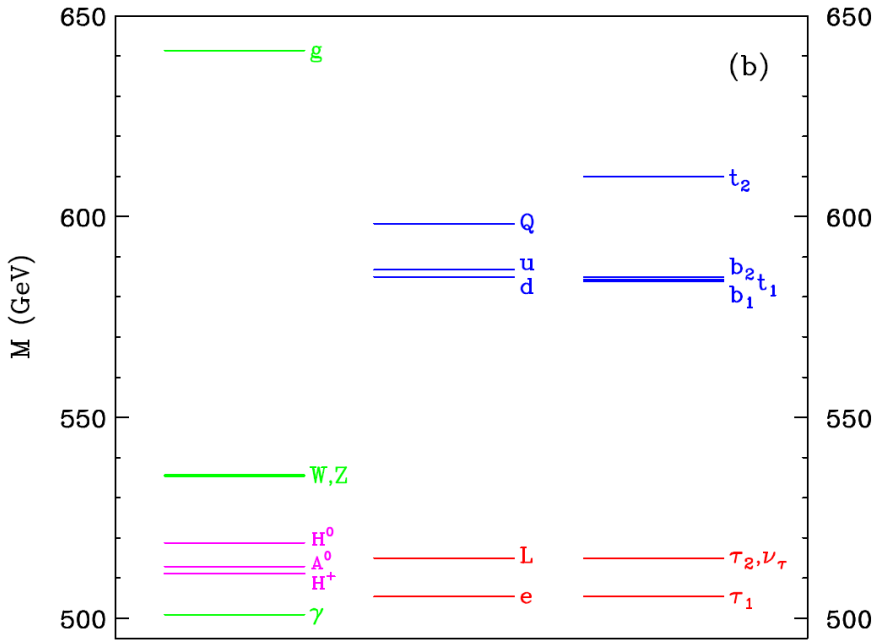

Figure 33: The mass spectrum of (the lightest) additional particles in a simple UED model (5D). It (almost) only depends on the size of the extra dimension r_c and the energy cutoff of the theoretical description (here: $r_c^{-1} = 500$ GeV). Taken from [174].

Part II

SIMULATION AND ANALYSIS

I don't believe it. Prove it to me and I still won't believe it.

— Douglas Adams, *Life, the Universe and Everything*

7 NEUTRINO INDUCED DOUBLE TRACKS

Taken together the considerations from the previous chapters can be used to build a plausible model for experimentally observable exotic physics at km^3-sized neutrino telescopes. A PeV (or higher) energy neutrino hits the Earth reaching possible center of momentum energies in the TeV range. Thus it is able to produce exotic particles expected in this energy range in many BSM-models. These particles will probably be produced in even numbers due to required symmetries (e.g. R-parity) and then decay fast to at least two of the lightest, possibly meta-stable particles (e.g. NLSP) in the respective exotic physics models (see Chapter 6).

Why exactly the particles are meta-stable does not matter in this scenario. So, whether it is due to the decay being suppressed, like in the case of decay into gravitinos, or due to a lack of phase space when the lighest (neutral) and next-to-lightest (charged) particle are almost degenerate in mass does not play a role for the detector signature.

If these particles are charged they can be observed in a neutrino detector as two tracks. The particles can traverse large parts of the Earth due to the large mass suppression of energy losses (see Chapter 3). This long range has a distinct effect on the later observed detector signature: the tracks will be almost completely parallel and some have much higher track separations than possible for similar Standard Model interactions. This is sketched in Figure 34.

Secondly, the much higher range compared to muons also means that the tracks can come from much further away and still reach the detector. This increases the effective volume of any detector searching for this signal. Even though exotic interactions are expected to be suppressed compared to SM-interactions by orders of magnitude the enhancement might still make it possible to reach an observable event rate for favorable models.

7.1 AIR SHOWER MUON AND NEUTRINO SIMULATION

Events in IceCube are generally either caused by muons produced in air showers or secondary leptons created in neutrino interactions. Both have to be simulated in order to account for background events. Air showers are simulated using the software package CORSIKA [56] used in many astroparticle experiments. It handles the simulation of air showers from the initial interaction in the atmosphere through the evolution and properties of the secondary particles. CORSIKA supports multiple models describing the hadronic interactions in the atmosphere that show conflicting data when comparing observables like the number of muons [175]. The CORSIKA datasets described in this work are based on the SIBYLL interaction model [176]. The CORSIKA simulation in use for IceCube has been adjusted to account for the South Pole atmosphere and location of the detector. If done for

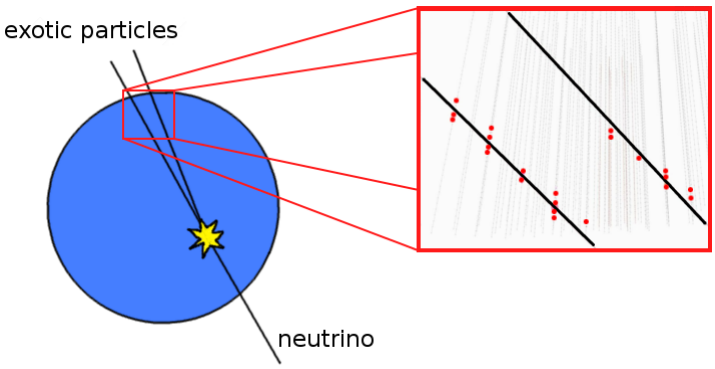

Figure 34: A high energy neutrino interacts in the Earth to produce two $\tilde{\tau}$-like particles that can be seen as two parallel tracks far from the interaction point. Due to the long range of these heavy, charged particles the tracks are extremely parallel and can have much higher track distances than can be achieved by Standard Model Particles.

the in-ice IceCube detector it only considers muons that have enough energy to reach the array. These are then injected in the MMC [80] simulation at ground level. The MMC code then handles the further propagation in the ice. The initial Cosmic Ray spectrum injected into CORSIKA for the datasets used in this work are based on a polygonato model [177].

Neutrino simulation within IceCube is usually done assuming a generic power law energy spectrum for the primary neutrinos. The index of the power law for a specific dataset is chosen in order to generate sufficient statistics for the energy range in question with both E^{-2} general purpose datasets and E^{-1} high energy datasets being the most common indices. The energy of the individual neutrinos is then re-weighted in order to reproduce any desired neutrino flux model. In this work the model considered is the one of Honda et al. [178] for the conventional neutrino flux. Higher energy neutrinos in the range of the prompt flux do not play a role for the double track background and so no model had to be specifically chosen for this energy. The generation and propagation of neutrinos is handled by the neutrino simulation package NUGEN. Each generated neutrino is forced to produce a secondary charged lepton near or in the detector volume. This particle, its kinematics, and its respective weight are then passed on to other modules for further simulation.

7.2 DOUBLE TRACK SIMULATION

While standard simulations for normal air shower and neutrino events already exist for use of the whole IceCube collaboration, most of the double track simulation had to be redone from scratch. Existing modules that had been started to do similar simulations were either non-

existent, faulty or largely incomplete. The simulation was done to model the two most important types of double tracks: signal tracks and di-muon events caused by a neutrino near the detector.

7.2.1 *Simulation of Exotic Double Tracks*

The first step in signal simulation is to get hold of a model and all its associated model parameters. Models are usually defined by a combination of high energy scale parameters as described in the previous chapter for constrained SUSY or the UED parameters (number, size and cut-off scale of the dimensions, etc.). The parameters then need to be translated into low energy scale parameters that can be used to compute cross sections and masses.

High scale here means at some level a unification of masses or couplings, etc. occurs.

For some popular models, such as the MSSM in supersymmetry, this is quite easy due to the existence of the SLHA [179] convention that lays out how to organize SUSY data files for high compatibility between programs. So high scale inputs can be put into almost any tool (e.g. SuSpect, SPheno, etc.) that does the RGE running in order to get the low energy parameters (masses, coupling constant, decay times, etc.). For other models the situation is generally more complicated. So, for now, the choice was made to start with SUSY simulations but keep the tools used general enough to allow for other exotic models with minor modifications.

At this point, with access to all required data, it is possible to compute the cross sections of the primary neutrino-matter interactions and the subsequent particle decays all down to the level of metastable CHAMPs (i.e. $\tilde{\tau}$ for many SUSY models). However, due to the high number of possible interactions and decays it is impossible to compute every interaction by hand in all but the simplest cases. Additionally, processes like string fragmentation need to be taken into account for a completely accurate description since the *target particles*, the nucleons in the Earth that the neutrinos hit, are colored. PYTHIA [180] is a framework commonly used at colliders experiments and elsewhere to do these calculations. So it, or more precisely its FORTRAN based version 6.4, is also the code of choice for the double track simulation.

PYTHIA is employed by many LHC collaborations.

Being very collider based, PYTHIA is, however, mostly focused on interactions between charged particles (e.g. proton-proton). It does not directly support the event generation of neutrino-nucleon interactions. Additionally, there are other problems that are also connected to the implicit expectation that the simulation is done for a typical collider phenomenology. This is particularly noticeable for MSSM simulations. Here the assumption in PYTHIA is that the lightest neutralino is the lightest SUSY particle. Once produced, it does not decay even if the SLHA parameters provided have a slepton in it with a lower mass. Even though gravitinos are also allowed as LSP by an additional flag,

the neutralino decay channels still show the same problems and the lightest one still only decays to gravitinos.

Fortunately, the lightest stau and neutralino are very close in mass for many MSSM models explored here (e.g. see Figure 28) and the decay of a neutralino into a stau only creates a very small change of stau momentum. Thus, treating neutralinos that are *stuck* and have not decayed in the PYTHIA output for the interaction as staus only introduces a minor error and a reasonable solution for the results within this work. Ideally the dependence on PYTHIA should be removed at a later stage (like done in Section 7.2.3) to avoid the issue altogether.

Simulating the Primary Interaction

While PYTHIA does not provide a way to do the event generation of the primary neutrino interaction directly, it does allow for the introduction of externally generated events provided in the LHEF[1] format [181] for further processing. So the issue of non-supported neutrino-nucleon interactions can be resolved by the use of external event generators. A number of event generators exist that can supply LHEF event information - like CompHEP [182] or CalcHEP [183].

After some testing MadGraph 5 [184] was chosen due to ease of use. It allows both for the calculation of cross sections as well as acting as tree level event generator. At a basic level it only provides access to protons and not neutron as a composite target. For the time being, the decision was thus made to treat all nucleons as protons for further simulation. This does mean, however, that the relative quark content within the Earth is not modeled quite correctly, a bias that should be kept in mind. Under this assumption, it is possible to calculate a good approximation of both the neutrino-nucleon ($\nu - n$) cross section and the branching ratio to exotic (SUSY) particles. The PDFs[2] used for the proton description is CTEQ6 [185] - a set assembled by the CTEQ[3] collaboration.

For simplicity the SM neutrino cross sections already in use elsewhere for IceCube can also be chosen.

Both MadGraph and PYTHIA interactions are computed at fixed *beam* (i.e. initial particle) energies. This means that the code is optimized to be fast when additional events at the same energy are being done but there is a significant overhead for initialization when changing the energy. The strategy employed here is thus the following: generate a high number of events ($\approx 1000 - 10000$) at each primary neutrino energy E and write out all the outgoing particles, associated kinematics, as well as cross sections. Then proceed with simulating again at a slightly higher energy $E + \Delta E$ and repeat the process. Do this until the whole energy range is covered. The energy separation $\Delta E(E)$ is chosen so that there is a good coverage of the whole energy

1 Les Houches Event Files
2 patron distribution functions
3 Coordinated Theoretical-Experimental Project on QCD

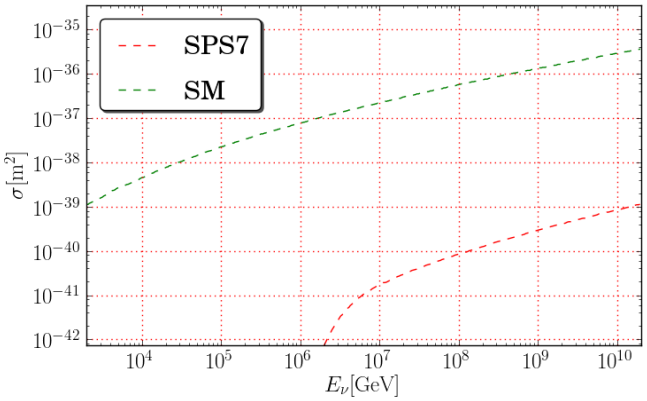

Figure 35: Result for the cross section calculation at the SPS7 [149] MSSM benchmark point compared to the Standard Model.

spectrum. For improved accuracy at intermediate energies and for easier handling of further calculations the cross-sections are fitted by a spline. For an example see Figure 35.

The points E are chosen mostly equidistant in center-of-momentum energy of the $\nu - n$ system $\propto \sqrt{E}$.

With this preparatory work done, all the parts for a basic double track simulation are in place. The simulation can be now done in the following way. The energy of the primary neutrino is generated by sampling from the presupposed spectrum. For now the hypothesis is that the flux follows a power law $\Phi_\nu \propto E^{-2}$ as is usually assumed for a generic cosmogenic neutrino source (see Chapter 1). The neutrinos are generated with a uniform arrival direction at the edge of Earth's atmosphere.

The next step is determining whether the neutrino interacts on the way to IceCube. Postulating a neutrino is lost during any SM interaction on the small path through Earth dl one gets

An additional assumption done here is $\sigma_{SM} \approx \sigma_{total}$.

$$dN = -N(l) \cdot \sigma_{SM} N_A \rho_{Earth}(l) dl$$

with N being the number of neutrinos and N_A being the (approximate) relation of mass and nucleon number and ρ_{Earth} the density of the Earth. The probability p of a neutrino interaction is then

$$p = \frac{N(0) - N(l)}{N(0)} = 1 - \exp(-\sigma_{SM} N_A \int \rho_{Earth}(l) dl) \ .$$

Here the density of the Earth $\rho_{Earth}(l)$ is modeled by the PREM[4] [186] model that is re-parametrized according to the incident neutrino angle. One can easily see that for high energies the interaction probability gets close to 1, so there is an option in the simulation code for skipping the previous simulation step and just assuming a neutrino interaction - if so desired . This can, however, lead to overestimation of the double track flux near the horizon for models with a

4 Preliminary Reference Earth Model

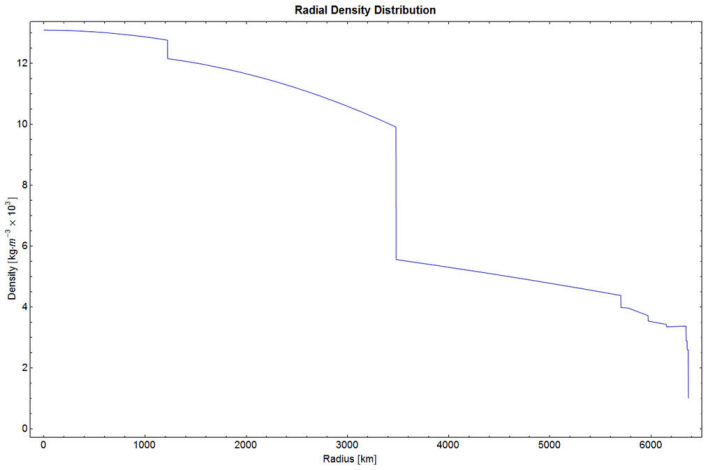

Figure 36: The preliminary reference Earth model [186] used for the density calculation within the simulation.

very low production threshold and should only be done with caution. The probability of an *exotic* neutrino interaction p_{exotic} is then simply determined by the branching ratio to exotic particles

$$p_{exotic} = p \cdot \frac{\sigma_{exotic}}{\sigma_{exotic} + \sigma_{SM}} \approx p \cdot \frac{\sigma_{exotic}}{\sigma_{SM}} \ .$$

In any case, the depth of the interaction l is randomly drawn from the distribution $N(l)$ in order to generate the position of the interaction vertex within the Earth in a separate step once an interaction has been determined.

It should be noted that the procedures described so far are not actually done in separate calculations but in a single M.C. operation. This avoids a high number of unnecessary calculations. If there are any interdependent variables (e.g. energy and direction) in a simulated event and the event itself is discarded the M.C. generation of them have to be redone for the next event. This is especially an issue in the case of highly unlikely events that can potentially happen a lot - for example neutrino interactions with low cross sections but high flux. In this situation it is much more efficient to directly draw an event from the convolution of the incoming neutrino energy distribution with the interaction cross section. This approach has been chosen in the double track simulation in all cases where it was easily possible (convolution of primary energy E_ν, $\frac{\sigma_{exotic}}{\sigma_{SM}}$ ratio, etc.) though the situation gets more complicated once multiple variables play a role and the distributions the event parameters have to be drawn from become multi-dimensional. The total interaction probability within the Earth, for example, is dependent on both the neutrino energy and its related variables as well as the amount of matter between the neutrino and the detector - a variable dependent on arrival direction.

For maximum accuracy all the simulation steps so far should be performed for each kind of neutrino separately - including the distinc-

tion between neutrino and anti-neutrino. The cross sections for high energy neutrinos and anti-neutrinos, however, become quite similar for the energy range considered here ($\approx 10^3$ TeV) [187] due to the dominating impact of the quark sea to the nucleon PDF. So, for simplicity, the calculations shown in this work have simply been done with an average contribution of all neutrinos in each step.

Finally a point is reached where an event describing an exotic neutrino interaction with known primary energy, direction and distance from the detector is generated. Now data from the pre-simulated $\nu - n$-interactions at this energy can be randomly drawn to get the kinematics (i.e. energy and opening angle) of the CHAMP pair. This pair of particles has to be *propagated* to the detector. In this step of the simulation some specific properties of the particular exotic model could be simulated: the losses of the double track flux due to metastable CHAMP decay, energy losses along the way to IceCube, as well as scattering and the effect on the double track opening angle. As such it has been kept highly modular. For now it has been set to a simple hypothesis. There is no significant effect on the opening angle from scattering, the CHAMPs do *not* decay and the energy losses are approximated [68] by the muon energy losses

$$\frac{dE_{CHAMP}}{dX} \approx \frac{m_\mu}{m_{CHAMP}} \cdot \frac{dE_\mu}{dX} \,.$$

This extremely simple model is not quiet correct but captures the basic dependencies and energy scaling for a wide array of models and has the huge advantage of only using a single parameter m_{CHAMP} of the exotic model. The energy losses of the exotic particle on the path to the IceCube detector can be treated in a very simple way by this continuous function. Unlike for similar muon simulations, this can be done because catastrophic energy losses - like bremsstrahlung - do not play a role for the CHAMPs considered here. If the distance of the CHAMPs to the detector is smaller than the range calculated by the energy loss of the lower energy CHAMP the event is discarded. Else the energy loss calculation is done for the other CHAMP and both can be assumed to have reached the detector with the calculated energies. The track opening angle and their energies can be used to calculate the respective track distance at the detector. These are now written out along with other data of note (primary energy, zenith direction, opening angle, etc.) for future use (see Figure 37) or directly be put into the next part of the simulation.

As will be seen later on, the detector simulation from here on only has to be done a single time with a simple model.

In a second step this data is used for the detector simulation itself. There are two minor considerations to be made. Among all kinds of CHAMPS, the MMC particle propagation code used in IceCube only simulates $\tilde{\tau}$ particles, though the mass parameter can be freely configured. Also the energy of the $\tilde{\tau}$ and all other exotic heavy particles is kept *constant* within the MMC simulation - no matter how big the energy losses are. So stopping $\tilde{\tau}$-tracks can not be simulated. This is,

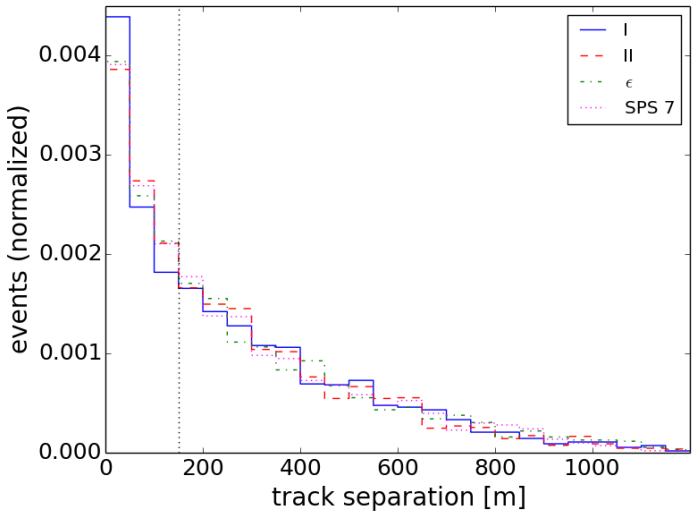

Figure 37: Simulated track separation distribution for a detector like IceCube for some SUSY models. For the exact parameter values, please see [188, 149]. Note that the SUSY particle masses here do not vary much from model to model.

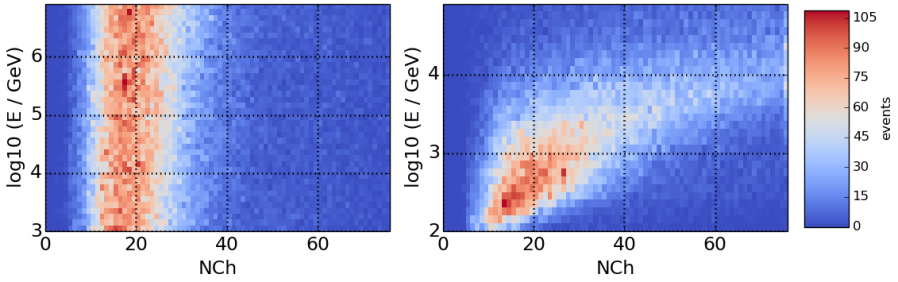

Figure 38: Simulated IceCube detector response for a CHAMP (*left:* $\tilde{\tau}$ with $m_{\tilde{\tau}} = 200$ GeV) and a muon (*right*). Shown is a very simple energy estimator, the number of DOMs with a signal (NCh).

however, not a big constraint. It is quite unlikely that a particle that has propagated through hundreds if not thousands of kilometers of the Earth stops exactly in the $\mathcal{O}(1$ km) path intersecting the detector volume. The restriction to only $\tilde{\tau}$ particles is also not very problematic. Comparing the models in [64] and [67] for example shows that there should be no distinction between any of the double track CHAMP candidates, no matter if they are scalar particles or fermions. Both can be treated the same, as can be assumed for any exotic particle with an energy loss low enough to reach the high track separations needed for a double track signal in the first place. Additionally, the exact energy of a $\tilde{\tau}$ or $\tilde{\tau}$-like CHAMP only plays an extremely minor role in the detector response at the expected energy range (Figure 38). Other factors, like the track distance from the optical modules or the incident track angle, have a much more dominating impact.

The simulation near the detector volume is done with the usual IceCube simulation framework [189]. To generate a realistic double track at the edge of the detector the same techniques can be used as for a single track. This is done by first calculating the mean direction and position of the two tracks. These two values can be used to generate a straight line that should be in the middle of both tracks. This line can now be treated like a single "track" and the M.C. sampling near the detector can be done following the usual steps.

The direction of the "track" and the middle of the detector volume is used to construct a disk that is perpendicular to the line connecting them. Now the starting point of the "track" is moved to this point while keeping the "track" direction the same. The disk radius is chosen big enough to not lose any potential "tracks" hitting the detector. This disk has to be placed well outside the detector volume. Now the problem can be treated again like a double track by putting the two tracks back to their relative positions around the mean "track". For some additional safety of the calculation and to avoid computational artifacts it makes sense to randomly rotate the track tracks around the mean "track" at this point. At this point both tracks can safely inserted into the normal IceCube simulation chain and propagated by MMC. The simulation of light and detector response follows the same scheme as for any other IC79 simulation. To save some simulation time, the double track signal assumption can be minimally enforced by demanding *both* tracks to be within $\approx 100 - 200$ m of the detector volume.

The size of the disk be used to calculate the effective area once the efficiency is known.

7.2.2 *Simplifications*

Apart from this more detailed and very model-specific simulation, another, much simpler but very generalized, simulation was created for this work. Due to the negligible impact of the CHAMP energy on detector response (compare Figure 38) and the fact that most particles will be produced far from the detector, and thus be extremely parallel (see Figure 39), one can simplify the simulation *near the detector*. This is done by assuming some arbitrary CHAMP candidates, like $\tilde{\tau}$-particles with a reasonable mass ≈ 200 GeV and energy $\approx 10^5$ GeV, as perfectly parallel tracks and directly throwing them into the IceCube detector simulation in the vicinity of the detector. Arrival direction and track separation distances can be drawn from uniform distributions and later re-weighted to any particular exotic model. This disentangles the highly model-dependent simulation of the generation and propagation through the Earth from the simulation of the IceCube detector response to these tracks.

Using data from this simple simulation as a baseline, all results of the current analysis can thus be presented in a form that does *not* depend on any of the model assumptions and specific approximations

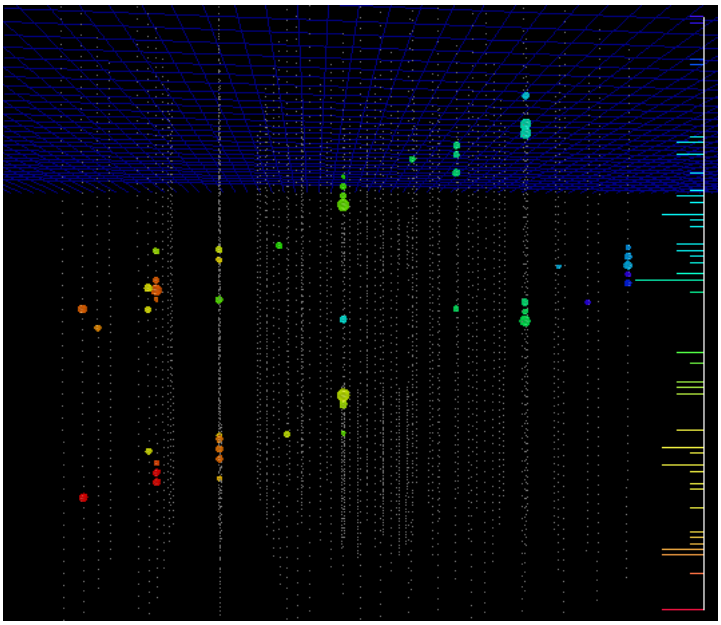

Figure 39: A simulated exotic double track. The tracks are extremely parallel once they have reached the detector.

described in Section 7.2.1. Moreover, model expectation and special cases like scattering [190] and energy losses can be added or refined *after* the analysis is complete if any particular model warrants it. None of the IceCube specific simulations have to be redone.

7.2.3 *Di-Muon Signal*

The di-muon simulation developed for this work shares many concepts with the signal simulation. Still, there are a number of differences that result from the different origin of the tracks. Note that results of the simulation were not used to inform any analysis cuts for this work, so not all parts will be discussed in detail.

The simulation models the SM di-muon background caused by charm production during neutrino interactions with a nucleon n within the Earth and subsequent decay:

$$\nu n \to \mu_- H_c \to \mu_- \mu_+ H_x \nu \,.$$

Here H_c denotes a charmed hadron and H_x any generic hadron (i.e. strange or non-strange). This is not the only di-muon process that could lead to separated tracks, but probably the dominating one and it is refereed to in the respective proposals for double track detection [64]. So it serves here as an example of typical high separation SM processes to be considered.

Unlike for exotic events, the energy is in the range where atmospheric neutrinos dominate. This makes the situation slightly more complicated. Instead of following a E^{-2} spectrum and a uniform

arrival direction for the neutrinos, the distributions are taken from existing models for conventional [178] and prompt [191] neutrino fluxes. Due to compatibility issues when injecting this class of events into PYTHIA, the matrix element event generator had to be switched from MadGraph5 to WHIZARD 2 [192, 193]. Unlike MadGraph, this code can access the string fragmentation routines used by PYTHIA internally directly and so could be used to simulate the whole decay process without needing to pass events from one event generator to another. For consistency, the PDFs provided to WHIZARD are the same ones used for the NUGEN simulation (i.e. CTEQ4-DIS [194]).

One of the problems seems to be the break down of the commonly used approximations for the center of mass and momentum energies at lower energies if one of the incoming particles is massless.

As a simplification, all particles apart from muons are forced to decay directly at the interaction vertex and only muon particle information and kinematics are written out. This was done to avoid having to do additional steps like using a toolkit such as Geant4 [195] to simulate all interactions in matter and speeding up the simulation process. Comparing the situation with interactions in the atmosphere (see Chapter 2) where the number of potential high energy muons goes down when mesons re-interact instead of decaying, this immediate decay can be seen as a conservative assumption that will produce additional muons and thus additional background events.

The goal of the di-muon simulation here is not an exact prediction, but a dataset that is enriched in SM double tracks and has at least *the expected number of di-muon events.*

Unlike CHAMPs, muons need to be generated close - $\mathcal{O}(10^1 - 10^2$ km$)$ for the highest energies - to IceCube to have a chance of reaching the detector. The simulation is thus done in two steps. First the calculation of the number of ν_μ reaching the vicinity of the detector along with their direction and energy. The maximum possible distance to the detector a muon can have and still be able to reach it is then determined. This is a highly energy dependent variable. It is chosen following the same principles as in the MMC simulation code.

The range is parameterized like in Section 3.2.1. Instead of using the parameter values a and b for the *mean* muon energy loss, however, these two parameters are adjusted as to incorporate outliers in the energy loss distributions. The values are the same ones as used in the MMC code to ensure that *at least* 99.9% of muons do not lose all their energy in a given range. Only neutrino interactions that take place within this range ($E_\nu > E_\mu$) are further simulated. The same applies for muons produced in the interaction. The simulation is then concluded in the IceCube simulation framework as described for the exotic double tracks.

Additionally, because not all muon events in charm production are interesting as a double track background, all events that can not possibly generate a double muon signal in IceCube are discarded. This is done in almost all intermediate simulation steps. Examples of discarded events are neutrinos that can not produce two muons with enough energy ($E_\nu < 2 \cdot E_{\mu,\,\mathrm{min}}$) to reach the detector, events that only produce single muons, and events where it is impossible to reach mid-detector separations > 50 m with a certain energy-opening angle

combination at the neutrino interaction vertex. Removing non suitable events makes it easily possible to generate > 10 years of livetime within the simulated di-muon dataset. Due to the many intermediate cuts on the phase space, it is not easy to picture in detail what the simulated event and their flux mean as a total dataset. Still, they can be used to estimate an upper limit to the total charm double track background after all analyses cuts since they *include* all interesting di-muon events.

7.3 COINCIDENT EVENTS

Simple considerations lead to a fraction of coincident muons for a typical event at the order of 10^{-1} at trigger level.

Due to the large size of the IceCube detector and the accordingly high rate of muons, coincident events (i.e. events with two independent particles entering the detector within the same trigger window) are common in IceCube data. This means that this special class of events also has to be simulated to correctly describe the data, especially since it poses special challenges when it comes to reconstruction and background rejection for almost every IceCube analysis. Within the IceCube simulation software this is done by merging the previously individually simulated events in a realistic fashion. This can be done in three ways. The first way is realized by merging events within pure CORSIKA simulation according to their expected (fixed) event rate. This results in a dataset consisting of both single events and coincident ones up to any arbitrarily high order (i.e. double, triple, quadruple, etc.). This yields a more or less realistic mix of air shower events and so is used for most IC79 air shower simulations without writing the single air shower data to disk. There also exist methods for merging events with a fixed number of coincidences (e.g. *only* triple coincidences) which can be useful for special cases. But since this information can now also be extracted from the normal simulation, generating a data set of this kind is often redundant. The third kind of merging functionality deals with coincidences of neutrino (or signal) events and air showers. Other coincidences, like two neutrino events in the same trigger time, are rare due to the low rates of individual events involved and generally do not need to be simulated.

7.4 PHOTON PROPAGATION AND DETECTOR SIMULATION

Once particles reach the detector and are propagated through the detector volume by the MMC module [80], their energy losses and secondary particles are written out and are treated in the same way from this point on - no matter if they are muons or exotic in origin. The next step is considering the light emitted by these particles along with their secondaries and determining the number of photons reaching each IceCube DOM as well as their respective arrival times. For the IC79 simulation this was done in two different ways. One option

was the PHOTONICS software [115] working with tabulated photon arrival times. It requires the input of an ice model made up by horizontal layers of wavelength dependent ice properties (i.e. scattering and absorption). Models of note are the AHA model based on data taken in 2005 with the AMANDA-II detector and the more recent SPICE model [93]. In use for most simulation for the IC79 data was the model internally known as SPICE-MIE, a SPICE variation with more realistic scattering following the angular expectation for Mie-scattering in ice. Using these inputs, PHOTONICS determines the photon arrival probability and time distributions depending on the relative position of the DOM to the photon source. So, for each DOM, the single photons can be sampled from these distributions according to the absolute light yield expected. These calculations are all is done within the *HitMaker* module.

The other option for photon propagation is the direct propagation of single photons. This is done using the PPC [93] code. Direct propagation is more processing intensive than sampling from look-up tables, but has the advantage of not needing huge pre-processed datasets in memory and the absence of sampling artifacts due to binned data. Single photons and their propagation can be treated independent from each other which allows for parallelization. This means PPC could be developed for use on GPUs - thus speeding up simulation time considerably and counteracting the previously mentioned disadvantage in processing speed. It should be noted that many newer IceCube simulations are being done using direct photon propagation codes, but most IC79 datasets are still based on PHOTONICS.

The simulated photons are often referred to as MChits. Additional noise hits are then added by the *noise-generator* module that assumes an additional constant Poissonian background noise of hits. A newer noise generating module that can also simulate correlated noise bursts has been developed since then but it is not used yet in the current analysis. The raw M.C. hit data is then given to the *pmt-simulator* and *DOMsimulator* modules that respectively simulate the PMT response (including the discriminator threshold) and the DOM main board response (including the local coincidence conditions). The result is a collection of simulated digitized waveforms modeling the hardware output presented in Section 5.3.2. The final step of the simulation is then the application of the known trigger logic and shifting all simulated time stamps in the data to match a realistic event according to the trigger time.

The newer module is fittingly named Vuvuzela.

There is an art to flying, or rather a knack. Its knack lies in learning to throw yourself at the ground and miss.

— Douglas Adams, *Life, the Universe and Everything*

8 DOUBLE TRACK RECONSTRUCTION AND CUT VARIABLES

The double track reconstruction is realized in several steps within the *icetray* software framework [189]. It starts at a basic level with event data comprised of reconstructed photon arrival times in the DOMs (compare Section 5.4.1). The reconstruction itself does not distinguish between signal (parallel tracks) and background events (single or non-parallel tracks) but the finished reconstruction can be used to better establish cut variables to do so. The main focus is maintaining a high signal efficiency while recovering the properties of simulated double track events.

The first step is the rough separation of DOM pulses and assigning them to two tracks. Since the tracks are assumed to be parallel there exist a number of planes between them that separate the tracks from each other. If such a plane is roughly in the middle of both tracks any hit in a DOM on one side of the plane is usually more likely to be caused by the track on the same side of the plane than the one on the other side. Thus the pulse series is approximately separated in a geometric fashion. All that remains to do is to find such a plane.

Note that the assumption for the reconstruction is that there are always exactly two *parallel tracks in the detector.*

8.1 TENSOR OF INERTIA BASED RECONSTRUCTION

One way to do so is to calculate the *tensor of inertia* (ToI) of the charge distribution caused be the event in the detector. The amount of charge in a DOM takes the place of a mass point in a classic tensor of inertia. The center of gravity is the center of charge. In most circumstances this point should be somewhere between the two tracks - probably close to the middle of both of them if their respective particle characteristics (energy losses, track length, etc.) are not too unlike each other. If one takes this as the reference point used in the ToI calculation one can take advantage of its eigenvalues and eigenvectors. The relative size of the eigenvalues can be easily visualized by correspondence of a rotation of the DOMs with hits around the symmetry axes given by the eigenvectors (compare Figure 40).

If one now looks at the eigenvalues of the tensor and the symmetry of the problem one can see that the smallest eigenvalue belongs to the eigenvector that aligns with the direction of the double track event. The next biggest eigenvalue is the one corresponding to the direction pointing from any position on one track to the closest point on the other track. The last and biggest eigenvalue belongs to a vector perpendicular to the plane both tracks lie in. Using this direction

and the direction along the tracks one can construct the separating plane in question. In this analysis though, the eigenvector along the track has been replaced with a simple single track fit (compare *linefit* in Chapter 5) on the whole charge distribution of the detector. The additional time information implicitly used this way helps to make a more accurate guess for the double track direction. For the eigenvector perpendicular to the tracks this is less critical since even a heavily *tilted* plane will still separate the pulses close to the tracks almost as well as well the *correct* one.

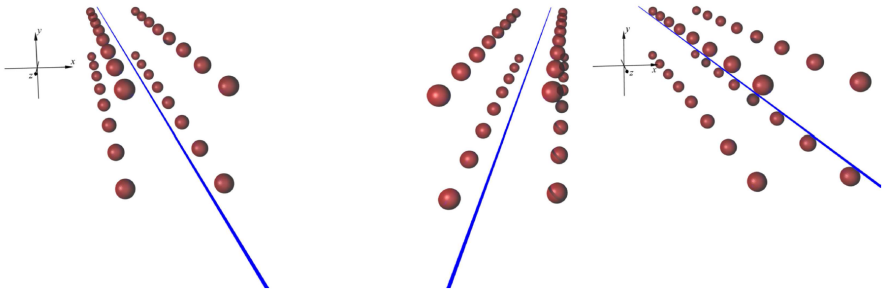

(a) Single Track (b) Double Track

Figure 40: The basics of the tensor of inertia reconstruction can be easily visualized by a simple, schematic DOM hit pattern around each track. An imaginary rotation of the pattern around the center of gravity yields a eigenvector aligning with the x,y, and z axes. A plane generated by the smallest (z) and the largest (y) eigenvalue/eigenvector combination then divides a double track (*right*). For a single track (*left*) the method only yields a small separation of the hit pattern. The simple picture breaks down once the track separation gets closer to the size of the detector or the tracks are too close to each other so that the DOMs with significant amounts of hits overlap for both tracks. Taken from [196].

The predicted efficiency using only tensor of inertia variables was 1% *even if allowing a high air shower passing rate of* 1 *Hz - too low for an efficient IceCube filter.*

The rough tensor of inertia behavior has been used in [196] in order to try and establish a filter for double track events - though ultimately it did not work to a satisfactory degree. While it works for a large number of events, just as many good events that can easily be split up into two pulse series by eye are mis-reconstructed due to the finite detector geometry. Tracks with large track separation (close to the size of the detector) for example will have a smallest eigenvalue that no longer aligns with the direction of the two tracks through the detector as seen in Figure 43.

Here this done with a simple linefit.

It is possible to recover these - very common - mis-reconstructed events though by finding a better guess for the initially assumed double track direction. A relatively simple way to do this is to look at track fits done on each of the two clusters of (possibly falsely) split DOM pulses. Very often a mis-reconstruction results in a quite uneven false assignment of pulses to the two tracks. If this is the case, one track reconstruction is heavily affected and only of very limited worth to recover the double track direction. The other cluster

of pulses, though, often has no or very few pulses from the unrelated track. In this case a track fit on the latter will give a good estimate of its direction and thus - for parallel tracks - the direction of both tracks. Repeating the reconstruction with this new direction as input now leads to a good - or at least better - result. If one wishes to do so this technique can be repeated multiple times to get further improvements. The end result is then fitted with a more robust linefit technique that reduces the effect of outliers [197].

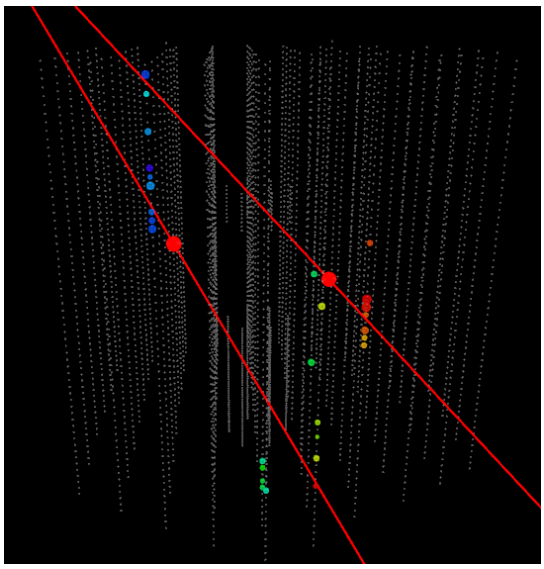

Figure 41: In a non ideal (i.e. finite) detector the reconstruction can fail for large track separations, especially if the tracks are not parallel to begin with or have a significant time delay (like for many random coincidences). In such a case the event either needs a refined track reconstruction (signal) or additional parameters to remove it (background).

8.2 k-means based reconstruction

In order to automate this procedure, however, one needs to find a method of pulse splitting that not only separates the tracks in multiple, recursive reconstructions but also gives a way to choose which of these possible results is the best reconstruction and which one is more likely to be a mis-reconstruction. Since the simple tensor-of-inertia method mentioned so far does not intrinsically provide such a measure, another way of separating the pulses using a k-*means* clustering algorithm [198] is used here instead. Note that k is the number of reconstructed centers of this algorithm, so here one could also call it 2-*means clustering*.

The tensor-of-inertia reconstruction can still be used to find a better initial double track direction. Still, the final reconstruction chosen is always the result of the k-means method.

Again, one starts with a simple fit like a linefit to get a rough direction of the tracks. Now all DOM positions are projected onto a plane that is perpendicular to this direction (see Figure 42). This is

done so that the shortest distance of the hits to a cluster center is a meaningful variable to separate the pulses with and the algorithm does not separate the pulses at the start of the track and the pulses close to where the particles exit the detector (or stop). Technically, since one can assume that the double tracks move with the speed of light, it is possible to use the k-means algorithm also in all 3 dimensions by using a co-moving reference frame that follows the double track propagation. This requires, however, a very good estimate of the track direction in the first place and thus is not helpful at this step. This 3D-clustering could give some additional time information to further separate random coincident events. Even so, it is ultimately not used for this analysis as it can be unstable and hard to interpret for badly reconstructed initial directions. Still - with further refinement - it could be serve as an additional step for future analyses, especially when the direction of the event is already well defined.

The initial guess is still needed to find the direction of this reference frame.

A good example would be the bright core of an air shower and a single laterally well separated muon to reconstruct.

A k-means clustering algorithm assigns the clusters by the shortest distance to a cluster center. With $k = 2$ only two clusters are present and the reconstruction again ultimately defines a plane that separates the DOMs in the detector. And just like before the reconstruction can be repeated using the fits emerging from the separated pulses. The average distance of hits to a cluster center, however, can now be used to measure how well the clustering has worked depending on initial projected direction: the one with the smallest spread around the centers can be assumed to be the best direction. The spread S is defined via the sum of the quadratic distances of the cluster constituents at location $\mathbf{x}_{k,i}$ to their center $\mathbf{c}_k$:

$$S^2 = \sum_i \sum_{k=1,2} (\mathbf{x}_{k,i} - \mathbf{c}_k)^2$$

The spread S is also the value that is being optimized by the k-means clustering algorithm. The smallest spread usually means the best splitting of the DOM signals, though in some cases the regular IceCube geometry can favour sub-optimal cluster locations.

8.3 LIKELIHOOD RECONSTRUCTIONS

So far the reconstructions have assumed that each DOM can only have some signal from a single track at a time. Of course, especially for not too well separated tracks and a certain amount of scattering of light, this it not the case. Thus, to get a better description, the reconstructed *best* track pair serves as a seed for a fit using a two track likelihood hypothesis. It no longer uses the geometrically split pulse series but instead tries to fit both tracks at the same time based on the complete information of *all* DOMs. The word *best* here means that the fits are based on the pair of clusters with the smallest spread S.

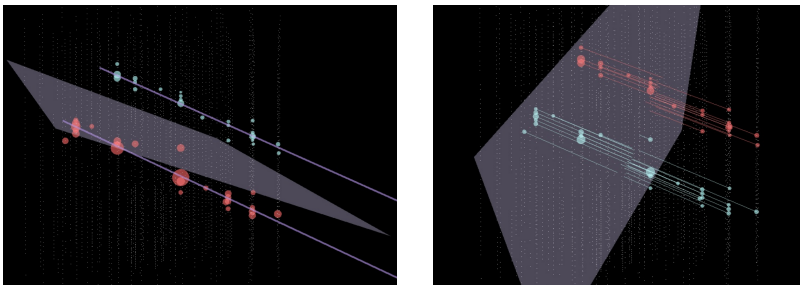

(a) The hits are separated by a plane constructed with the help of the tensor-of-inertia (DOM charge) of the event.

(b) Projection of the events into a common plane perpendicular to the approximate track directions, followed by k-means clustering (k=2).

Figure 42: Visualization of the two alternative reconstructions.

This gives a much more detailed and accurate angular information about the event. Unlike the linefit procedure that describes the tracks as plane waves with variable speed the likelihood fit not only fixes the speed at c, like expected for high energy muons and muon-like tracks, but also takes the Cherenkov cone and scattering effects into account (see *likelihood fit* in Chapter 5).

$c \approx 3 \cdot 10^8$ *m/s is the speed of light*

There already exists such a double track fit for muons in the IceCube reconstruction software. It has been used in the past to fit laterally separated muons and muon bundles at the same time [199]. Unfortunately, it often has problems with convergence due to the high number of free parameters.

For roughly half of all signal events the fit fails completely. Using only these events in the final analysis would lead to a big and unneeded loss in signal efficiency. So instead of the full likelihood information only the improved angular resolution of the fit is used if the fit is successful. If not, angular cuts at this stage fall back the original double track linefit *seed* the likelihood fit is based on.

To amend the problems of the fit and make sure it succeeds for most signal events it has been adjusted to automatically mirror parallel double tracks. This removes some degrees of freedom in the fit parameters. Instead of using two totally independent fits with a start point (3 d.o.f.[1]), and a direction (2 d.o.f.) each (10 d.o.f. total), the tracks are forced to be parallel by having a common direction (8 d.o.f. total). An additional degree of freedom could be removed by also requiring the particle distance along both tracks to be always the same as the track separation and thus assuming that they arrive in the detector at the exact same time. But because the fit convergence problem already had been solved at this point and in order to have a fit parameter that can possibly absorb small irregularities in the ice

The arrival time of both particles could be slightly divergent due to scattering while transversing the Earth or similar effects.

1 degrees of freedom

and light propagation modeling the 8 parameter fit was deemed to be the better choice.

The (reduced) likelihood value of this adjusted fit can now be used directly as a cut variable and is by far the most effective and efficient variable used in this analysis. The number of fit parameters is still high compared to a single track fit and this makes the fit much more computationally intensive. So necessarily the fit can *not* be used on *all data* but some previous data reduction cuts are required. These cuts will be discussed in the next section.

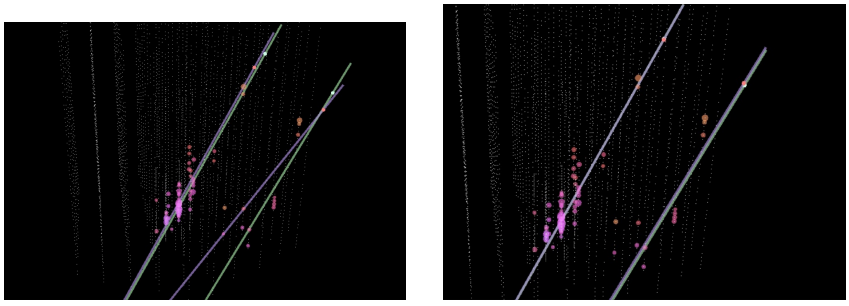

(a) 10 parameter double track fit (b) 8 parameter (parallel) double track fit

Figure 43: Two kinds of likelihood fits are used in this analysis. The non-parallel likelihood still retains angular information but can not be used on many signal events, the parallel one has no explicit angular information but has fewer problems with convergence and automatically describes the signal events better.

8.4 DATA SELECTION CUTS

The cuts used in this analysis can be roughly categorized into those cuts that improve basic data quality and make reconstructions meaningful and those that separate double track events from *background* events. The latter can be further distinguished between single (muon) track events that are an important background for double tracks with only very small track separation and *coincident* events where multiple particles (usually muons) trigger the detector at the same time. For coincident events the true properties of the primary particles causing it, especially the directionality, have little in common with the result of basic reconstructions and fits. This is especially true if none of the sub-events is clearly dominating - contrary to, for example, an extremely high energy particle cascade and a low energy muon. This is very unlike signal events of completely parallel tracks where the direction of simple fits very often aligns - at least roughly - with the true arrival direction.

Small separation here is roughly around the IceCube string spacing of 125 m.

The most common source of coincident events is two muons from separate air showers. Due to the sheer number of this class of events

it is also the most relevant background for this analysis, especially for well separated double tracks. Technically any kind of physics event can fall into this class if another event just happens to fall into the same trigger window, but random coincidence with an air shower muon is almost always the most relevant one. In practice cuts designed to remove uncorrelated (down-going) air shower muons prove to work almost just as well for muons caused by (possibly up-going) neutrino paired with an air shower muon. The potentially dangerous combination of two muons caused by independent atmospheric neutrinos is very low at ≈ 0.0008 events per year before even requiring them to have roughly the same direction [200].

i.e. several hundred meters

The irreducible background of two neutrinos from the *same* air shower producing two correlated muons is also extremely low (≈ 0.07 events per year [200]). Double muon production in charmed neutrino interactions has been discussed in literature as a typical background [64] and has been simulated as discussed in Chapter 7. It never proved to be dominant at any level of the analysis and so requires no specific additional cuts.

Thus coming from exactly the same direction!

In a strict sense there is another class of events which does not fall in the previous categories of track-like or very low quality events: large particle cascades such as those caused by ν_e or ν_τ. None of these events, however, are very signal-like or very common in the detector and no dedicated cuts are needed to remove them. They never get close to dominating the background expectation at any cut level and get inadvertently removed by cuts dedicated for more common background events.

8.4.1 *Muon Filter*

Due to a lack of a better alternative the muon filter is the start of the current double track analysis. It is a zenith dependent filter that selects for reasonably well reconstructed up-going tracks. It has by far the highest passing rate for double tracks among the IC79 filters. Around 1/2 to 2/3 of simulated CHAMP double tracks that cause at least 1 hit each in some DOM pass the filter. Still, there is a undeniable pre-selection for track that look more like single track within the filter.

8.4.2 *Basic Quality Cuts*

Data quality cuts are made so that the output of fits and other reconstructions can be trusted. Only then can the latter be used to inform cuts on data. Most of them are done early in the processing chain and remove a high number of useless events. In this way they save CPU time for later analysis steps.

NCh and NString

Requiring a number of DOM channels with a signal (NCh), either as a SLC or a HLC hit, is one of the most simple quality cuts. Defining two parallel tracks using only DOMs on a single string is impossible. A sensible reconstruction also needs a minimum of DOM hits on a number of different strings (NString).

Zenith Angle Cuts

Most events coming from above the horizon are muons that can be removed by a cut on the zenith angle of a linefit reconstruction. Neutrino-induced CHAMPs are also almost always coming from well below the horizon. Doing a global fit based on the hits in the *whole* event without trying to recover the individual tracks is good enough to not lose many ($< 1\%$) signal events by just cutting at the horizon. The zenith angle cut is repeated on the likelihood fits of the *individual* tracks once they become available.

Opening Angle and Track Separation

When looking for parallel, well separated events both the opening angle and the distance from one track to the other are useful cut variables. After the first ToI reconstruction, though, these variables are not yet good enough to correctly describe the signal events in many cases. So only events where the reconstruction can be trusted are being cut. These are clear single track events with a low reconstructed track separation and opening angle at the same time.

After the iterative k-means clustering later on, the reconstruction of signal events has become good enough to also cut away events with a large opening angle.

It should be noted that the *mathematic* distance of two infinitely long straight lines is not a useful description of track separation. Often the distance can become very small for points far outside the detector, which can arbitrarily lead to large spread of distances even for only minor changes in track direction. The track separation parameter used in this work is defined differently. The *mean direction* of both tracks is used to construct a plane that is perpendicular to it and goes through the middle of the detector. Now the distance of the points where the tracks intersect this plane is a stable description for track distance *at the detector* for parallel or nearly parallel tracks. For extremely non-parallel tracks, however, this definition of track separation remains rather meaningless and is not useful for cuts.

CoG Position

The z-position (i.e. depth) of the center of gravity is useful to describe where in the detector (i.e. top/bottom) most of the light output of

the event has taken place. So events that only clip the top or bottom of IceCube will have a CoG that is not too far from the top ($z \approx 500$ m) or bottom ($z \approx -500$ m) edge. Events clipping the detector can often not be properly reconstructed or the reconstruction follows the detector edges. For neutrino background events, most up-going events clipping the detector will be at the bottom.

8.4.3 *Coincident Event Cuts*

Cuts to remove coincident events mostly aim for the randomness of time and space pattern the individual sub-event cause in the detector and the associated gaps this leaves in reconstructed tracks and other parameters.

Opening Angle

The opening angle can be a useful tool to detect non parallel coincident events. So the cut is redone once the reconstruction of the individual tracks becomes stable (i.e. after the k-means reconstruction).

Linefit Speed

The linefit assumes a plane wave, but the speed of the wave is a variable. CHAMPs and muons can be assumed to move with the speed of light c and the linefit speed of the individual track linefits recovers the speed reasonably well. Exceptions are often due to scattering and the break down of the linefit description for light far from the actual track. Especially cases where high energy particle cascades are triggered within the detector that lead to a lot of scattering of lower energy particles will lead to a reduction of the linefit speed from c. This is rare for the case for the kind of CHAMPs assumed in this work though.

Coincident events have a random time pattern because the linefit usually connects the first and second series of hits. This leads to a large spread of linefit speeds, both bigger and smaller than c.

Likelihood Cut

The likelihood of the double track hypothesis obtained during the fitting procedure is a strong cut variable. It is, however, dependent on the the number of degrees of freedom and thus the number of DOMs with a signal (NCh). If nuisance parameter like NCh is removed from a likelihood $\mathtt{l}$, it is called the *reduced* likelihood. For computational reasons a likelihood is often expressed as a (negative) logarithmic likelihood $\mathtt{logl}$ instead.

Computers usually use minimization *algorithms, so negative likelihood are minimized during maximum likelihood fitting.*

The cut parameter $\mathtt{logl}/(\mathtt{NCh}-4)$ used here is very close to the negative reduced likelihood (rlogl = logl / d.o.f.) from now on called

that for simplicity. It can now be used as a 1-dimensional cut parameter independently from the NCh - and thus energy - of the event (compare Figure 44).

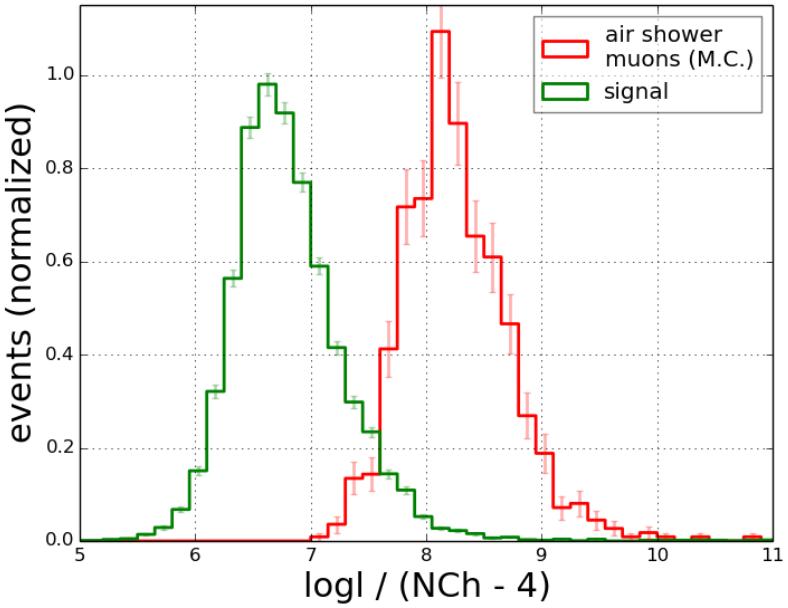

Figure 44: The (negative, logarithmic) likelihood of the double track hypothesis is a strong variable separating it from air shower background events. There scaling of the parameter with the number of channels that has to be removed in order to make it a 1-dimensional cut variable. The distribution is shown for a late cut level.

Z Pattern

Coincident events can fool a linefit reconstruction to connect the first sets of hits of one event and the second set of the other to get an overall up-going behavior. Still, the individual hit patterns of the sub events will be down-going for air shower muons and this can be exploited.

If the hits in the detector are ordered in time one can form pairs of hits that directly follow each other. Any down-going sub-event will usually have more pairs of hits that are also down-going (i.e. the z coordinate of the second hit will be lower). If there is some time overlap between events there will be some pairs that show no clear preference but overall the hit pairs with the correct pattern will generally outnumber the wrong or random ones.

The cut variable z *pattern* is made up of all these pairs of hits: starting with 0, each time a pair of hits is up-going ($z_2 > z_1$) the variable is increased by 1, each time it is down-going ($z_2 < z_1$) it is decreased by one. Up-going single and double tracks will have a z *pattern* > 0.

Events dominated by air shower muons mostly have $z\ pattern < 0$ and are cut.

Time Gaps

Coincident events have a random, and thus often long, time gap between the individual sub events. This can be used by cutting on the maximum time between one hit and the next within an event.

T Pattern

Even if there is some overlap in the arrival time of the sub-events or there are noise hits spoiling the time gap, the time structure of hits can still be used to identify them. Most hits of the sub-events will be spread into two parts instead of being spread over the whole event. Moreover, such events tend to be longer than non-coincident ones. The spread of the hit pattern in time - defined by its standard deviation - is a useful parameter that increases with both factors.

The standard deviation gives different answers depending on if a pulse gets reconstructed into a single hit with a higher charge or multiple hits with lower charges. This is sometimes not perfectly modeled by simulation. Thus, to ensure data to M.C. agreement, the variable was modified and each hit is weighted according to its charge relative to the charge of the whole event.

K-Means Distortion Parameter

The k-means technique has a distortion parameter that is used during the optimization of the clusters that can also be used as a cut variable. A higher distortion (i.e. standard deviation of the distance of hits to their cluster center) can indicate a mis-reconstruction.

8.4.4 *Single Track Cuts*

Single track cuts use reconstructions to find and remove events that are mostly single track like. Examples are (single) muon neutrino events and track-like events with very low track separations.

Track Separation

The track separation is a useful variable to detect single tracks showing a small (i.e. usually 50 - 150 m) reconstructed track distance. Failed reconstructions generally lead to a high track distance. For parallel fits this often happens when one track hypothesis is outside the detector. This is a valid assumption for a single track, but leads to a meaningless high track separation. The same is the case for non-parallel fits where mis-reconstructions lead to large, random opening

angles and thus often a large - and again meaningless - high track distance in the middle of the detector.

Likelihood Ratio

Comparing how single track like a reconstruction looks compared to double track like can be done in a likelihood ratio test. The reduced likelihood variables are used instead of the likelihood in order to remove the energy dependence of the parameter.

Using a monotonous logarithmic transformation the likelihood ratio $\frac{l_{double}}{l_{single}}$ becomes

$$\log(\frac{l_{double}}{l_{single}}) = \log(l_{double}) - \log(l_{single}) =$$

$$= \mathrm{logl}_{single} - \mathrm{logl}_{double} \propto \mathrm{rlogl}_{single} - \mathrm{rlogl}_{double} \,.$$

Remember the definition of logl *as* negative *logarithmic likelihood.*

For events that are clearly more double track like than single track like $\mathrm{rlogl}_{double} - \mathrm{rlogl}_{single}$ decreases and is an effective cut variable.

8.4.5 *Final Quality Cut*

As will be discussed in the next chapter, a final quality cut was introduced at the end of the analysis. Is has properties that remove both single track and coincident background events. It is defined for each track after the associated hits are (orthogonally) projected on onto it. The quality parameter Q is defined as

$$Q = \sum_i i \log(1 + d_i/f) \cdot f < \sum_i d_i$$

with d_i being the distance from a hit i to the next hit i+1 (Figure 45) and the scale factor $f = 100$ m. For small steps in d_i between hits compared to f one thus gets $Q \approx \sum_i d_i$. To increase effectiveness of the Quality parameter, only HLC hits are counted for computation of Q. The parameter gets bigger for long tracks that have many hits along them and gets smaller for tracks with short length or big gaps with no HLC hits.

8.4.6 *Data / M.C. Mismatch*

There is a well known data/M.C. rate mismatch at the level of the muon filter for IC79. There is a $\approx 30\%$ higher data rate for real data compared to air shower simulation and for down-going reconstructions there is a shape mismatch at high zenith angles. For the up-going part the rate mismatch approaches a factor ≈ 2. This larger mismatch can be partially understood. The rate of coincidences rises

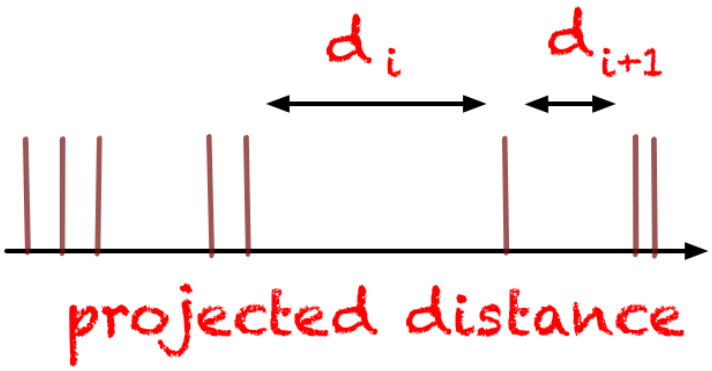

Figure 45: Sketch of the final quality parameter Q.

faster than linearly with the mean rate of air-showers and up-going tracks at this analysis level are actually mis-reconstructed coincident events.

Fortunately - unlike for the down-going part - the shape for parameter distributions agrees well for up-going events (see Figure 46). Only the total rate of M.C. events has to be adjusted upwards.

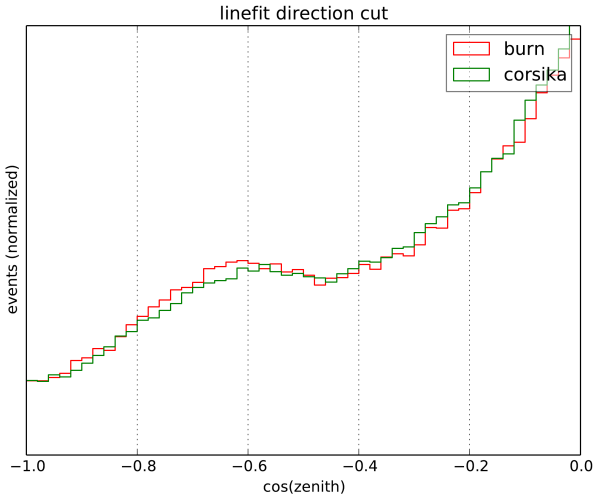

Figure 46: Zenith angle distribution after the zenith cut for simulation data normalized to real data at this cut level. Data is dominated by coincident showers and the data/M.C. mismatch has mostly been removed apart from a constant factor.

Clearly, it is this second part, the missing, that presents the difficulties.

— Douglas Adams, *Life, the Universe and Everything*

9 CHOICE OF CUTS

The cuts described in the last chapter form the basis of the analysis. This chapter now deals with the principles of how the explicit values of the cut parameters were chosen and the data sets used to do so.

9.1 DATA SETS

Before going into the details about how cut parameters it is important to understand all the data sets involved in the process. They can be divided into simulated data sets for signal and background contributions and real data that is also required for verification of the simulation/data agreement.

9.1.1 *Simulated Data*

The data sets mostly contributing to the overall cut strategy in the analysis are a weighted NUGEN neutrino dataset (ν_μ, E^{-1} spectrum) for single tracks that still had the highest number of events of all available neutrino datasets for the 79 string configuration and an unweighted CORSIKA dataset including both single and coincident air showers. Datasets with coincident neutrino and air shower events were also viewed but the relatively low statistics of the data sets made them not important for any choice of cuts. Cuts removing pure coincident air shower muons also proved to be effective at removing all these events. As discussed, the same is true for the di-muon simulation data set compared to the NUGEN (single muon) neutrino dataset. Signal data is made up of a SUSY dataset of $\tilde{\tau}$ double tracks with uniform arrival direction and track separation. While the livetime of the simulated di-muon and exotic double tracks is easily sufficient, the livetime of the air shower dataset is in the order of 1:100 compared to the full IC79 data gathered during a year of data taking. The livetime of the NUGEN dataset is overall higher than the CORSIKA dataset, especially for high energies. But due to the weighted spectrum its statistics also breaks down in the lower energy part that is also important for this analysis.

9.1.2 *Real Data and Burn Sample*

In order to ensure high data quality, all runs of IceCube data-taking are monitored and later assembled into a so called *good run list*. The list does not contain runs with issues like significant hardware faults,

A run is a data taking segment with a length of up to 8 hours.

very short runs or runs where artificial light (like used for calibration) have been introduced into the detector. It also contains additional information and flags that show if the detector was only operated with a partial configuration (e.g. no IceTop, missing strings, etc.). The current analysis is based on the good run list for the 79 string configuration (May 2010 - May 2011) [201]. From this list only runs were chosen that had consisted of a complete detector geometry for the in-ice array (i.e. no inactive strings).

Blind Analysis and the Burn Sample

Like many other IceCube analyses, the search for double tracks deals with extremely rare events. Thus one has to exercise caution when viewing the events to be analyzed before finalizing search strategies, cuts and determining the procedure for setting the confidence intervals. Knowledge of the data introduces a bias that is impossible to quantify and the bias can go in any direction. Especially high dimensional data is prone to these effects: any event is rare if the dimensionality of parameters gets higher. Thus machine learning algorithms also heavily affected and are practically never trained directly on the data to be analyzed.

The reason is trivial: the probability for things being seen as they have been seen is 1. The probability for anything else if infinitely small. Thus the size of the bias is only governed by how detailed the data is treated.

A solution to these problems is to *blind* the scientist from knowledge about the data as much as possible. Still, only depending on simulations without verifying its accuracy at least on a basic level is not practical and equally problematic. The strategy for many IceCube analyses, and this one in particular, is to keep most of the data *hidden* to be used in the finished analysis. Only $\approx 10\%$ of the data is viewed to verify the data/simulation agreement and possibly inform analysis cuts. This data, know as the *burn sample*, is then discarded and not used anymore once the reconstruction strategy has been finalized. Only then the analysis is run on the previously blinded data. The total livetime of this final data set in the current analysis is approximately 280 days.

To be exact: every run with a run number ending in a 0.

9.2 OPTIMIZATION OF CUT PARAMETERS

The various cuts used here fall into three areas that differ in the way they are optimized. The first pre-cuts are simple basic cuts that ensure the basic event topology: somewhat up-going events (linefit) that might be separated tracks are kept. The focus lies on data quality improvement for further reconstructions and the retention of high quality signal events, even if their reconstruction might have failed. It does no lie on signal to background rate optimization at this time. Since none of the events are restrictive on signal events and the knowledge about high quality tracks is hard to define, all cut values were chosen by hand. Another principle here was data reduction to enable more intricate reconstructions that need a higher amount of CPU processing

time. The cut on the number of DOMs and strings hit, for example, is chosen close to the one required for further reconstructions.

Most single air shower muons are removed by the basic cuts as well as some neutrinos and double tracks that are reconstructed as clear single tracks (i.e. below 70 m reconstructed separation). The main background from here on are coincident muons. After doing improved reconstructions, like k-means clustering and later on likelihood reconstructions, the situation is in a state where signal double tracks are successfully and quite accurately reconstructed and optimization makes sense.

Most signal double tracks removed this way have one of the tracks almost completely outside the detector. Only one of the tracks is reconstructed.

Removal of Coincident Events

The dominant fraction of coincident events is air shower muons, so the CORSIKA dataset was exclusively used for optimization. Half the dataset was passed to a machine learning algorithm for cut optimization, the other half kept for evaluation. Since efficiency of many of the weaker, but computationally cheap, cuts is somewhat correlated to the efficiency of the extremely strong likelihood cut, a very general optimization algorithm, a genetic algorithm, was chosen for the task. A genetic algorithm is a population based evolutionary algorithm that is modeled after inheritance in genetics with *crossover* of parent genomes (i.e. in this specific case: cut values). For simplicity it this was done with the help of the TMVA (Toolkit for MultiVariate data Analysis) toolkit [202] with a standard population of 300. Initial conditions were set around reasonable cut values set by hand at the stage most cut variables were first explored to improve chances of convergence near a global instead of a random local maximum. The cut parameter combination being optimized are all cuts described in Section 8.4.3.

The optimization was chosen for maximum number of signal events while removing all background in the evaluation data set. This is almost identical to requiring maximum significance or comparable requirements because a realistic exotic signal can be assumed to be of the order of only a few events per year *at best*, a rate that is two orders of magnitude lower than the available air shower M.C. statistics.

Single Track Cuts

Having removed the background of coincident air shower muons up to the level possible by simulations data alone without further assumptions, one has reached a background purity where the number of muon tracks induced by neutrinos can no longer be ignored. Optimizing cuts for significance by a machine learning does not make much sense anymore for the remaining events if the optimization is

done down to a level that is 1 - 2 orders of magnitude lower than the air shower statistics.

This is best illustrated in an example: A low $\mathcal{O}(1)$ event signal expectation could possibly benefit from cuts with a reduction of single track background events from 1 to 0.1 if that is the only contributing background, even at the cost of sizable $(10 - 20\%)$ loss in signal efficiency if this is the only contributing background. If another, unknown, background is added that can be in the range of $\mathcal{O}(100)$ events, however, one clearly is going to lose significance from the same cut in a large amount of cases.

Technically, the unknown background expectation can be taken into account in a (semi-)Bayesian way when optimizing but this only leads to an optimization close to the known uncertainty of the background rate $\mathcal{O}(100)$. None such optimization has any effect on the ability of claiming a discovery of exotic double tracks in a completely *blind* fashion using statistics alone. The real flux of exotic double tracks at the detector would have to be in the range of $\mathcal{O}(1000)$ well separated tracks per year. No model predicts even close to such an amount of flux. Moreover, any model like this would already have been clearly visible in the burn sample events.

The choice was thus made to do the cuts removing single track events in a heuristic fashion. The surviving events in the neutrino dataset as well as exotic events with a small track separation (< 100 m) served as a baseline for single track events.

While some of the previous quality cuts do remove a certain percentage of very clear single track events, the reconstruction and cut parameters so far are rather inefficient at removing tracks below 100-150 m of reconstructed separation. Signal simulation with 1-100 m separation (M.C. truth) shows that the reconstruction at these low separations scatters up to 150 m - irrespective of the true separation. This amount of minimum separation was thus chosen as a reliable cut value. Before doing the cut and losing all but a few (low weight) neutrino events, the events were also used to inform the *likelihood ratio*-like cut. Due to the relatively large amount of neutrino events clipping the *flat* bottom of the detector volume producing parallel tracks a cut on the center of (charge) gravity was also implemented. The cut values here were chosen by eye. Doing these three cuts has the effect of removing all simulated background events - apart from a handful neutrino events with very low weight.

Due to the danger of ending up with a high number of events in the final data set and thus getting only a very bad upper limit from the available data, several attempts were made to model background rates at the after the 150 m track separation cut level. Both predictions using a generalized linear model that reproduces the effects of the cuts and their correlations as well as predictions using multivariate *decision trees* - or rather forests - were tried. Ultimately no solution

that was deemed both stable and clearly without bias was found that yielded a prediction below the already known rates of the burn sample.

One has to see though, that even the burn sample has to be treated as a non-blind data sample here that could also already have parts of signal in it.

The lack of a reliable background prediction means that the analysis can not make any signal discovery and so it was decided to treat any event as possible signal for a pure - and very robust - upper limit. Figure 47 shows how an upper limit compares with a confidence interval encompassing the approximate knowledge of CORSIKA air showers due to the M.C. statistics. However, due to the danger of still finding multiple events and a final quality cut (see Section 8.4.5) was introduced that removes more typical background events. The cut can be seen as a gamble, since it was not clear at this point to what degree the loss in signal efficiency associated with it would undo its potential. It is tuned for at least one of the tracks to show a clean signature of a long track (removing coincident events) and the other track having at least mediocre quality (removing extra *tracks* that are only made up by low quality scattered photons or noise hits).

The quality cut also happens to remove all remaining neutrino events.

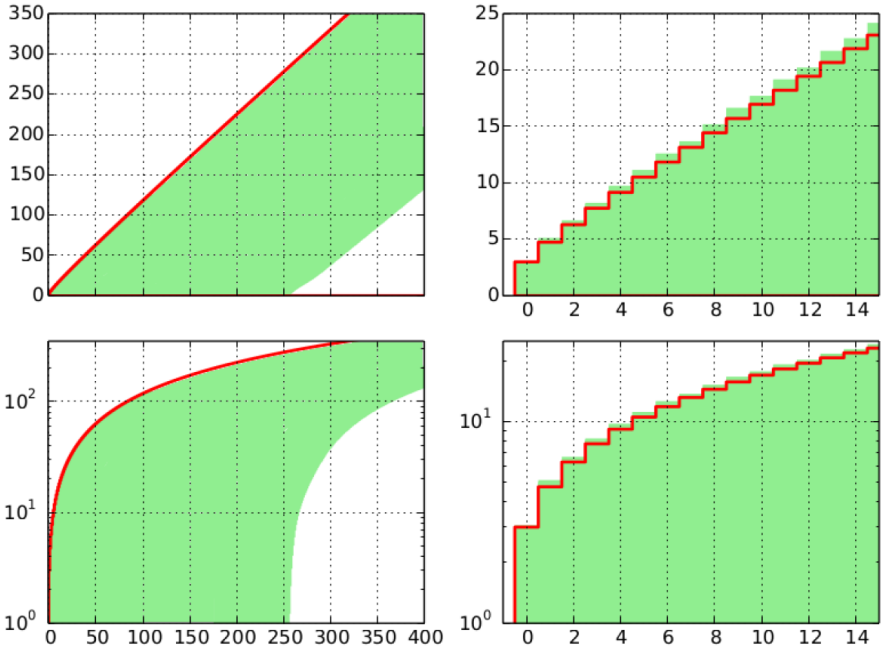

Figure 47: Comparing the number of events seen (x-axis) with the confidence interval of the signal events. The pure upper limit is shown in red. The green area is the union of the Feldman-Cousins confidence intervals when varying the background from null to the approximate knowledge of CORSIKA data M.C. statistics for a year of data taking. Note that these are event number confidence intervals and not fluxes - efficiencies are not included.

Cut Order

Having set and finalized all cut values (compare Table 2), only the order of cuts was changed to improve the processing time. Some of the fast quality cuts imposed further to the end of the analysis were swapped and moved to the start and any of the extremely slow likelihood reconstructions were moved to a later cut level. The datasets at their respective cut level are shown and discussed in Appendix A.

cut name	min	max	notes	optimized
DOMs with signal (a.k.a. NCh)	18	300	quality cut	-
strings with signal (a.k.a. NString)	4		quality cut	-
distance of ToI linefits [m] angle of ToI linefits [rad]	70 0.2		THIS OR THIS	-
z position of CoG [m]	-350		0 is the center of IceCube	-
zenith angle (linefit) [°]	90	180	require up-going tracks	-
zpattern	0		remove down-going topology	+
tpattern [ns]	28.3	195	charge weighted standard deviation of pulse hits	+
time gap [ns]	0	1294	biggest time gap between one hit and the next	+
speed of each k-means linefit [m/ns]	0.23	0.36	remove coincident events that do not match $v \approx c = 0.3$ m/ns	+
distance of k-means linefits [m] angle of k-means linefits [rad]	70 0	 0.3	single and coincident quality cut THIS AND THIS	-
zenith angle of each k-means linefit [°]	90	180	require up-going tracks	-
k-means distortion	76.1		removes coincident events	+
angle of likelihood fit [rad]	0	0.39	only optimized opening angle cut (linefit is fallback)	+
parallel likelihood variable $\text{logl}_{\text{double track fit}}/(\text{NCh} - 4)$		6.9	strongest cut variable, heavily correlated to other cuts	+
likelihood ratio variable $\text{rlogl}_{\text{single track fit}} - \text{rlogl}_{\text{double track fit}}$		-1.2	remove events that do not look much more like double tracks	-
distance of closest pair of fits [m]	150		mostly removes the random (but rare) upward fluctuations	-
quality parameter Q [m] (other, lower Q track)	500 (150)		remove tracks with few HLC hits along them	-

Table 2: Cuts and their respective parameters.

'The Answer to the Great Question... Of Life, the Universe and Everything... Is... Forty-two', said Deep Thought, with infinite majesty and calm.

— Douglas Adams, *The Hitch Hiker's Guide to the Galaxy*

10 RESULTS

At this point of the analysis all parameters had been fixed and the analysis strategy fixed as a pure upper limit search. The analysis was thus performed on the remaining data set that had not been *burned* before (compare Section 9.1.2). The complete livetime of data used was 279 days, 17 hours and 54 minutes. Of all planned runs, only a single 1h run (117014) was not used due to a missing calibration file.

The result was no data surviving the complete chain of cuts.

In order to see if the additional quality cut was warranted, the events surviving all but this cut were examined - yet knowing that it would not be possible to remove this final cut without introducing a bias. In the end, two events could be observed at this level (see Figure 48 and Figure 49). Both are fine examples of exactly the kind of events the cut was designed to suppress. One event resembles a coincident topology with a very divided clusters of hits and one with a clear track going through DeepCore accompanied by only two SLC hits that make up the total light yield of the second *reconstructed* track. This track so is with high probability just noise, but in any case of extremely low quality. Comparing a possible limit that could have been computed using these two events with the final limit calculations (no events) shows a small improvement in the overall limit for most cases. Only for double tracks that are just slightly below the horizon there is a small loss in efficiency when applying the additional quality cut.

Overall the question about the importance of the final quality cut for further analyses stays somewhat inconclusive due to the low statistics, but clearly the cut variable does remove relevant background events and it should be studied further. The consequences of the null finding and limit result is shown in the next chapter where the systematic uncertainties are also dealt with.

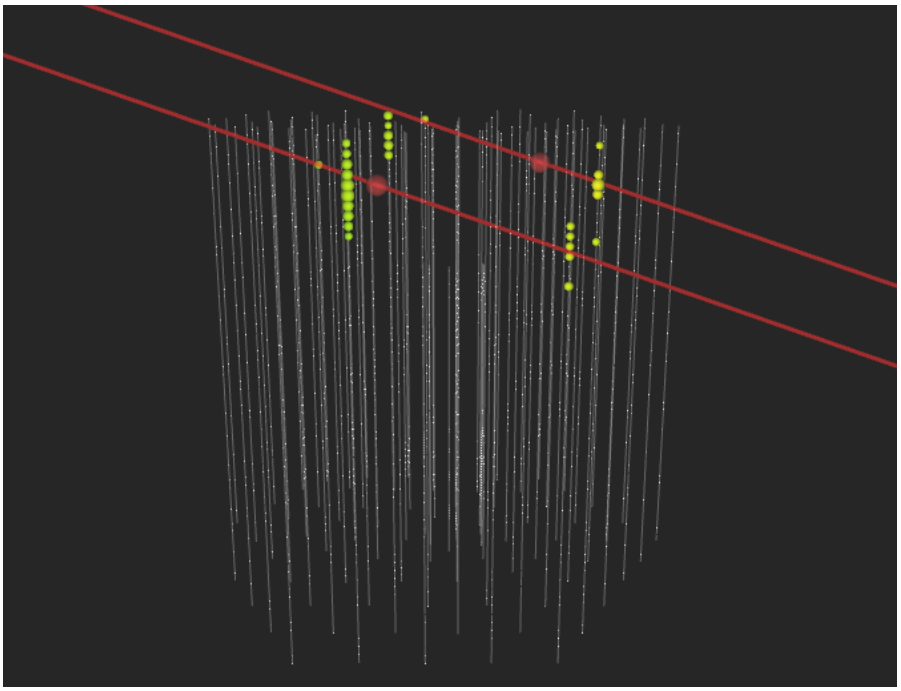

Figure 48: An event that shows the typical *coincident topology* it has in common with most background events in the analysis.

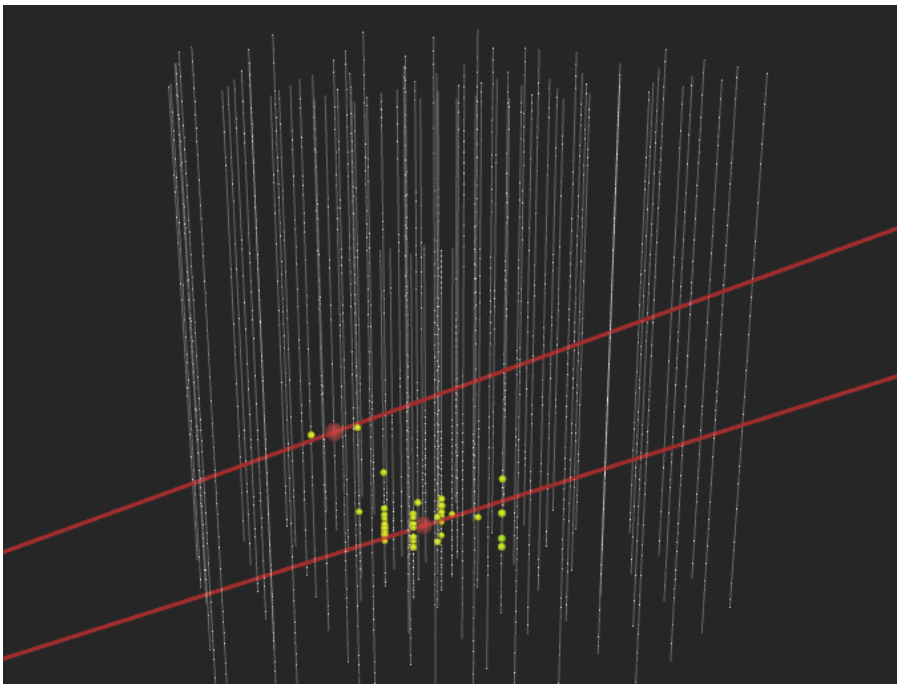

Figure 49: An event with a clear track through DeepCore. The other reconstructed *track* only consists of two SLC hits.

The Guide is definitive.
Reality is frequently inaccurate.

.

— Douglas Adams, *The Hitchhiker's Guide to the Galaxy*

11

SYSTEMATIC UNCERTAINTIES

With an ideal experiment and full knowledge about all possible outside factors as well as a complete and perfectly accurate modeling of the experiment itself, the uncertainty of the measurement of a variable only really depends on the statistics of the measured variable. The longer such an experiment goes on or the more often it is repeated, the more accurate the measurement generally gets - though there are often diminishing returns.

Note that perfect modeling of an experiment is not the same as it perfectly measuring the variable in question.

No real experiment, however, is perfectly modeled. Measurement errors that are caused by inaccurate modeling are generally known as systematic errors. Unlike statistical errors, repeating an experiment or (increasing the exposure for a counting experiment) does not help to reduce their impact on the measurement. The contributions to the systematic uncertainties are often quite varied. They can, for example, be simply tied to the imperfect knowledge of the quantum efficiency of a detector. They can also be tied to imprecisions in some parts of the theoretical description. For instance, the background modeling, like an air shower computer code, always has a multitude of inaccuracies in its underlying variables. Sometimes the systematic uncertainties can also be quite subtle. The commonly used Monte-Carlo technique has an intrinsic uncertainty. Even with perfect knowledge of all variables, the (pseudo)probabilistic approach means that the precision is also limited by the amount of simulated data. The associated problems this has in the current analysis have been discussed in the previous chapters.

Of course, air showers are also often part of the signal modeling.

How well the boundaries and interdependencies of these uncertainties are known can often vary wildly. Sometimes one has only, at best, a handful of different models for some aspect of the experiment. The detector medium a neutrino telescope is surrounded by or the air of the atmosphere an air shower develops in are prime examples. In this case one often has to fall back to varying between the models and seeing the effects of the (simulated) experiment to at least get an approximation of the effects. The interdependence of this modeling with other detector effects - like the aforementioned quantum efficiency of optical modules - can sometimes be quite opaque. On the other hand effects like the uncertainties introduced by limited M.C. statistics are quite easy to narrow down by statistical analysis and are in many cases almost guaranteed to be perfectly independent of other errors.

This chapter discusses all the main systematic errors that are involved both in this analysis specifically as well as similar analyses that could be built upon it and how they effect the results of the anal-

ysis. Taking all the uncertainties into account one can put the null observation of the previous chapter into an upper limit for double tracks *at the detector*. This is shown at the end of the chapter.

11.1 MONTE CARL STATISTICS

The lack of Monte Carlo statistics for the most common kinds of background simulation has already been discussed in detail. In the current analysis the background exact uncertainty plays no role in the resulting limit calculation. There are two equivalent ways to rationalize the situation depending on one's point of view. It could be so because the background rate is also being measured - it is the upper limit of *all* events, including the background events. The alternative view is that the background event uncertainty does play a role but it is conservatively assumed to be *infinitely high*.

Conversely, the M.C. statistics of the *signal* simulation does not play a role in any case. Since it is easy to simulate many thousands to millions of years of lifetime of rare double track events in a comparatively short time frame, the number of simulated events is not a limiting factor unless one wants to study the correlations of a high number of signal variables. This is not the case in the current work: only two variables - the track distance and the zenith angle of the incoming double tracks - are considered.

11.2 ICE MODE AND PHOTON PROPAGATOR

The modeling and measurement of the ice properties IceCube vicinity have already been mentioned in Section 5.2. The ice models considered in this analysis were the SPICE MIE ice model and the (older) AHA ice model. They describe the scattering and absorption of the ice at varying depths. It is very hard to accurately quantify the error introduced by the fitting procedure used to generate these models in a general way. They depend highly on the cuts of an individual analysis. In this work an approximation is used. The error introduced by the fitting procedure itself is estimated by comparing the event rates of the baseline SPICE MIE and the AHA models. In addition to the fitting procedure there can also be global effects that change these models *at all depths* of the ice layer. For example, an uncertainty in calibration of measurement devices will change the measured scattering of all ice layers in a fixed direction, no matter what fitting strategy is used to produce the ice model. To account for this, the scattering and absorption of all the model ice layers are shifted *globally* by up to 10%. It should be noted here that the measurement of scattering and absorption of the ice is not fully independent. The main effect is in both cases the same and a DOM will see fewer incoming photons

These variations are commonly used for most IceCube analysis.

from a fixed source no matter which of these variables is increased. The further away from the source, the bigger the effect.

Additionally, the properties of the so called *hole ice* near the strings with the optical modules can also be varied in the simulation to account for incorrect modeling.

Even for a fixed ice model, there are still other parameters that can be changed that affect the simulated light propagation. Within the IceCube software framework there exist various computer codes for photon propagation as discussed in Section 7.4. Just like the ice model itself, they can also be changed in order to get an approximate estimate on their effect on event rates. Not all ice models currently in use by the IceCube collaboration are compatible with every photon propagator though, so some cross-variations are not easily possible. The photon propagation codes used in this work are the PHOTONICS and the PPC module.

11.3 DOM EFFICIENCY

A very straightforward error is the uncertainty of the relative DOM efficiency. At first glance it appears similar to the problem of uncertainties in scattering and absorption. Lowered DOM efficiency also reduces the amount of photons that can reach a DOM, just like increased absorption does. Unlike absorption though, this is independent on the distance the photon has to travel to reach the DOM. So the relative effects of uncertainties in the DOM efficiency and the ice modeling and their effects heavily depend on the analysis cuts and reconstructions. The stronger the cleaning and selection of data for photons arriving directly without scattering and produced close to the DOMs, the less important scattering and absorption become. The uncertainties introduced by the effects of DOM efficiency, however, can not be so easily reduced.

11.4 BACKGROUND EVENTS

Although the limit calculation in this analysis uses no information about the background rates and thus is also completely independent on their theoretical errors, it is still instructional to consider the effects in light of possible future double track searches with access to higher M.C. statistics.

11.4.1 *Atmospheric Muons*

As one of the most important backgrounds, the properties of simulated atmospheric muon events must be studied further if one wants to use them for a dependable prediction of mis-reconstructed background events. As discussed in 8.4.2 the air-shower simulation data

used for the IC79 Icecube configuration exhibits a too low muon event rate that influences the rate of coincident events in a non-linear way. Even though simple rescaling of events that are mostly coincident muons showed promise in this work when comparing simulated to real event ratios, there is a need to quantify the error introduced by this approximation. Ideally, new muon simulation datasets will show the right rates and remove the need for this rescaling. It should be noted, though, that even simulation with an adjusted and correct *mean* muon event rate will need further consideration. Any signification varability in muon rates on any time scale - there is *at least* the annual muon flux modulation [203] - will have a higher rate of coincident events than the simple assumption of a fixed muon rate that is assumed in the current IceCube simulation tools. Again, this has to be either accounted for, or fixed in the simulation code itself.

11.4.2 *Neutrino Events*

Adding simple single neutrino events to the background expectation does not introduce many big additional errors beyond their statistics. If any absolute event rate rescaling is needed, this seems to be less problematic. The neutrinos falling into the category of producing double track background event candidates are typically not too far from the TeV range and so in a range that still has a high amount of statistics. They can be well measured without any extrapolation and the errors introduced here will be small. Stringent energy dependent cuts uncertainties in neutrino simulation and specific neutrino-cross sections probably do not play a large role as long as the total rate can be fixed because an analysis like the current one does not rely on a detailed energy reconstruction.

Regarding neutrinos that are part of coincident IceCube events, though, the same considerations as in Section 11.4.1 must be taken. Since these events are so similiar to the much more common situation with two coincident muons, it might be possible that this kind of event stays sub-dominant even with higher M.C. statistics.

11.4.3 *Di-Muon Events*

Like discussed before, for a single year of data and the current analysis scheme, di-muon events are another clearly sub-dominant background compared to mis-reconstructions. In a significantly improved analysis (i.e. multi year, considerable increase in background M.C. statistics, etc.; compare Chapter 12) one will eventually come to a point where these events do play a role. Then they have to be included in the analysis or - at the very least - treated as additional systematic uncertainty that shows up as irreducible background rate. If a similar di-muon simulation is done as conducted within this work

(see Section 7.2.3) a variation of the respective cross sections within their known limits and the inclusion of additional di-muon production channels should also be explored as systematic uncertainty.

11.5 SIGNAL MODELING

Within reasonable explored energy limits 10^3 to 10^7 GeV for a 200 GeV $\tilde{\tau}$ - no clear effect of the energy dependence of the exotic particle energy on the reconstruction efficiency could be found.

Though it seems reasonable that due to the chosen cuts and reconstruction - a minimum required pulses for reconstructions and a very loose maximum measured pulses - higher energy and thus brighter events will be slightly preferred. As such, the later shown limit should automatically also prove to be quite model independent even if some exotic model somehow produces slightly brighter events.

To be exact: DOM channels

There are many additional uncertainties tied to various aspects like production, primary neutrino flux and propagation of exotic particles through the Earth that can have significant effects. All of these effects - including the relevant high energy cosmic neutrino flux - are extremely model dependent. But since these only change the expected signal flux and track separation distribution near the detector - but not the signal efficiency - they can be ignored when calculating an upper limit of the double track flux *in the immediate vicinity of* IceCube.

Of course, this has to be done for each possible track separation.

When this limit is then used to test a *specific* double track model later on, however, these considerations can no longer be avoided.

11.6 INCLUSION OF SYSTEMATIC UNCERTAINTIES

As discussed before, the only remaining uncertainties for the current double track search that treats all potential events as signal, and thus produces a pure upper limit, are the uncertainties for the signal efficiency. These uncertainties were calculated for a fixed track separation (M.C. truth) by combining the effects of the main sources of errors: the DOM efficiency, various effects within the ice model, and the simulated signal statistics of a given track separation bin. The track separation binning was chosen big enough so that the error introduced by signal M.C. statistics is always sub-dominant. The signal simulation was done for double tracks with a separation of up to 1000 m for a number of datasets (see Table 3) while varying the main systematic variables. The chosen combinations of variables follow the typically used variations for systematic datasets of the IC79 season within the IceCube collaboration.

For each track separation bin the result with the highest signal efficiency - and thus most conservative limit - was chosen for the final limit calculation. This automatically takes co-variation between the systematic uncertainties into account and does so in a conservative

icel mode	absorp.	scatt.	photon propagator	DOM sensitivity	modified hole ice?
AHA			PHOTONICS		
SPICE 1			PHOTONICS		
SPICE MIE			PHOTONICS	90%	
SPICE MIE			PHOTONICS		
SPICE MIE			PHOTONICS	110%	
SPICE MIE			PPC		
SPICE MIE	-10%	-10%	PPC	90%	
SPICE MIE			PPC	120%	
SPICE MIE	-10%	-10%	PPC	110%	
SPICE MIE	-10%	-10%	PPC	120%	
SPICE MIE	+10%	+10%	PPC		
SPICE MIE			PPC		100 cm
SPICE MIE			PPC		30 cm
SPICE MIE	-10%	-10%	PHOTONICS		
SPICE MIE	-7.1%	-7.1%	PPC	120%	
SPICE MIE	+10%	+10%	PHOTONICS		
SPICE MIE	+10%	+10%	PPC	90%	

Table 3: Datasets generated for the inclusion of systematic effects. Note that 110% Dom Efficiency is probably closer to the true DOM efficiency. 100% DOM efficiency refers to an outdated baseline still used in the simulation software. This - possibly slightly confusing - labeling has been kept for clarity of the software settings used.

fashion. The small additional error from M.C. statistics of the bin is independent and taken into account by assuming a simple 1-σ interval of the M.C. statistics. The resulting upper limit can be seen in Figure 50. It shows also the dependency of the zenith angle of the incoming double track compared to this *mean upper limit* for an *isotropic* double track flux at the detector. This is computed in a similar fashion by replacing the track separation bins by zenith angle bins. The effects of both these variables are only very weakly correlated.

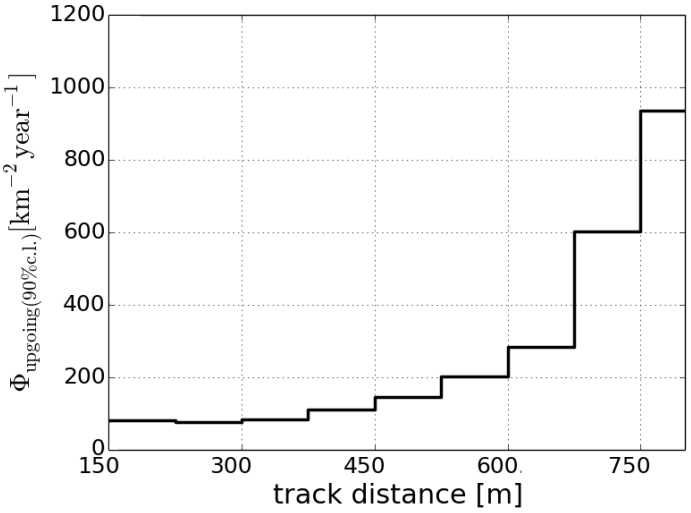

(a) Upper limit of the double track search - including systematic and statistical uncertainties - for varying track separations. The calculation assumes a uniform arrival direction distribution in cos(zenith) for the up-going tracks.

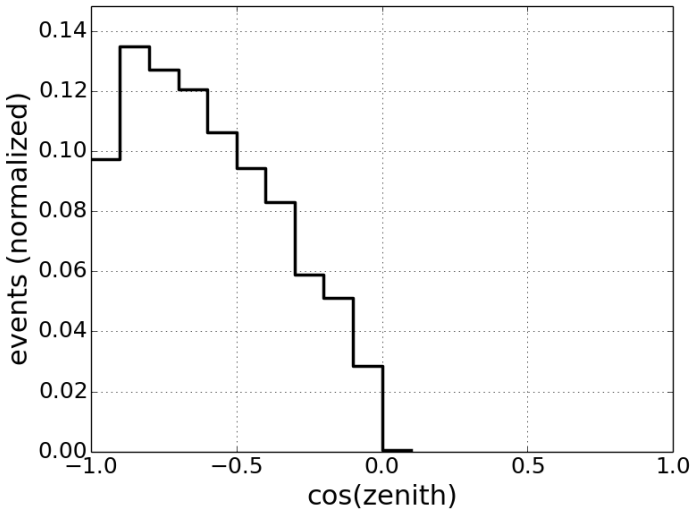

(b) The relative efficiency for different zenith directions of the incoming double tracks. The distribution is only weakly correlated to the track distance efficiency.

Figure 50: Results of the double track search. In order to get specific results the limits shown here have to be convoluted with the separation and zenith probability distributions of the model in question.

Time affords us the ability to blame past errors on others while whole heartedly pronouncing our futures successes.

— Douglas Adams

12

DISCUSSION AND FUTURE IMPROVEMENTS

The results in the previous chapter suggest that an exotic model that is on the verge of being detected could easily accommodate ≈ 100 double tracks with a separation of above 150 m without being detected. In light of this, one can easily see that there still is both room and need for improvement when it comes to the reconstruction efficiency and sensitivity beyond just combining multiple years of data. Moreover, in view of undefined background rates, the inclusion of additional data using the full 86-string IceCube configuration is not even guaranteed to improve the limit one can set on double tracks.

This bears further discussion, especially since any SUSY or UED not in tension with the current collider experiments easily requires improvements of more than an order of magnitude in background-less sensitivity. The most straightforward conceivable improvement is the inclusion of a *double track filter* guided by the reconstruction cuts used in this work and thus no longer being reliant on the muon filter. Its pre-selection of tracks that have a high likelihood of being a single track is, in a way, antithetical to the proposition of looking for two distinct tracks. Removing this requirement has a good chance of significantly improving signal efficiency without adding many additional background events. Furthermore, eventual IceCube detector upgrades might also lead to some opportunities for an enhanced double track search. Combining all these factors might be essential in probing more interesting parameter space.

Additional M.C. Data

Any improvement of the analysis that has the goal of a sensitivity in the single-track-per-year range has an important feature: the need for additional M.C. statistics for standard (both single *and* coincident) neutrino as well as muon backgrounds. Not only does this allow one to actually claim the discovery of a potential double track signal or - at least - improve limit calculations, but it also can be used to inform cuts. It seems plausible that the final quality cuts used in this analysis could then be replaced by precisely tailored cuts, easily leading to an improvement of signal efficiency by a factor of two - if not more.

Adjusted Search Strategies

It is useful to consider two general cases why an exotic double track model - assuming it is realized in nature - would not yet have been detected. One option is that the track separation, while high for SM

particles, is almost exclusively below the chosen reconstruction window of separation (150 m). By comparison with the UED and SUSY models considered by Albuquerque et al. [64, 67] one can assume that this means the model will have rather low particle masses (there: $\approx$ 450 GeV center-of-mass production threshold and squarks/KK[1]-quark masses of $\approx$ 300 GeV). Realistically such models should have been easily observed by the experiments at the LHC.

Still, in the unlikely event that a model has special properties that somehow hide it at collider experiments, it might be desirable to probe for double tracks with separations in the range $100 - 150$ m with IceCube. The best and cleanest option to do searches in this region without upgrades to the detector is to look for *mostly vertical* track separation. After all, inter-DOM spacing is much closer than inter-string spacing. One can not only look for vertical *gaps* in the DOM hit distribution but can also try to reconstruct overlapping light patterns if restricting the reconstruction to direct (i.e. non-scattered) photons.

The downside of this technique is the somewhat limited efficiency: For it to work, the tracks have to both travel close to the string and be mostly vertically separated - a requirement not met by a large fraction of tracks.

Prospects of Detector Upgrades

Using a tighter string space, like it already exists for the DeepCore sub-detector, would be another solution for the problem of detecting tracks with only small separations. Two tracks intersecting DeepCore with a separation of 50 to 100 m should be easily reconstructed as two individual tracks. The issue here is that the current volume of DeepCore, and thus achievable effective area, is not big enough. Even the ideal, purely geometric size of the sub-detector is too small to allow for any measurable flux of double tracks that *both* intersect the more densely instrumented section. Having a detector extension of the size of the *whole* IceCube array with the string separation of DeepCore would be a technical solution. But this is a scenario that is both cost prohibitive and lacking virtually any other physics cases.

The other option for a hidden signal is that, like expected, the double track signal shows a significant amount of high separation tracks in it. The total flux is just too low to be detected. Here the search strategy can mostly be kept as it is - with the exception of a few key areas and detector extensions could be more relevant. A popular consideration for IceCube is a high energy extension with additional strings added outside the current detector volume [204]. The increased geometric area, of course, is directly a chance for an increase of the effective area for double tracks, assuming the exotic tracks do not slip through wide inter-string spacings. Seeing how this is already partially the case for the current instrumentation this will be a chal-

lenge. A less regular string spacing than for the existing array might, however, alleviate the problem. Additional simulations are required to answer this question.

A bigger detector could also help the analysis beyond just improving the geometric cross section of the detector. Muons, unlike CHAMPs, have a limited range on a scale at least somewhat close to the scale of IceCube. If the size of the extended detector is big enough and the energy reconstruction can be done accurately enough, it might be possible to distinguish them from standard model muons when observing very long tracks. This idea also requires further studies. Especially the energy estimation has to be quite exact seeing how while a 400 GeV muon only has a range of up to $\approx$ 1.5 km, a 2 TeV muon already can reach track lengths of $5-6$ km [80] - enough to fully traverse even some extended IceCube array. At the very least, a coincident air shower event can definitely not be mistaken for a long track. These events are the events most prone to be mistaken for a high track separation signal. An interesting aspect here is that, if feasible, this method of CHAMP search does *not* require a double track signature. Only needing a single track to hit the detector is an automatic gain in efficiency.

For a useful energy reconstruction such a multi km track will probably have to pass the current IceCube volume first.

Whether as double tracks or not, CHAMPs remain an interesting signature for exotic Physics and large neutrino observatories are an ideal instrument to further explore this signal.

Part III

APPENDIX

A

ADDITIONAL PLOTS

This appendix shows most of the cut variables at their respective cut order used in the final analysis. It should be stressed again that this cut order is mostly optimized for processing speed and not to show a maximum signal to background improvement at each cut level. Specifically very simple cuts that only require the application of the cut and no additional reconstructions are done very early.

The center of gravity cut is a prime example. It is a quality cut that is done to remove neutrino events that clip the bottom of the detector. The variable is, however, already computed during the tensor-of-inertia reconstruction.

For all cuts shown the horizontal (and vertical) red lines highlight the choices of the cut parameters used in the analysis (see Chapter 9). The histograms are normalized and show the relative distributions for each dataset on a linear scale. For the 2-dimensional plots the color bars show the relative amount of events in the 2-dimensional histogram. Note that these numbers can not necessarily be compared between different datasets. Especially the neutrino dataset has a much higher normalization than the other datasets.

All simulation datasets shown are based on PHOTONICS with SPICE MIE photon tables. The dataset names are:

STAU
: An signal dataset with uniform track separations (1 to 1000 m) and arrival directions

BURN
: The IC79 burn sample

CORSIKA
: Unweighted muon air shower simulation done with CORSIKA (dataset 6451)

NEUTRINO
: NUGEN neutrino dataset with a E^{-1} spectrum weighted to an atmospheric [178] model (dataset 6454)

DIMUON (CHARM)
: A di-muon enriched unweighted dataset for neutrino interactions involving charmed hadrons; based on same atmospheric neutrino model as the NUGEN dataset above (see Chapter 7)

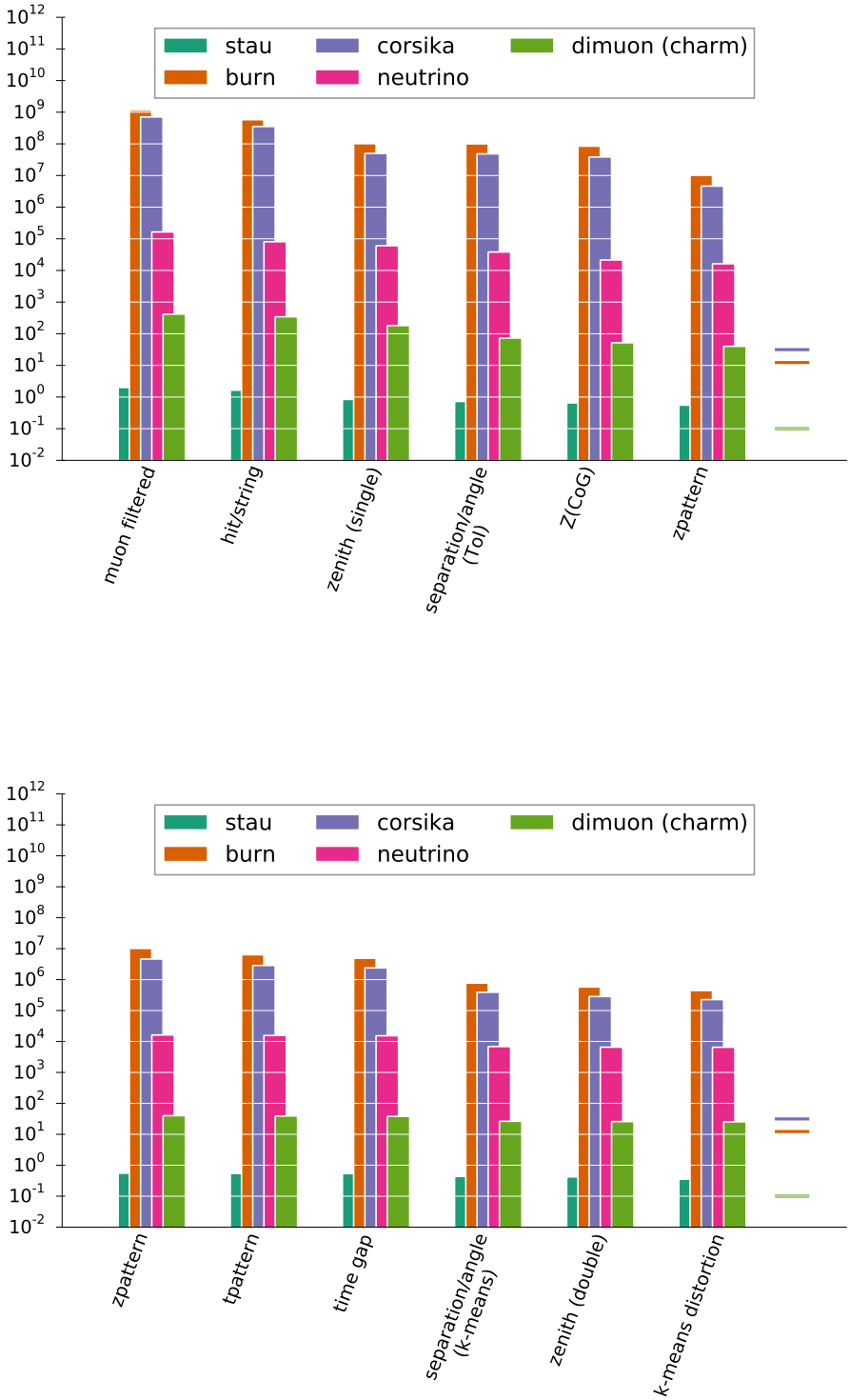

Figure 51: Rate (events per year) for various signal and background datasets. The makers on the right hand side show the limit of statistics (i.e. weight of *one* event for each M.C. limited dataset. The neutrino dataset is an exception and weighted on the per event level.

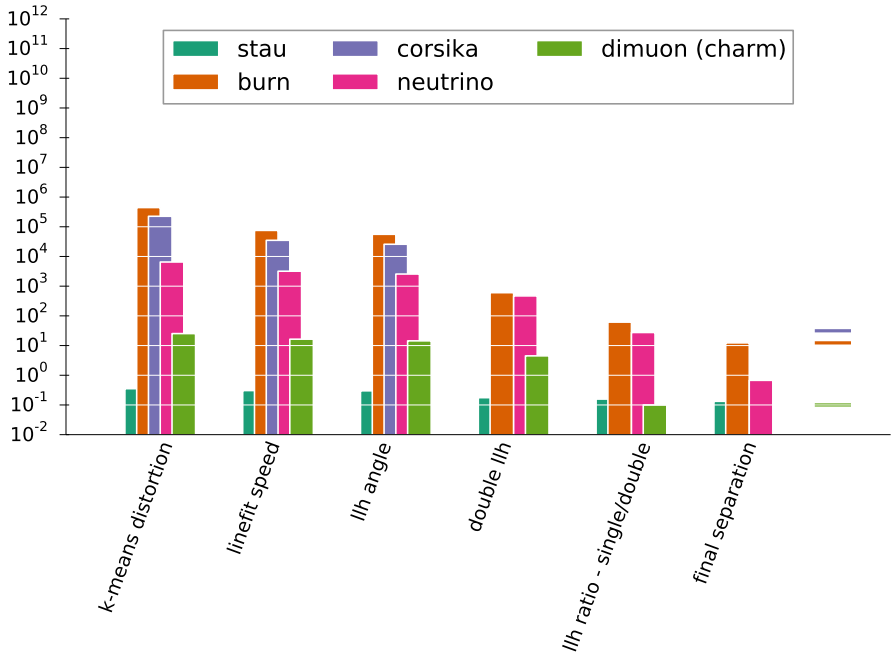

Figure 52: Rate for various signal and background datasets (continued). Not shown is the last data quality cut introduced at the end of the analysis that removes all simulated background events as well as the last burn sample event.

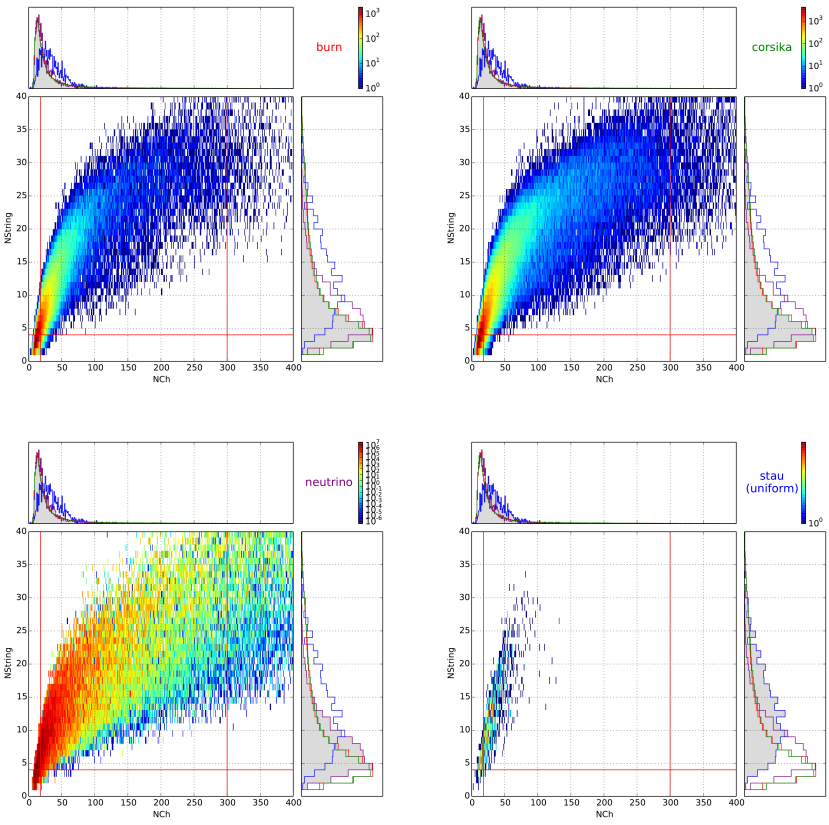

Figure 53: Minimal data quality cut on number of DOMs triggered (*NCh*) and number of DOMs on different strings triggered (*NString*). Mostly a cut for data reduction to speed up reconstruction. First analysis specific cuts.

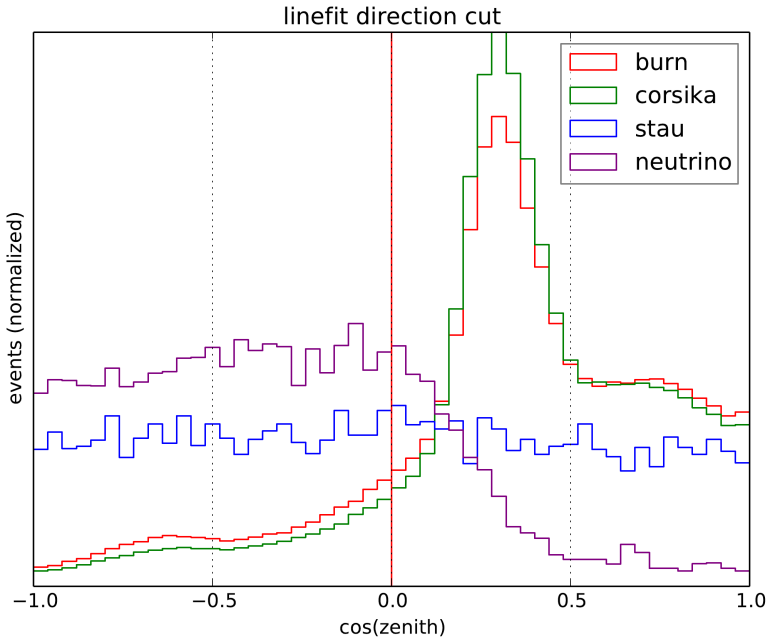

Figure 54: Simple *cut on down-going events* after a global linefit reconstruction. Background data is dominated by single air shower muons at this level. Note that the signal for neutrino induced CHAMPs will be made up of up-going tracks but the simulation was done with a completely uniform arrival direction including down-going tracks.

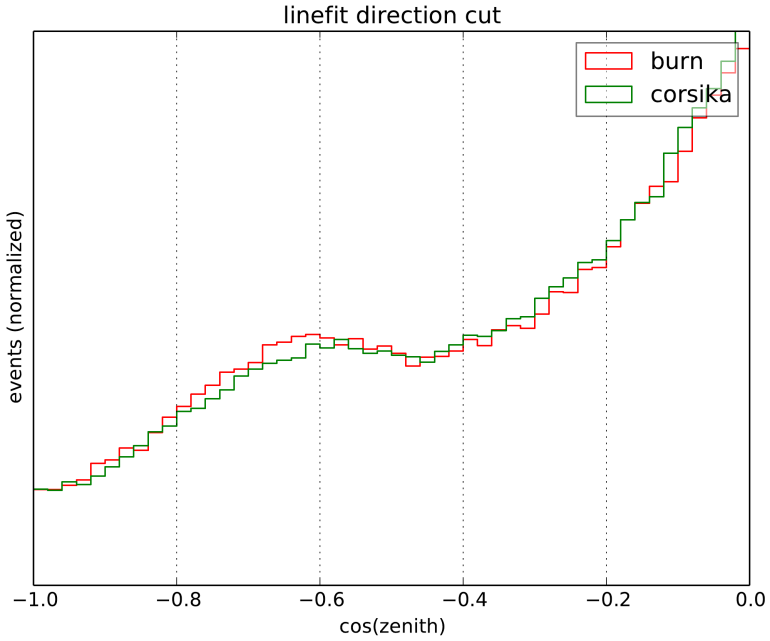

Figure 55: Zenith angle distribution after the zenith cut for simulation data normalized to real data at this cut level. Data is dominated by coincident showers at this level. Data and M.C. shapes agree now.

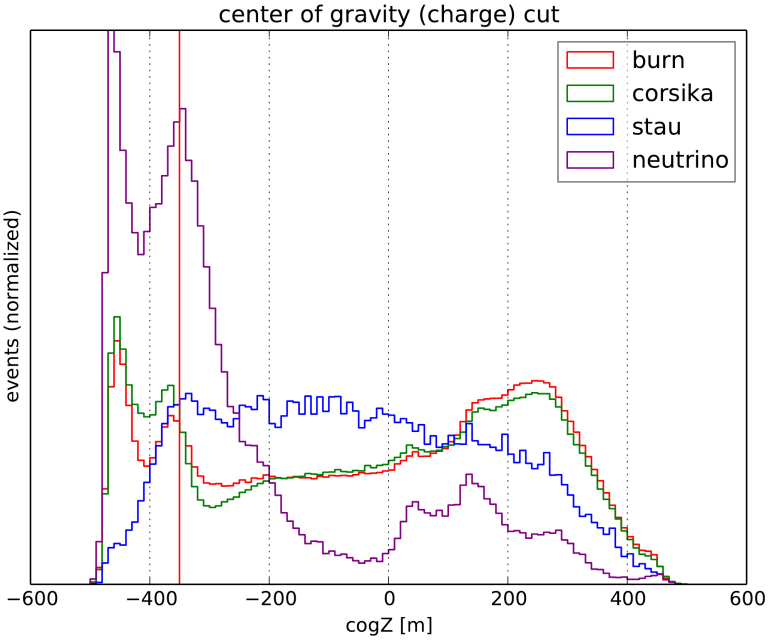

Figure 56: Cut on the *center-of-gravity* of the charge distribution to remove events only clipping at the bottom of the detector. This cut also helps to improve data/M.C. matching.

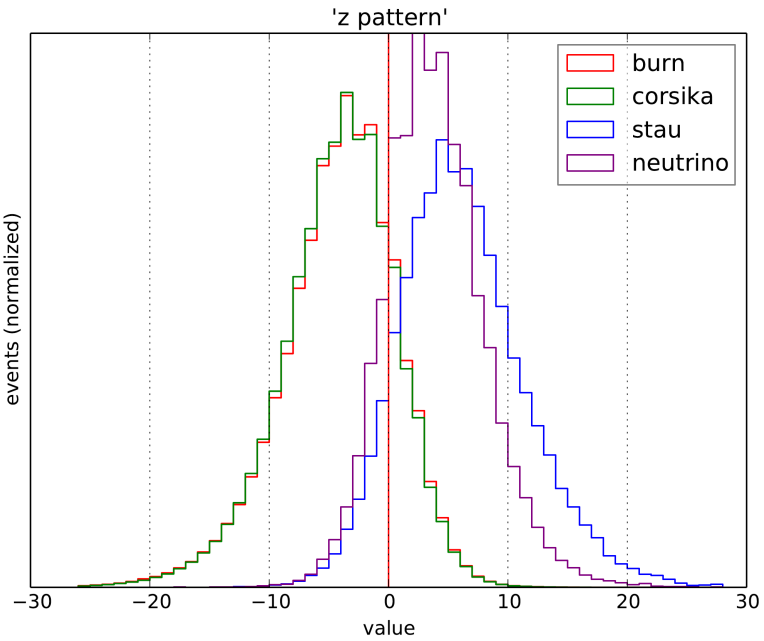

Figure 57: Cut on a parameter that selects for overall up- (z *pattern* > 0) or down-going (z *pattern* < 0) topology of the light pattern in the DOMs. Efficiently removes even coincident down-going muons.

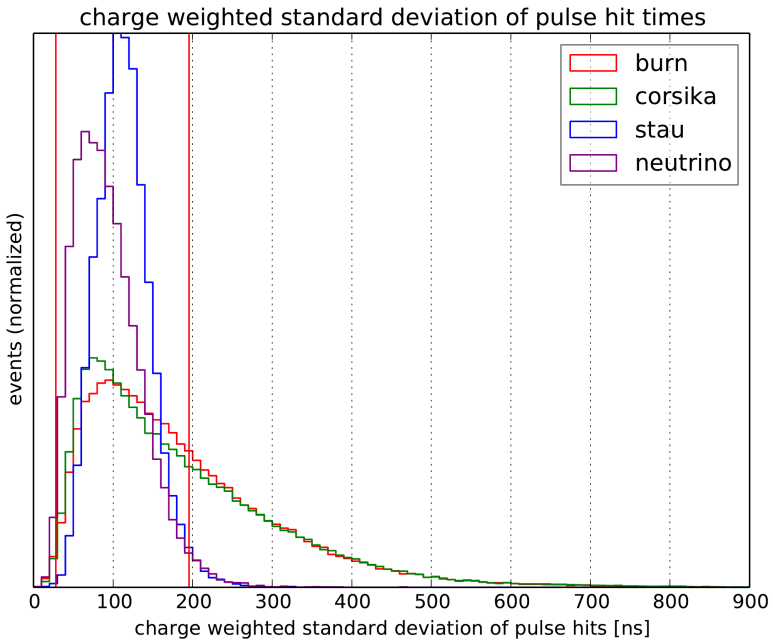

Figure 58: The charge weighted standard deviation of hits in time. A variable that grows with long events, especially if they have large gaps in the time pattern.

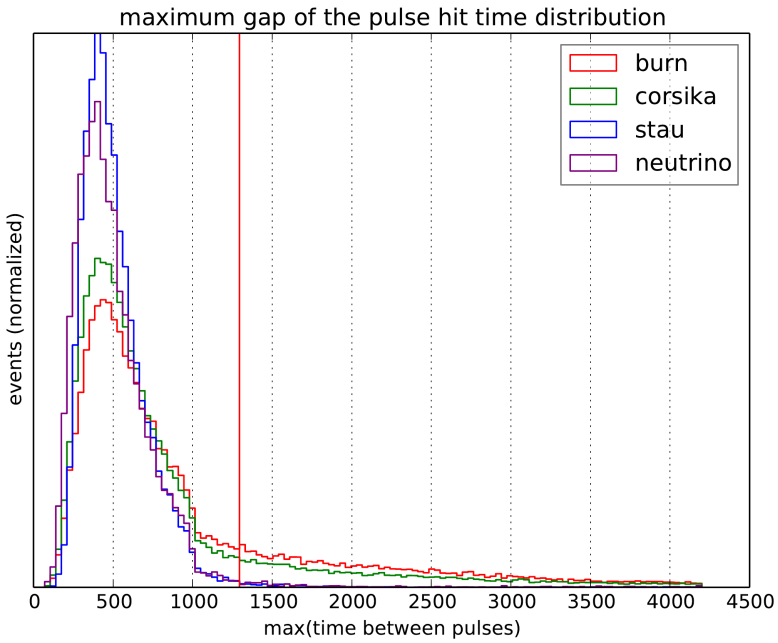

Figure 59: Another time based parameter - the maximum time between each DOM hit to the next within an event. Like the previous cut it removes coincident events with long time gaps between events.

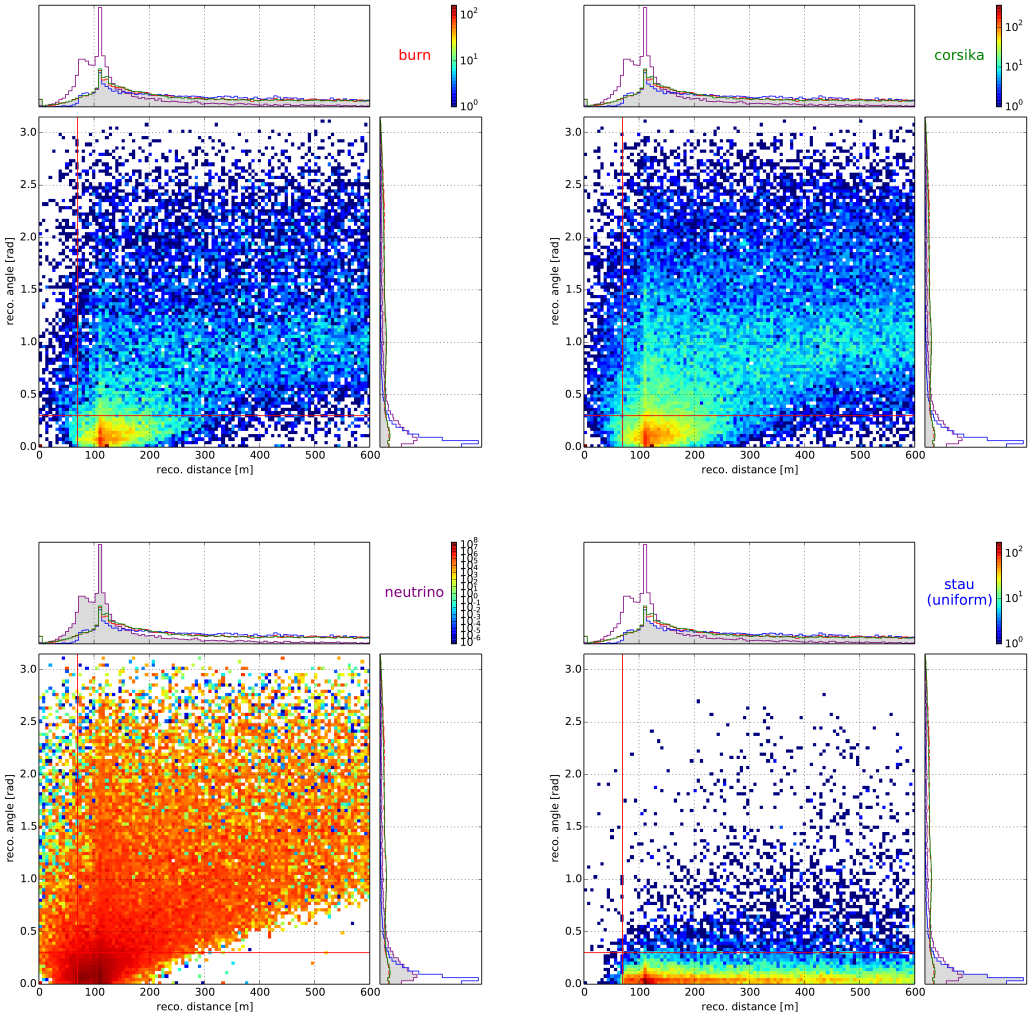

Figure 60: Cut on the double track opening angle and separation distances for the iterative *k-means* reconstructions after which many exotic tracks are already fairly well reconstructed. Removes obvious single track events (low separation), obvious coincident events (large opening angles) and extremely badly reconstructed signal events that are hard to recover in the following reconstruction steps.

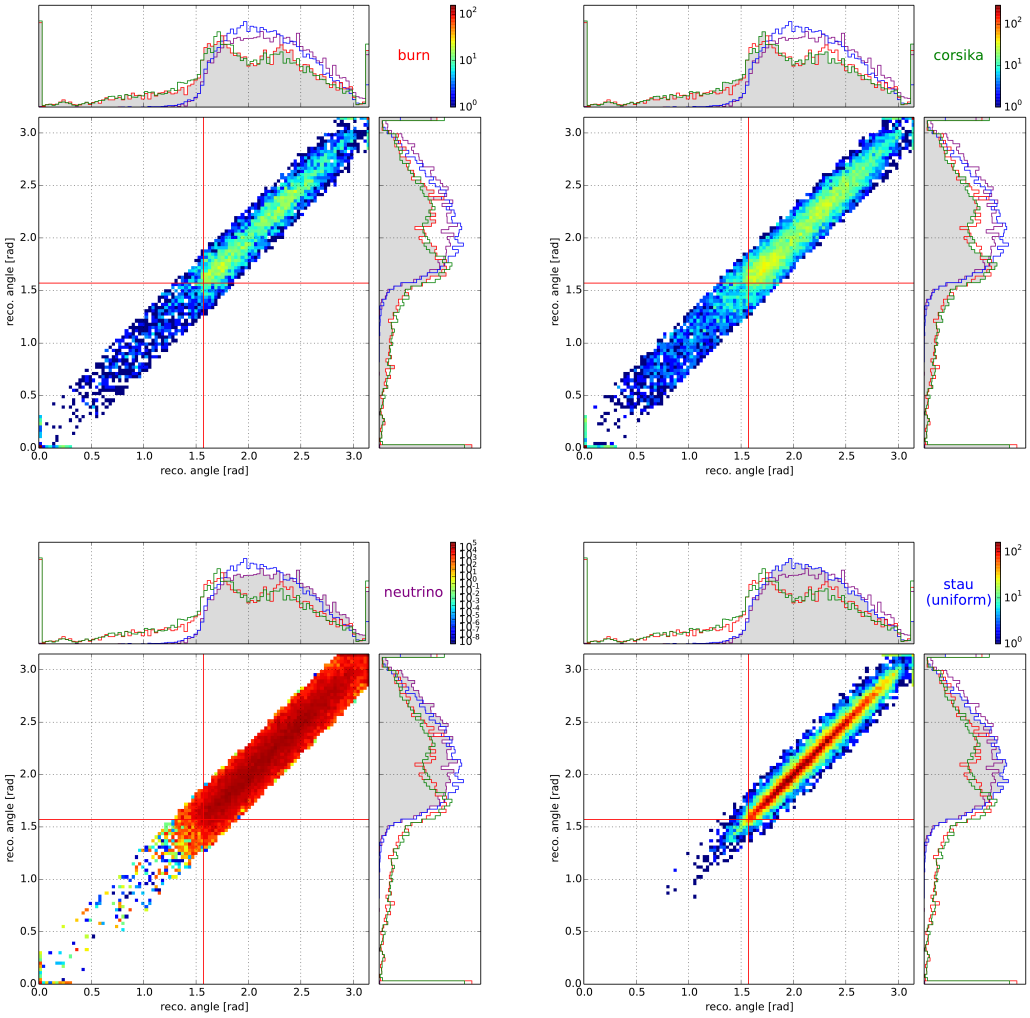

Figure 61: Another cut on down-going events, this time on the separately reconstructed tracks after the k-means reconstruction. It serves as a minor Quality Cut.

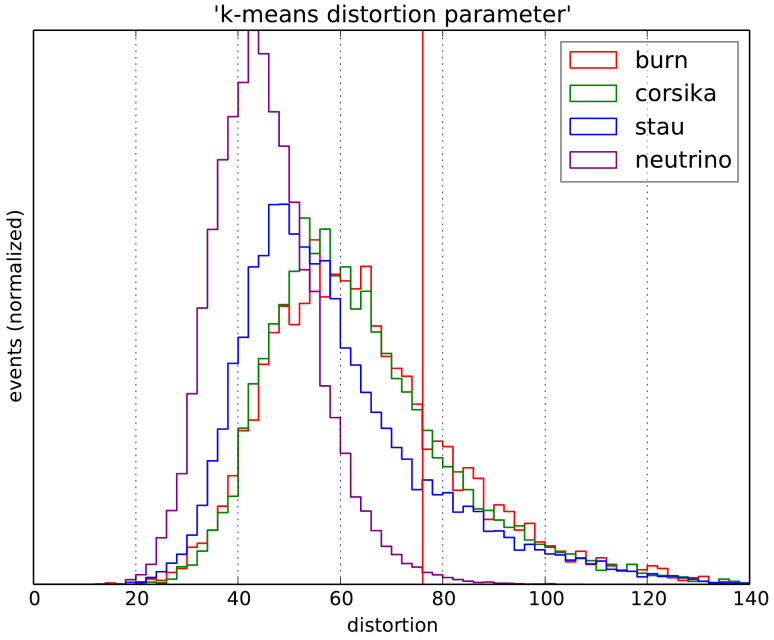

Figure 62: The clustering algorithm is based on minimizing the standard deviation of the hits in the clusters from their respective cluster center. The directions of coincident muons tend to not align with their reconstructed direction. This often causes an additional spread. The same is true for badly reconstructed signal events.

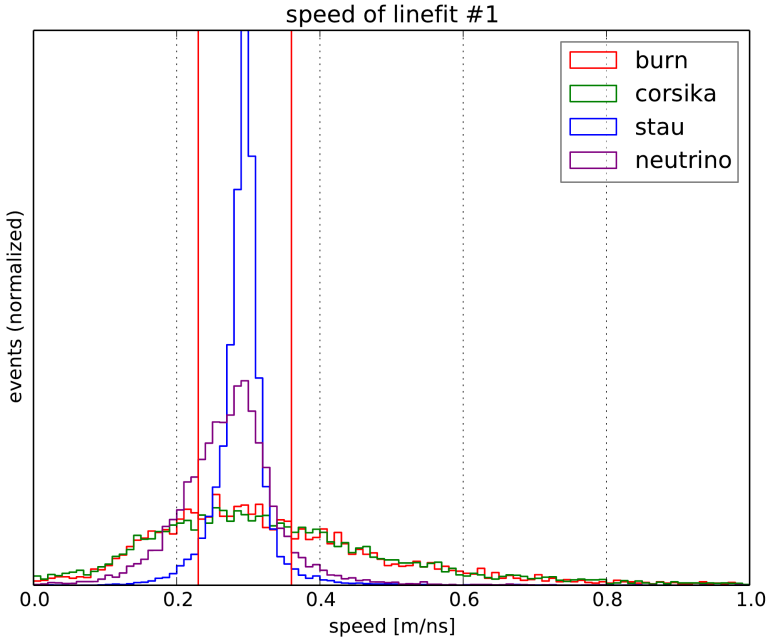

Figure 63: Cut on the variable linefit speed reconstruction. True double tracks have both the speed of light while random coincidences of two events within the trigger time have a larger spread of reconstructed speed. Cut is done for both fits.

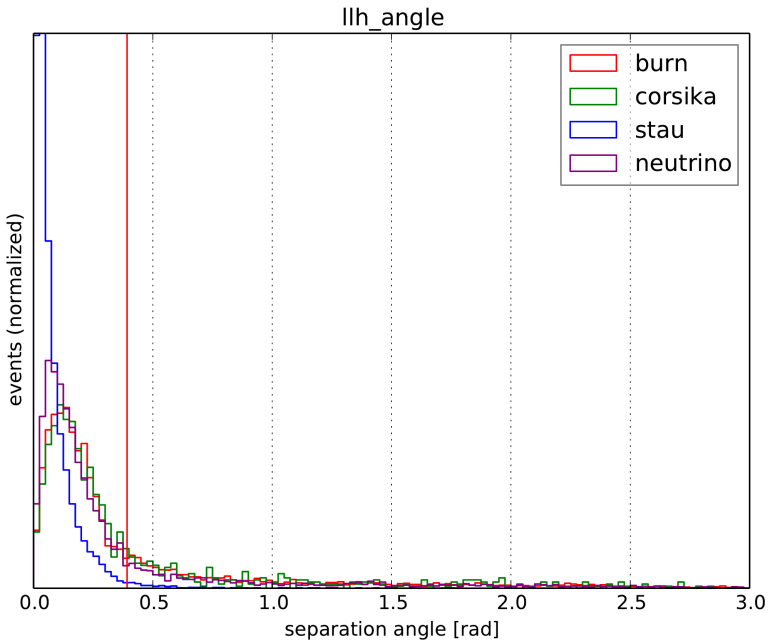

Figure 64: Cut on the opening angle after the (non-parallel) likelihood fit. This is done for each track. Minor quality cut due to the improved reconstruction. If the likelihood fit is not successful the cut is not applied.

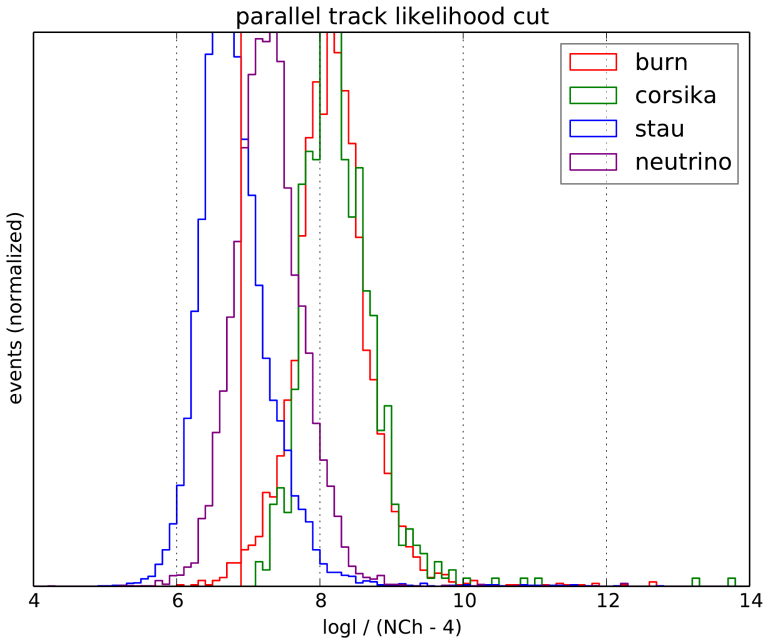

Figure 65: Cut on a likelihood parameter closely related to the (negative) reduced log-likelihood of the fit. Efficient at removing coincident events but can also remove some neutrino events.

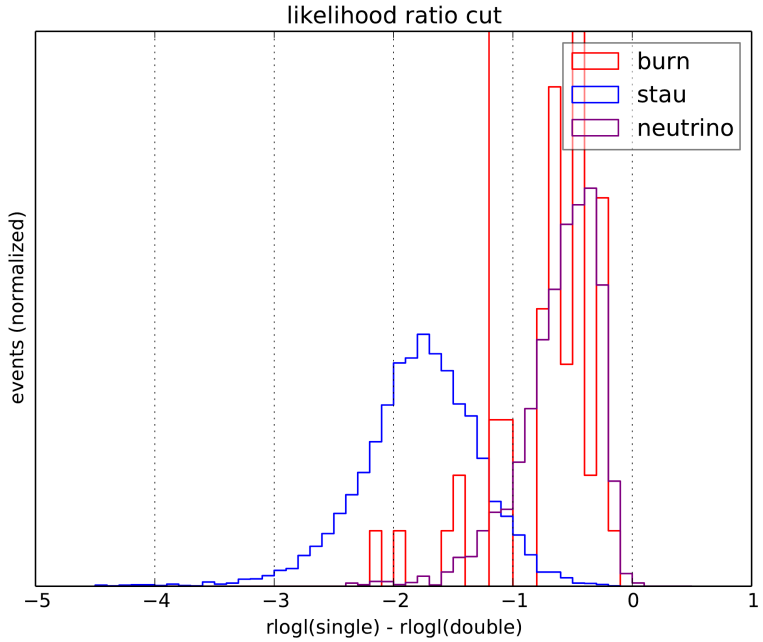

Figure 66: A cut closely related to a kind of likelihood ratio. A cut to remove events that are not clearly more double track like than single track like. (Note that unlike in the rest of this work `rlogl` in this picture is the *positive* logarithmic likelihood - and the sign is reversed.)

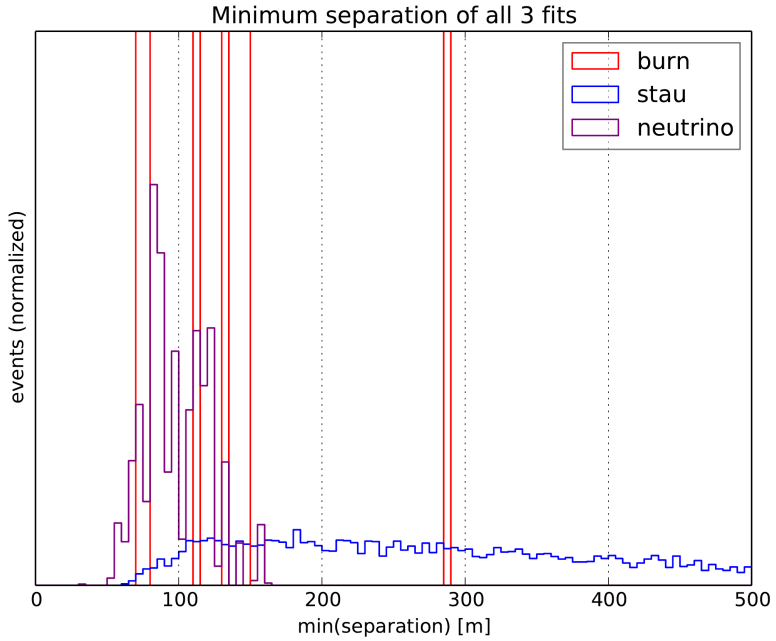

Figure 67: Track separation cut that removes tracks with a separation lower than 150 m. The track separation used for this cut is the *minimum* of the results of any of the fit pairs - i.e. linefit (k-means reco.) and likelihood fits (parallel and non parallel).

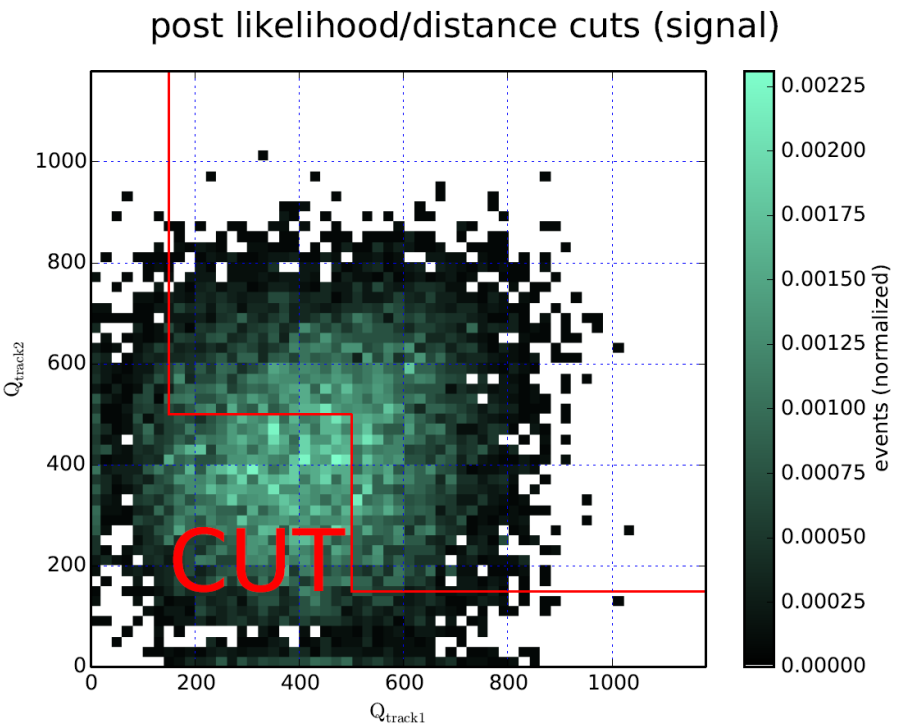

Figure 68: The quality parameter Q for signal events. The cut removes tracks that have only very few HLC hits along or are very short. The cut is chosen in order to require a high quality track and another of at least mediocre quality.

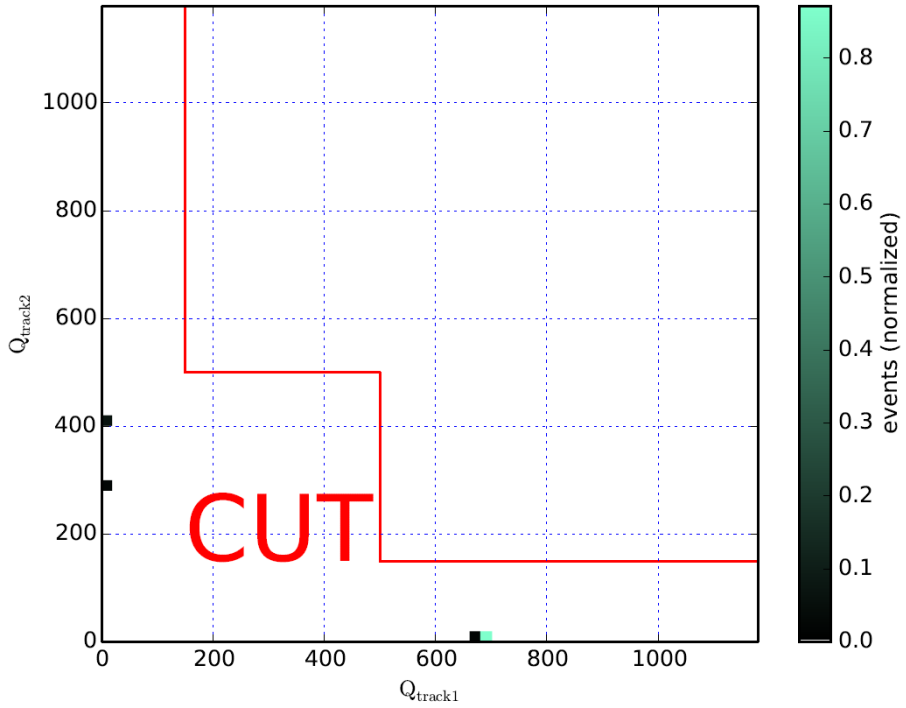

Figure 69: The quality parameter Q for the last surviving neutrino events. They can reach high lengths but one track is usually only scattered light or noise hits (often SLC hits).

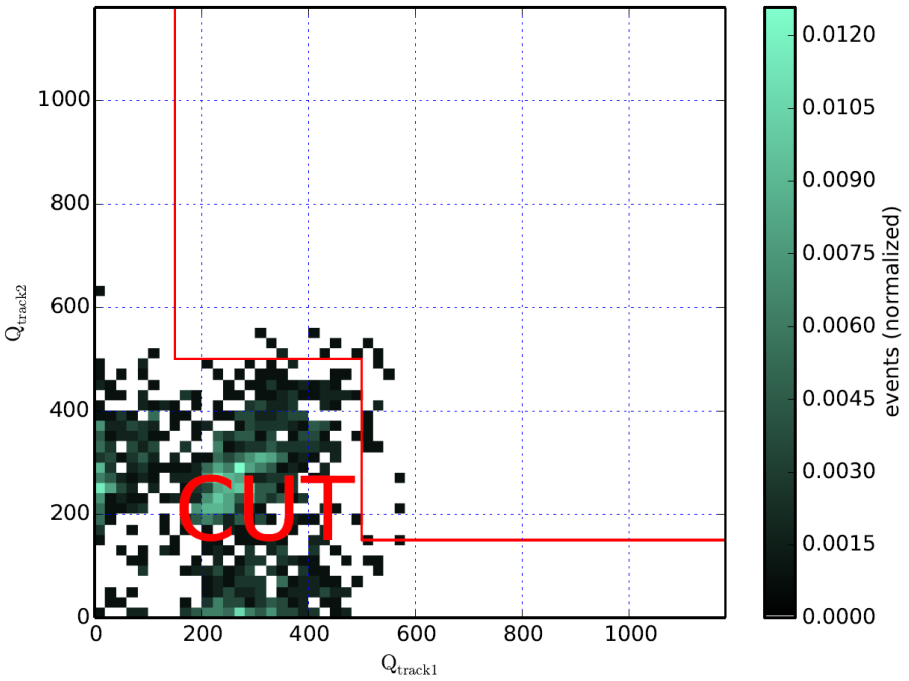

Figure 70: The quality parameter Q for CORSIKA events at an earlier cut level (just before the likelihood and more restrictive track separation cuts). Coincident events tend not to have the highest quality tracks with gaps along the tracks.

BIBLIOGRAPHY

[1] V. Hess, "Über Beobachtungen der durchdringenden Strahlung bei sieben Freiballonfahrten, journal = Physikalische Zeitschrift", 1912.

[2] J. Blumer, R. Engel, and J. R. Horandel, "Cosmic Rays from the Knee to the Highest Energies", *Prog. Part. Nucl. Phys.* **63** (2009) 293–338.

[3] T. K. Gaisser, "Cosmic Rays and Particle Physics", Cambridge University Press, Cambridge, 1990.

[4] **HiRes** Collaboration, R. U. Abbasi *et al.*, "First observation of the Greisen-Zatsepin-Kuzmin suppression", *Phys. Rev. Lett.* **100** (2008) 101101.

[5] M. Takeda *et al.*, "Energy determination in the Akeno Giant Air Shower Array experiment", *Astropart. Phys.* **19** (2003) 447–462.

[6] **Pierre Auger** Collaboration, J. Abraham *et al.*, "Observation of the suppression of the flux of cosmic rays above 4×10^{19}eV", *Phys. Rev. Lett.* **101** (2008) 061101.

[7] M. Nagano, "Search for the end of the energy spectrum of primary cosmic rays", *New J. Phys.* **11** (2009) 065012.

[8] **Particle Data Group** Collaboration, K. Nakamura *et al.*, "Review of Particle Physics", *J. Phys. G* **37** (2010), no. 7A, 075021.

[9] D. R. Bergman and J. W. Belz, "Cosmic Rays: The Second Knee and Beyond", *J. Phys.* **G34** (2007) R359.

[10] M. Nagano, M. Teshima, Y. Matsubara, H. Y. Dai, T. Hara, N. Hayashida, M. Honda, H. Ohoka, and S. Yoshida, "Energy spectrum of primary cosmic rays above 10**17-eV determined from the extensive air shower experiment at Akeno", *J. Phys.* **G18** (1992) 423–442.

[11] **HiRes** Collaboration, D. J. Bird *et al.*, "Evidence for correlated changes in the spectrum and composition of cosmic rays at extremely high-energies", *Phys. Rev. Lett.* **71** (1993) 3401–3404.

[12] A. V. Glushkov and M. I. Pravdin, "Yakutsk EAS array data on the variations in intensities of the highest energy cosmic rays", *JETP Lett.* **73** (2001) 115–117, [Pisma Zh. Eksp. Teor. Fiz.73,131(2001)].

[13] K. Greisen, "End to the cosmic ray spectrum?", *Phys. Rev. Lett.* **16** (1966) 748–750.

[14] G. T. Zatsepin and V. A. Kuzmin, "Upper limit of the spectrum of cosmic rays", *JETP Lett.* **4** (1966) 78–80, [Pisma Zh. Eksp. Teor. Fiz. 4 (1966) 114].

[15] F. W. Stecker, "Photodisintegration of ultrahigh-energy cosmic rays by the universal radiation field", *Phys. Rev.* **180** (1969) 1264–1266.

[16] J. L. Puget, F. W. Stecker, and J. H. Bredekamp, "Photonuclear Interactions of Ultrahigh-Energy Cosmic Rays and their Astrophysical Consequences", *Astrophys. J.* **205** (1976) 638–654.

[17] M. A. Malkan and F. W. Stecker, "An empirically based model for predicting infrared luminosity functions, deep infrared galaxy counts and the diffuse infrared background", *Astrophys. J.* **555** (2001) 641–649.

[18] F. W. Stecker and M. H. Salamon, "Photodisintegration of ultrahigh-energy cosmic rays: A New determination", *Astrophys. J.* **512** (1999) 521–526.

[19] F. W. Stecker, M. A. Malkan, and S. T. Scully, "Intergalactic photon spectra from the far ir to the uv lyman limit for $0 < Z < 6$ and the optical depth of the universe to high energy gamma-rays", *Astrophys. J.* **648** (2006) 774–783.

[20] M. de Naurois and D. Mazin, "Ground-based detectors in very-high-energy gamma-ray astronomy", *Comptes Rendus Physique* **16** (2015) 610–627.

[21] **Fermi-LAT** Collaboration, W. B. Atwood *et al.*, "The Large Area Telescope on the Fermi Gamma-ray Space Telescope Mission", *Astrophys. J.* **697** (2009) 1071–1102.

[22] W. I. Axford, E. Leer, and J. McKenzie, "The structure of cosmic ray shocks", *Astronomy and Astrophysics* **111** (1982) 317–325.

[23] E. Dorfi, "Cosmic ray production rates in supernova remnants", *Astrophysics and Space Science* **272** no. 1, 227–238.

[24] D. Lazzati and R. Perna, "Short Gamma Ray Bursts: Marking the Birth of Black Holes from Coalescing Compact Binaries", arXiv:1001.0538.

[25] W. S. Paciesas *et al.*, "The Fourth batse gamma-ray burst catalog (revised)", *Astrophys. J. Suppl.* **122** (1999) 465–495.

[26] J. S. Bloom, S. R. Kulkarni, and S. G. Djorgovski, "The Observed offset distribution of gamma-ray bursts from their host galaxies: A Robust clue to the nature of the progenitors", *Astron. J.* **123** (2002) 1111–1148.

[27] S. Campana *et al.*, "The shock break-out of grb 060218/sn 2006aj", *Nature* **442** (2006) 1008–1010.

[28] H.-T. Lieb, Elliott H.; Yau, "A rigorous examination of the Chandrasekhar theory of stellar collapse", *Astrophysical Journal.* 140–144.

[29] C. D. Dermer, "The Collapsar and supranova models", in "On recent developments in theoretical and experimental general relativity, gravitation, and relativistic field theories. Proceedings, 10th Marcel Grossmann Meeting, MG10, Rio de Janeiro, Brazil, July 20-26, 2003. Pt. A-C", pp. 461–482. 2004.

[30] J. Arons, "Magnetars in the metagalaxy: an origin for ultrahigh-energy cosmic rays in the nearby universe", *Astrophys. J.* **589** (2003) 871–892.

[31] G. Henri, G. Pelletier, P. O. Petrucci, and N. Renaud, "Active galactic nuclei as high-energy engines", *Astropart. Phys.* **11** (1999) 347–356.

[32] P. Bhattacharjee and G. Sigl, "Origin and propagation of extremely high-energy cosmic rays", *Phys. Rept.* **327** (2000) 109–247.

[33] H. C. Spruit, "Essential Magnetohydrodynamics for Astrophysics", arXiv:1301.5572.

[34] E. M. d. G. D. Pino, P. P. Piovezan, and L. H. S. Kadowaki, "The role of magnetic reconnection on jet/accretion disk systems", *Astron. Astrophys.* **518** (2010) A5.

[35] M. G. Baring, "Diffusive shock acceleration: The Fermi mechanism", in "Very high-energy phenomena in the universe. Proceedings, 32nd Rencontres de Moriond, Les Arcs, France, January 18-25, 1997", pp. 97–106. 1997.

[36] E. Fermi, "On the Origin of the Cosmic Radiation", *Phys. Rev.* **75** (1949) 1169–1174.

[37] M. Bustamante *et al.*, "High-energy cosmic-ray acceleration", 2010, https://cds.cern.ch/record/1249755.

[38] G. Sigl, "High Energy Neutrinos and Cosmic Rays", *Proc. Int. Sch. Phys. Fermi* **182** (2012) 145–184.

[39] F. Halzen, R. A. Vazquez, T. Stanev, and H. P. Vankov, "The highest energy cosmic ray", *Astropart. Phys.* **3** (1995) 151–156.

[40] F. Halzen and E. Zas, "Neutrino fluxes from active galaxies: A Model independent estimate", *Astrophys. J.* **488** (1997) 669–674.

[41] F. W. Stecker, C. Done, M. H. Salamon, and P. Sommers, "High-energy neutrinos from active galactic nuclei", *Phys. Rev. Lett.* **66** (1991) 2697–2700, [Erratum: Phys. Rev. Lett.69,2738(1992)].

[42] E. Waxman and J. N. Bahcall, "High-energy neutrinos from cosmological gamma-ray burst fireballs", *Phys. Rev. Lett.* **78** (1997) 2292–2295.

[43] F. W. Stecker, C. Done, M. H. Salamon, and P. Sommers, "High-energy neutrinos from active galactic nuclei", *Phys. Rev. Lett.* **66** May (1991) 2697–2700.

[44] E. Waxman and J. N. Bahcall, "High-energy neutrinos from astrophysical sources: An Upper bound", *Phys. Rev.* **D59** (1999) 023002.

[45] **IceCube** Collaboration, R. Abbasi *et al.*, "An absence of neutrinos associated with cosmic-ray acceleration in γ-ray bursts", *Nature* **484** (2012) 351–353.

[46] H.-N. He, R.-Y. Liu, X.-Y. Wang, S. Nagataki, K. Murase, and Z.-G. Dai, "Icecube non-detection of GRBs: Constraints on the fireball properties", *Astrophys. J.* **752** (2012) 29.

[47] **IceCube** Collaboration, M. G. Aartsen *et al.*, "First Observation of PeV-Energy Neutrinos with IceCube", *Phys. Rev. Lett.* **111** (2013) 021103.

[48] P. Auger, P. Ehrenfest, R. Maze, J. Daudin, and R. A. Fréon, "Extensive Cosmic-Ray Showers", *Rev. Mod. Phys.* **11** Jul (1939) 288–291.

[49] W. Heitler, "The Quantum Theory of Radiation", Ox-ford University Press, London, 3 ed., 1954.

[50] J. Matthews, "A Heitler model of extensive air showers", *Astropart. Phys.* **22** (2005) 387–397.

[51] **Particle Data Group** Collaboration, J. Beringer *et al.*, "Review of Particle Physics", *Phys. Rev.* **D86** (2012) 010001.

[52] A. A. Kochanov, T. S. Sinegovskaya, and S. I. Sinegovsky, "High-energy cosmic ray fluxes in the Earth atmosphere: calculations vs experiments", *Astropart. Phys.* **30** (2008) 219–233.

[53] J. I. Illana, M. Masip, and D. Meloni, "Atmospheric lepton fluxes at ultrahigh energies", *JCAP* **0909** (2009) 008.

[54] T. K. Gaisser, "Atmospheric neutrinos in the context of muon and neutrino radiography", *Earth Planets Space* **62** (2010) 195–199.

[55] P. Gondolo, G. Ingelman, and M. Thunman, "Charm production and high-energy atmospheric muon and neutrino fluxes", *Astropart. Phys.* **5** (1996) 309–332.

[56] D. Heck, G. Schatz, T. Thouw, J. Knapp, and J. N. Capdevielle, "CORSIKA: A Monte Carlo code to simulate extensive air showers", *FZKA-6019*, 1998.

[57] **Super-Kamiokande** Collaboration, Y. Fukuda *et al.*, "Evidence for Oscillation of Atmospheric Neutrinos", *Phys. Rev. Lett.* **81** (1998) 1562–1567.

[58] P. Jain, J. P. Ralston, and G. M. Frichter, "Neutrino absorption tomography of the earth's interior using isotropic ultrahigh-energy flux", *Astropart. Phys.* **12** (1999) 193–198.

[59] P. A. Cherenkov, "Visible emission of clean liquids by action of gamma radiation", *Doklady Akademii Nauk SSSR* **2** (1934) 451.

[60] S. Buitink, J. Bacelar, R. Braun, G. de Bruyn, H. Falcke, O. Scholten, K. Singh, B. Stappers, R. Strom, and R. a. Yahyaoui, "The NuMoon experiment: first results", arXiv:0808.1878.

[61] G. A. Askar'yan, "Excess negative charge of an electron-photon shower and its coherent radio emission", *Sov. Phys. JETP* **14** (1962), no. 2, 441–443, [Zh. Eksp. Teor. Fiz.41,616(1961)].

[62] L. Radel, "Simulation studies of the cherenkov light yield from relativistic particles in high-energy neutrino telescopes with geant4", Master's thesis, RWTH Aachen, 2012.

[63] K. Hagiwara *et al.*, "Review of Particle Physics", *The European Physical Journal* **C15** (2000) 163–173.

[64] I. F. M. Albuquerque, G. Burdman, and Z. Chacko, "Direct detection of supersymmetric particles in neutrino telescopes", *Phys. Rev.* **D75** (2007) 035006.

[65] D. E. Groom, N. V. Mokhov, and S. I. Striganov, "Muon stopping power and range tables 10-MeV to 100-TeV", *Atom. Data Nucl. Data Tabl.* **78** (2001) 183–356.

[66] M. H. Reno, I. Sarcevic, and S. Su, "Propagation of supersymmetric charged sleptons at high energies", *Astropart. Phys.* **24** (2005) 107–115.

[67] I. F. M. Albuquerque *et al.*, "Direct detection of Kaluza-Klein particles in neutrino telescopes", *Phys. Rev. D* **78** (2008) 015010.

[68] M. Ahlers, J. Kersten, and A. Ringwald, "Long-lived staus at neutrino telescopes", *JCAP* **0607** (2006) 005.

[69] J. Blumer, R. Engel, and J. R. Horandel, "Cosmic Rays from the Knee to the Highest Energies", *Prog. Part. Nucl. Phys.* **63** (2009) 293–338.

[70] F. Reines and C. L. Cowan, "The neutrino", *Nature* **178** (1956) 446–449.

[71] **Planck** Collaboration, P. A. R. Ade *et al.*, "Planck 2013 results. XVI. Cosmological parameters", *Astron. Astrophys.* **571** (2014) A16.

[72] F. Halzen and D. Hooper, "High-energy neutrino astronomy: The Cosmic ray connection", *Rept. Prog. Phys.* **65** (2002) 1025–1078.

[73] A. Roberts, "The Birth of high-energy neutrino astronomy: A Personal history of the DUMAND project", *Rev. Mod. Phys.* **64** (1992) 259–312.

[74] **DUMAND** Collaboration, J. Babson *et al.*, "Cosmic Ray Muons in the Deep Ocean", *Phys. Rev.* **D42** (1990) 3613–3620.

[75] **BAIKAL** Collaboration, V. Aynutdinov *et al.*, "Search for a diffuse flux of high-energy extraterrestrial neutrinos with the nt200 neutrino telescope", *Astropart. Phys.* **25** (2006) 140–150.

[76] **NESTOR** Collaboration, G. Aggouras *et al.*, "A measurement of the cosmic-ray muon flux with a module of the NESTOR neutrino telescope", *Astropart. Phys.* **23** (2005) 377–392.

[77] **ANTARES** Collaboration, J. A. Aguilar *et al.*, "First results of the Instrumentation Line for the deep-sea ANTARES neutrino telescope", *Astropart. Phys.* **26** (2006) 314–324.

[78] E. Migneco, "Progress and latest results from Baikal, Nestor, NEMO and KM3NeT", *J. Phys. Conf. Ser.* **136** (2008) 022048.

[79] E. Bugaev, T. Montaruli, Y. Shlepin, and I. A. Sokalski, "Propagation of tau neutrinos and tau leptons through the earth and their detection in underwater / ice neutrino telescopes", *Astropart. Phys.* **21** (2004) 491–509.

[80] D. Chirkin and W. Rhode, "Muon Monte Carlo: A High-precision tool for muon propagation through matter", arXiv:hep-ph/0407075.

[81] M. Kowalski, "On the reconstruction of cascade-like events in the amanda detector", Master's thesis, Humboldt Universitat zu Berlin, 1999.

[82] O. B. Bigas, O. Deligny, K. Payet, and V. Van Elewyck, "UHE tau neutrino flux regeneration while skimming the Earth", *Phys. Rev.* **D78** (2008) 063002.

[83] S. L. Glashow, "Resonant Scattering of Antineutrinos", *Phys. Rev.* **118** (1960) 316–317.

[84] **IceCube** Collaboration, M. G. Aartsen *et al.*, "Probing the origin of cosmic rays with extremely high energy neutrinos using the IceCube Observatory", *Phys. Rev.* **D88** (2013) 112008.

[85] J. Ahrens *et al.*, "Icecube preliminary design document". http://www.icecube.wisc.edu/science/publications/pdd/pdd.pdf, 10 2001. Revision 1.24.

[86] F. Halzen and S. R. Klein, "IceCube: An Instrument for Neutrino Astronomy", *Rev. Sci. Instrum.* **81** (2010) 081101.

[87] F. Halzen and D. Hooper, "High-energy neutrino astronomy: The Cosmic ray connection", *Rept. Prog. Phys.* **65** (2002) 1025–1078.

[88] F. Halzen, "IceCube: The Rationale for Kilometer-Scale Neutrino Detectors", arXiv:0910.0436.

[89] **IceCube** Collaboration, R. Abbasi *et al.*, "IceTop: The surface component of IceCube", *Nucl. Instrum. Meth.* **A700** (2013) 188–220.

[90] **IceCube** Collaboration, S. Hussain, "Measurements of the cosmic ray spectrum and average mass with IceCube", *Adv. Space Res.* **53** (2014) 1470–1475.

[91] **IceCube** Collaboration, R. Abbasi *et al.*, "The Design and Performance of IceCube DeepCore", *Astropart. Phys.* **35** (2012) 615–624.

[92] M. Ackermann *et al.*, "Optical properties of deep glacial ice at the South Pole", *J. Geophys. Res.* **111** (2006), no. D13, D13203.

[93] **IceCube** Collaboration, M. G. Aartsen *et al.*, "Measurement of South Pole ice transparency with the IceCube LED calibration system", *grum. Meth.* **A711** (2013) 73–89.

[94] N. E. Bramall, R. C. Bay, K. Woschnagg, R. A. Rohde, and P. B. Price, "A deep high-resolution optical log of dust, ash, and stratigraphy in South Pole glacial ice", *Geophysical Research Letters* **32** (2005), no. 21, n/a–n/a, L21815.

[95] D. Chirkin, "Study of South Pole ice transparency with IceCube flashers", in "Proceedings, 32nd International Cosmic Ray Conference (ICRC 2011)", vol. 4, p. 161.

[96] **IceCube** Collaboration, A. Achterberg *et al.*, "First Year Performance of The IceCube Neutrino Telescope", *Astropart. Phys.* **26** (2006) 155–173.

[97] **IceCube** Collaboration, R. Abbasi *et al.*, "The IceCube Data Acquisition System: Signal Capture, Digitization, and Timestamping", *Nucl. Instrum. Meth.* **A601** (2009) 294–316.

[98] **IceCube** Collaboration, R. Abbasi *et al.*, "Calibration and Characterization of the IceCube Photomultiplier Tube", *Nucl. Instrum. Meth.* **A618** (2010) 139–152.

[99] S. Kleinfelder, "Gigahertz waveform sampling and digitization circuit design and implementation", *Nuclear Science, IEEE Transactions on* **50** Aug (2003) 955–962.

[100] "Internal document". http://wiki.icecube.wisc.edu/index.php/ATWD, accessed May 27, 2015.

[101] **IceCube** Collaboration, "The IceCube Collaboration: Contributions to the 30th International Cosmic Ray Conference (ICRC 2007)", in "Proceedings, 30th International Cosmic Ray Conference (ICRC 2007)". 2007.

[102] C. Bohm, H. Kavianipour, D. Nygren, C. Robson, C. Wernhoff, and G. Wikstrom, "A low energy muon trigger for Icecube", in "Proceedings, 2008 IEEE Nuclear Science Symposium, Medical Imaging Conference and 16th International Workshop on Room-Temperature Semiconductor X-Ray and Gamma-Ray Detectors (NSS/MIC 2008 / RTSD 2008)", pp. 2784–2787. 2008.

[103] "Internal document". http://docushare.icecube.wisc.edu/dsweb/Get/Document-45193/2010_TFT_StringTriggerProposal.pdf, accessed January 3, 2015.

[104] **IceCube** Collaboration, M. G. Aartsen *et al.*, "The IceCube Neutrino Observatory Part V: Neutrino Oscillations and Supernova Searches", in "Proceedings, 33rd International Cosmic Ray Conference (ICRC2013)". 2013.

[105] T. Glusenkamp, "On the detection of subrelativistic magnetic monopoles with the icecube neutrino observatory", Master's thesis, RWTH Aachen, 2010.

[106] "Internal document". http://wiki.icecube.wisc.edu/index.php/IC77EHEFilter, accessed May 27, 2015.

[107] "Internal document". http://docushare.icecube.wisc.edu/dsweb/Get/Document-52559/2010_TFT_CascadeFilter.pdf, accessed May 27, 2015.

[108] "Internal document". http://docushare.icecube.wisc.edu/dsweb/Get/Document-52485/2010_TFT_LowUp_proposal.pdf, accessed May 27, 2015.

[109] "Internal document". http://docushare.icecube.wisc.edu/dsweb/Get/Document-52488/2010_TFT_DeepCore_SMT_Filter_HLC.pdf, accessed May 27, 2015.

[110] "Internal document". http://docushare.icecube.wisc.edu/dsweb/Get/Document-52529/2010_TFT_MuonFilterv1p1-1.pdf, accessed April 15, 2015.

[111] G. D'Agostini, "A Multidimensional unfolding method based on Bayes' theorem", *Nucl. Instrum. Meth.* **A362** (1995) 487–498.

[112] G. Cowan, "A survey of unfolding methods for particle physics", *Conf. Proc.* **C0203181** (2002) 248–257.

[113] D. Chirkin, "Feature extraction of icecube waveforms. (Internal Document)". http://icecube.wisc.edu/~dima/work/LBNL/reader/docs/fe/fe.pdf, accessed February 22, 2015.

[114] **AMANDA** Collaboration, J. Ahrens *et al.*, "Muon track reconstruction and data selection techniques in AMANDA", *Nucl. Instrum. Meth.* **A524** (2004) 169–194.

[115] J. Lundberg, P. Miocinovic, T. Burgess, J. Adams, S. Hundertmark, P. Desiati, K. Woschnagg, and P. Niessen, "Light tracking for glaciers and oceans: Scattering and absorption in heterogeneous media with Photonics", *Nucl. Instrum. Meth.* **A581** (2007) 619–631.

[116] **IceCube** Collaboration, R. Abbasi *et al.*, "An improved method for measuring muon energy using the truncated mean of dE/dx", *Nucl. Instrum. Meth.* **A703** (2013) 190–198.

[117] **CMS** Collaboration, S. Chatrchyan *et al.*, "Observation of a new boson at a mass of 125 GeV with the CMS experiment at the LHC", *Phys. Lett.* **B716** (2012) 30–61.

[118] **ATLAS** Collaboration, G. Aad *et al.*, "Observation of a new particle in the search for the Standard Model Higgs boson with the ATLAS detector at the LHC", *Phys. Lett.* **B716** (2012) 1–29.

[119] C. Rovelli, "Notes for a brief history of quantum gravity", in "Recent developments in theoretical and experimental general relativity, gravitation and relativistic field theories. Proceedings, 9th Marcel Grossmann Meeting, MG'9, Rome, Italy, July 2-8, 2000. Pts. A-C", pp. 742–768. 2000.

[120] H. Georgi and S. L. Glashow, "Unity of All Elementary Particle Forces", *Phys. Rev. Lett.* **32** (1974) 438–441.

[121] A. J. Buras, J. R. Ellis, M. K. Gaillard, and D. V. Nanopoulos, "Aspects of the Grand Unification of Strong, Weak and Electromagnetic Interactions", *Nucl. Phys.* **B135** (1978) 66–92.

[122] S. P. Martin, "A Supersymmetry primer", arXiv:hep-ph/9709356, [Adv. Ser. Direct. High Energy Phys.18,1(1998)].

[123] F. Zwicky, "Die Rotverschiebung von extragalaktischen Nebeln", *Helvetica Physica Acta* **6** (1933) 110–127.

[124] C. S. Frenk and S. D. M. White, "Dark matter and cosmic structure", *Annalen Phys.* **524** (2012) 507–534.

[125] **Supernova Search Team** Collaboration, A. G. Riess *et al.*, "Observational evidence from supernovae for an accelerating universe and a cosmological constant", *Astron. J.* **116** (1998) 1009–1038.

[126] P. J. E. Peebles and B. Ratra, "The Cosmological constant and dark energy", *Rev. Mod. Phys.* **75** (2003) 559–606.

[127] **ATLAS and CMS** Collaboration, G. Aad *et al.*, "Combined Measurement of the Higgs Boson Mass in pp Collisions at $\sqrt{s} = 7$ and 8 TeV with the ATLAS and CMS Experiments", *Phys. Rev. Lett.* **114** (2015) 191803.

[128] H. Baer and X. Tata, "Experimental consequences of supersymmetry", in "Properties of SUSY particles. Proceedings, 23rd Workshop of the INFN Eloisatron project, Erice, Italy, September 28-October 4, 1992". 1992.

[129] A. Masiero and L. Silvestrini, "Pre-LHC SUSY searches: An Overview", in "Particle physics and cosmology. Proceedings, 1st Tropical Workshop, San Juan, Puerto Rico, April 1-7, 1998. High-energy physics. Proceedings, 2nd Latin American Symposium, SILAFAE'98, San Juan, Puerto Rico, April 8-11, 1998". 1998.

[130] M. Misiak, S. Pokorski, and J. Rosiek, "Supersymmetry and FCNC effects", *Adv. Ser. Direct. High Energy Phys.* **15** (1998) 795–828.

[131] S. Dimopoulos and H. Georgi, "Softly Broken Supersymmetry and SU(5)", *Nucl. Phys.* **B193** (1981) 150.

[132] A. Signer, "ABC of SUSY", *J. Phys.* **G36** (2009) 073002.

[133] I. J. R. Aitchison, "Supersymmetry and the MSSM: An Elementary introduction", arXiv:hep-ph/0505105.

[134] **Particle Data Group** Collaboration, K. A. Olive *et al.*, "Review of Particle Physics", *Chin. Phys.* **C38** (2014) 090001.

[135] G. C. Branco, P. M. Ferreira, L. Lavoura, M. N. Rebelo, M. Sher, and J. P. Silva, "Theory and phenomenology of two-Higgs-doublet models", *Phys. Rept.* **516** (2012) 1–102.

[136] K. Griest, "Cross-Sections, Relic Abundance and Detection Rates for Neutralino Dark Matter", *Phys. Rev.* **D38** (1988) 2357, [Erratum: Phys. Rev.D39,3802(1989)].

[137] J. R. Ellis, J. F. Gunion, H. E. Haber, L. Roszkowski, and F. Zwirner, "Higgs Bosons in a Nonminimal Supersymmetric Model", *Phys. Rev.* **D39** (1989) 844.

[138] Z. Komargodski and N. Seiberg, "From Linear SUSY to Constrained Superfields", *JHEP* **09** (2009) 066.

[139] S. Dimopoulos and D. W. Sutter, "The Supersymmetric flavor problem", *Nucl. Phys.* **B452** (1995) 496–512.

[140] C. F. Berger, J. S. Gainer, J. L. Hewett, and T. G. Rizzo, "Supersymmetry Without Prejudice", *JHEP* **02** (2009) 023.

[141] A. Djouadi, J.-L. Kneur, and G. Moultaka, "SuSpect: A Fortran code for the supersymmetric and Higgs particle spectrum in the MSSM", *Comput. Phys. Commun.* **176** (2007) 426–455.

[142] J. Bardeen, L. N. Cooper, and J. R. Schrieffer, "Theory of Superconductivity", *Phys. Rev.* **108** Dec (1957) 1175–1204.

[143] F. D'Eramo, J. Thaler, and Z. Thomas, "Anomaly Mediation from Unbroken Supergravity", *JHEP* **09** (2013) 125.

[144] G. F. Giudice and R. Rattazzi, "Theories with gauge mediated supersymmetry breaking", *Phys. Rept.* **322** (1999) 419–499.

[145] W. Porod, "SPheno, a program for calculating supersymmetric spectra, SUSY particle decays and SUSY particle production at e+ e- colliders", *Comput. Phys. Commun.* **153** (2003) 275–315.

[146] B. C. Allanach, "SOFTSUSY: a program for calculating supersymmetric spectra", *Comput. Phys. Commun.* **143** (2002) 305–331.

[147] A. H. Chamseddine, R. Arnowitt, and P. Nath, "Locally Supersymmetric Grand Unification", *Phys. Rev. Lett.* **49** Oct (1982) 970–974.

[148] G. F. Giudice and R. Rattazzi, "Theories with gauge mediated supersymmetry breaking", *Phys. Rept.* **322** (1999) 419–499.

[149] B. C. Allanach *et al.*, "The Snowmass points and slopes: Benchmarks for SUSY searches", *Eur. Phys. J.* **C25** (2002) 113–123.

[150] H. Murayama, "Supersymmetry phenomenology", in "Particle physics. Proceedings, Summer School, Trieste, Italy, June 21-July 9, 1999", pp. 296–335. 2000.

[151] S. Mukhopadhyay, M. M. Nojiri, and T. T. Yanagida, "Compressed SUSY search at the 13 TeV LHC using kinematic correlations and structure of ISR jets", *JHEP* **10** (2014) 12.

[152] **ATLAS** Collaboration, G. Aad *et al.*, "Summary of the searches for squarks and gluinos using $\sqrt{s} = 8$ TeV pp collisions with the ATLAS experiment at the LHC", *JHEP* **10** (2015) 054.

[153] **CMS** Collaboration, S. Chatrchyan *et al.*, "Searches for long-lived charged particles in pp collisions at $\sqrt{s}$=7 and 8 TeV", *JHEP* **07** (2013) 122.

[154] K. Kohri and F. Takayama, "Big bang nucleosynthesis with long lived charged massive particles", *Phys. Rev.* **D76** (2007) 063507.

[155] K. Jedamzik, "The cosmic Li-6 and Li-7 problems and BBN with long-lived charged massive particles", *Phys. Rev.* **D77** (2008) 063524.

[156] N. Craig, "The State of Supersymmetry after Run I of the LHC", in "Beyond the Standard Model after the first run of the LHC Arcetri, Florence, Italy, May 20-July 12, 2013". 2013.

[157] S. Iwamoto, "Supersymmetry after the Higgs discovery and its LHC phenomenology", arXiv:1305.0790.

[158] J. Alwall, P. Schuster, and N. Toro, "Simplified Models for a First Characterization of New Physics at the LHC", *Phys. Rev.* **D79** (2009) 075020.

[159] J. A. Evans and J. Shelton, "Long-Lived Staus and Displaced Leptons at the LHC", arXiv:1601.01326.

[160] T. Kaluza, "Zum Unitatsproblem der Physik", *Sitzungsberichte Preuszische Akademie der Wissenschaften*, 1921 966–972.

[161] O. Klein, "Quantentheorie und fünfdimensionale relativitätstheorie", *Zeitschrift für Physik* **37** no. 12, 895–906.

[162] R. Sundrum, "Tasi 2004 lectures: To the fifth dimension and back", in "Theoretical Advanced Study Institute in Elementary Particle Physics: Many Dimensions of String Theory, TASI 2005, Boulder, USA, June 5-July 1, 2005", pp. 585–630. 2005.

[163] L. Nilse, "Classification of 1D and 2D orbifolds", arXiv:hep-ph/0601015.

[164] N. Arkani-Hamed, S. Dimopoulos, and G. Dvali, "The hierarchy problem and new dimensions at a millimeter", *Physics Letters B* **429** (1998), no. 3-4, 263 – 272.

[165] N. Arkani-Hamed, S. Dimopoulos, and G. Dvali, "Phenomenology, astrophysics, and cosmology of theories with submillimeter dimensions and TeV scale quantum gravity", *Phys. Rev. D* **59** Mar (1999) 086004.

[166] J. W. Rohlf, "Modern Physics from α to Z_0", Wiley, 1994.

[167] L. Randall and R. Sundrum, "A Large mass hierarchy from a small extra dimension", *Phys. Rev. Lett.* **83** (1999) 3370–3373.

[168] Y.-b. Kim, C. O. Lee, I.-b. Lee, and J.-J. Lee, "Brane world of warp geometry: An Introductory review", *J. Korean Astron. Soc.* **37** (2004) 1–14.

[169] G. Burdman, "New solutions to the hierarchy problem", *Braz. J. Phys.* **37** (2007) 506–513.

[170] G. D. Kribs, "TASI 2004 lectures on the phenomenology of extra dimensions", in "Physics in D >= 4. Proceedings, Theoretical Advanced Study Institute in elementary particle physics, TASI 2004, Boulder, USA, June 6-July 2, 2004", pp. 633–699. 2006.

[171] K. Agashe, A. Falkowski, I. Low, and G. Servant, "KK Parity in Warped Extra Dimension", *JHEP* **04** (2008) 027.

[172] H.-C. Cheng, J. L. Feng, and K. T. Matchev, "Kaluza-Klein dark matter", *Phys. Rev. Lett.* **89** (2002) 211301.

[173] D. Hooper and S. Profumo, "Dark matter and collider phenomenology of universal extra dimensions", *Phys. Rept.* **453** (2007) 29–115.

[174] H.-C. Cheng, K. T. Matchev, and M. Schmaltz, "Radiative corrections to Kaluza-Klein masses", *Phys. Rev.* **D66** (2002) 036005.

[175] J. Knapp, D. Heck, and G. Schatz, "Comparison of hadronic interaction models used in air shower simulations and of their influence on shower development and observables", *FZKA-5828*, 1996.

[176] R. S. Fletcher, T. K. Gaisser, P. Lipari, and T. Stanev, "SIBYLL: An Event generator for simulation of high-energy cosmic ray cascades", *Phys. Rev.* **D50** (1994) 5710–5731.

[177] J. R. Horandel, "On the knee in the energy spectrum of cosmic rays", *Astroparticle Physics* **19** (2003), no. 2, 193 – 220.

[178] M. Honda, T. Kajita, K. Kasahara, S. Midorikawa, and T. Sanuki, "Calculation of atmospheric neutrino flux using the interaction model calibrated with atmospheric muon data", *Phys. Rev.* **D75** (2007) 043006.

[179] P. Z. Skands *et al.*, "SUSY Les Houches accord: Interfacing SUSY spectrum calculators, decay packages, and event generators", *JHEP* **07** (2004) 036.

[180] T. Sjostrand, S. Mrenna, and P. Z. Skands, "PYTHIA 6.4 Physics and Manual", *JHEP* **05** (2006) 026.

[181] J. Alwall *et al.*, "A Standard format for Les Houches event files", *Comput. Phys. Commun.* **176** (2007) 300–304.

[182] A. Belyaev, N. D. Christensen, and A. Pukhov, "CalcHEP 3.4 for collider physics within and beyond the Standard Model", *Comput. Phys. Commun.* **184** (2013) 1729–1769.

[183] **CompHEP** Collaboration, E. Boos, V. Bunichev, M. Dubinin, L. Dudko, V. Ilyin, A. Kryukov, V. Edneral, V. Savrin, A. Semenov, and A. Sherstnev, "CompHEP 4.4: Automatic computations from Lagrangians to events", *Nucl. Instrum. Meth.* **A534** (2004) 250–259.

[184] J. Alwall, M. Herquet, F. Maltoni, O. Mattelaer, and T. Stelzer, "MadGraph 5 : Going Beyond", *JHEP* **06** (2011) 128.

[185] J. Pumplin, D. R. Stump, J. Huston, H. L. Lai, P. M. Nadolsky, and W. K. Tung, "New generation of parton distributions with uncertainties from global QCD analysis", *JHEP* **07** (2002) 012.

[186] A. M. Dziewonski and D. L. Anderson, "Preliminary reference earth model", *Phys. Earth Planet. Interiors* **25** (1981) 297–356.

[187] R. Gandhi, C. Quigg, M. H. Reno, and I. Sarcevic, "Ultrahigh-energy neutrino interactions", *Astropart. Phys.* **5** (1996) 81–110.

[188] S. Ando, J. F. Beacom, S. Profumo, and D. Rainwater, "Probing new physics with long-lived charged particles produced by atmospheric and astrophysical neutrinos", *JCAP* **0804** (2008) 029.

[189] T. DeYoung, "IceTray: A software framework for IceCube", in "Computing in high energy physics and nuclear physics. Proceedings, Conference, CHEP'04, Interlaken, Switzerland, September 27-October 1, 2004", pp. 463–466. 2005.

[190] I. F. M. Albuquerque and S. R. Klein, "Supersymmetric and Kaluza-Klein Particles Multiple Scattering in the Earth", *Phys. Rev.* **D80** (2009) 015015.

[191] R. Enberg, M. H. Reno, and I. Sarcevic, "Prompt neutrino fluxes from atmospheric charm", *Phys. Rev.* **D78** (2008) 043005.

[192] W. Kilian, T. Ohl, and J. Reuter, "WHIZARD: Simulating Multi-Particle Processes at LHC and ILC", *Eur. Phys. J.* **C71** (2011) 1742.

[193] M. Moretti, T. Ohl, and J. Reuter, "O'Mega: An Optimizing matrix element generator", arXiv:hep-ph/0102195.

[194] R. Gandhi, C. Quigg, M. H. Reno, and I. Sarcevic, "Neutrino interactions at ultrahigh-energies", *Phys. Rev.* **D58** (1998) 093009.

[195] **GEANT4** Collaboration, S. Agostinelli *et al.*, "GEANT4: A Simulation toolkit", *Nucl. Instrum. Meth.* **A506** (2003) 250–303.

[196] A. Tepe, "Hardware Integration of the AMANDA into the IceCube Neutrino Telescope and Search for Supersymmetric Particles with the IceCube Neutrino Telescope", PhD thesis, BU Wuppertal, 8 2009.

[197] M. G. Aartsen *et al.*, "Improvement in Fast Particle Track Reconstruction with Robust Statistics", *Nucl. Instrum. Meth.* **A736** (2014) 143–149.

[198] J. MacQueen in "Proceedings of the Fifth Berkeley Symposium on Mathematical Statistics and Probability, Volume 1: Statistics", pp. 281–297. University of California Press, Berkeley, Calif.

[199] **IceCube** Collaboration, R. Abbasi *et al.*, "Lateral distribution of muons in IceCube cosmic ray events", *Phys. Rev. D* **87** (2013) 012005.

[200] D. van der Drift and S. R. Klein, "Double Neutrino Production and Detection in Neutrino Detectors", *Phys. Rev.* **D88** (2013) 033013.

[201] "Internal document". http://docushare.icecube.wisc.edu/dsweb/Get/Document-65251/Preliminary_IC79_inice_v2.9.txt, accessed May 27, 2015.

[202] **TMVA Core Developer Team** Collaboration, J. Therhaag, "TMVA: Toolkit for multivariate data analysis", *AIP Conf. Proc.* **1504** (2009) 1013–1016.

[203] **IceCube** Collaboration, T. Gaisser, "Seasonal variation of atmospheric neutrinos in IceCube", in "Proceedings, 33rd International Cosmic Ray Conference (ICRC2013): Rio de Janeiro, Brazil, July 2-9, 2013", p. 0492.

[204] **IceCube** Collaboration, M. G. Aartsen *et al.*, "IceCube-Gen2: A Vision for the Future of Neutrino Astronomy in Antarctica", arXiv:1412.5106.

It's not the fall that kills you;
it's the sudden stop at the end.

— Douglas Adams

COLOPHON

This document was typeset using the typographical look-and-feel `classicthesis` developed by André Miede.

http://code.google.com/p/classicthesis/